Peak-to-Average Power-Ratio and Intercarrier-Interference Reduction Algorithms for Orthogonal Frequency-Division Multiplexing Systems

by

Yajun Kou
M.Sc, Beijing University of Posts & Telecomm., 2000
B.Sc, Beijing University of Posts & Telecomm., 1997

A Dissertation Submitted in Partial Fulfillment of the Requirements
for the Degree of

DOCTOR OF PHILOSOPHY

in the Department of Electrical and Computer Engineering

Supervisor: Dr. A. Antoniou and Dr. W.-S. Lu

ABSTRACT

Several new peak-to-average power-ratio (PAPR) and intercarrier interference (ICI) reduction algorithms are developed for different orthogonal frequency-division multiplexing (OFDM) systems.

A new constellation extension technique is proposed for PAPR reduction for OFDM systems whereby the modulation constellation for active subcarriers and the modulation symbols in unused subcarriers are continuously modified. Based on this technique, the PAPR-reduction problem for OFDM systems with real-valued time-domain signals is formulated as a linear-programming (LP) problem where the number of constraints is much larger than that of the variables. The solution of the problem is obtained efficiently by using a new Newton algorithm. Simulations demonstrate that considerable performance improvement can be achieved by using the proposed algorithm relative to that achieved by using some existing algorithms.

The proposed constellation extension technique is applied for PAPR reduction for OFDM systems with complex-valued time-domain signals. In this case, the PAPR-reduction problem is formulated as a minimax optimization problem and an accelerated least-pth algorithm is proposed to obtain the solution. Simulations show that, in many practical situations, considerable performance improvement can be achieved by the proposed algorithm over that achieved by several existing algorithms. Furthermore, the accelerated algorithm offers a tradeoff between performance and computational complexity, which can be used to advantage in practical situations.

Yet another constellation extension technique for PAPR reduction is developed whereby, for each subcarrier, the same data may be represented by points in the original constellation or by extended points. In an attempt to find an optimal representation of the OFDM signal, two de-randomization algorithms are proposed by applying the so called conditional probablity method, i.e., the Chernoff-bound based

and polynomial-bound based algorithms. In order to further improve the performance, new algorithms based on the selective rotation (SR) and coordinate descent optimization (CDO) are proposed. It is shown that the proposed algorithms outperform several existing algorithms in terms of PAPR reduction and computational complexity. Compared with the proposed Chernoff-bound based algorithm, the proposed polynomial-bound based algorithm achieves a similar performance with much less computational complexity. The performance of the proposed algorithms can be further improved by combining the de-randomization, SR, and CDO algorithms with the selective mapping (SLM) algorithm.

The thesis also deals with ICI reduction in OFDM systems in fast time-varying channels. Two new algorithms are proposed for OFDM systems with complex-valued time-domain signals. A low-complexity ICI-reduction algorithm based on an iterative optimization algorithm is proposed for OFDM systems using 4-quadrature-amplitude-modulation (4-QAM) for all subcarriers. Then an ICI-reduction algorithm based on the sphere decoding (SD) algorithm is proposed for OFDM systems using high-order modulation. By taking channel information into account, a new search strategy to reduce the computational complexity of the SD algorithm is developed. Simulations demonstrate that the proposed iterative algorithm outperforms several existing algorithms in terms of BER performance and computational complexity, and the performance can be further improved by using the proposed SD algorithm. The proposed algorithms can exploit the frequency diversity introduced by channel variations and, therefore, improved performance can be achieved at higher Doppler frequencies.

Table of Contents

List of Tables

List of Figures

List of Abbreviations

ASE	Active Set Extension
AWGN	Additive White Guassian Noise
BER	Bit-Error Rate
CDF	Cumulative Density Function
CDO	Coordinate Descent Optimization
CFO	Carrier Frequency Offset
CIR	Channel Impulse Response
CP	Cyclic Prefix
DAB	Digital Audio Broadcasting
DF	Decision Feedback
DFT	Discrete Fourier Transform
DOA	Direction of Arrival
DVB	Digital Video Broadcasting
FDM	Frequency-Division Multiplexing
FFT	Fast Fourier Transform
IBO	Input Back-Off
ICI	Intercarrier Interference
IDFT	Inverse Discrete Fourier Transform
ISI	Inter-Symbol Interference
JD	Joint Detection
l.h.s.	Left Hand Side
LOS	Line of Sight
LP	Linear Programming

LS	Least-Square
MCP	Method of Conditional Probability
MIMO	Multiple-Input Multiple-Output
ML	Maximum Likelihood
MMSE	Minimum Mean-Square-Error
MSE	Mean-Square-Error
OFDM	Orthogonal Frequency-Division Multiplexing
OFDMA	Orthogonal Frequency-Division Multiple Access
PA	Power Amplifier
PAPR	Peak-to-Average Power-Ratio
PSK	Phase-Shift Keying
QAM	Quadratic Amplitude Modulation
r.h.s.	Right Hand Side
rms	root-mean-square
RRC	Root-Raised-Cosine
SCE	Symmetric Constellation Extension
SD	Sphere Decoding
SIR	Signal to Intercarrier-Interfercence Ratio
SL	Soft Limiter
SLM	Selective Mapping
SNR	Signal to Noise Power-Ratio
SR	Selective Rotation
TDL	Tapped Delay Line
VLSI	Very Large-Scale Integration
WLAN	Wireless Local Area Networks
WSSUS	Wide-Sense-Stationary Uncorrelated-Scattering

Acknowledgement

I would like to take this opportunity to express deep gratitude to my co-supervisors, Dr. Andreas Antoniou and Dr. Wu-Sheng Lu, for suggesting the topic of this thesis and for guiding me through the journey toward the completion of my Ph. D. degree. Their continuous encouragement and support along the way is appreciated.

I thank Dr. Aaron Gulliver, Dr. Zuoming Dong, and Dr. Chintha Tellambura for serving on the examining committee, and for providing suggestions, comments, and questions that greatly helped to improve the quality of the thesis.

I wish to thank the staff of the Department of Electrical Engineering Ms. Catherine Chang, Ms. Lynne Barrett, Ms. Vicky Smith, Ms. Moneca Bracken, and Ms. Mary-Anne Teo, and my past and present fellow students colleagues Dr. Xianmin Wang, Dr. M. Watheq El-Kharashi, Nanyan Wang, Mingjie Cai, Rajeev Nongpiur, Mohamed S. Yasein, Stuart Bergen, Sabbir Ahmad, Paramesh Ramachandran, Rafik Mikhael, Brad Riel, and many others for their generous friendship, enlightening discussions, and productive cooperation.

I would also like to thank Micronet, NSERC, and PMC-Sierra Inc. for supporting the research reported in this thesis. The financial support from these organizations is greatly appreciated.

I am greatly indebted to my parents and sister for their love, deep understanding, and continuous strong support in the pursuit of my Ph. D. degree.

Finally, I wish to express my deepest gratefulness to my wife, Beibei Wang, who has been accompanying and supporting me for many years. Without her encouragement and support, I could not have come even close to what I have achieved.

Chapter 1

Introduction

1.1 OFDM Basics

Recently, the demand for high data-rate services over wireless networks has been increasing very rapidly. These services require reliable data transmission over band-limited wireless channels, which experience many degradations, such as noise, multipath fading and nonlinearities. A physical-layer technique that has gained much popularity is orthogonal frequency-division multiplexing (OFDM) [1][2].

The concept of using parallel data transmission by means of frequency-division multiplexing (FDM) appeared in the middle 1960s [3][4]. In an FDM system, the total signal frequency band is divided into a number of nonoverlapping frequency subchannels, and each subchannel is modulated individually and then all subchannels are frequency-multiplexed. A guard band is inserted between each pair of neighbouring subchannels to eliminate interchannel interference. This however reduces the spectral utilization efficiency. To deal with this inefficiency, the ideas proposed in the middle 1960s were to use parallel data transmission and FDM with overlapping subchannels. The term "orthogonal frequency-division multiplexing" was first used in a patent filed and issued in 1970 [5]. The idea is to use parallel data streams and FDM with overlapping subcarriers to increase the spectral efficiency, to avoid the use of high-speed equalization, and to combat multipath fading as well as narrowband interference. Since the subcarriers of OFDM are orthogonal to each other, the signals

on each subcarrier are received without intercarrier interference (ICI). The spectral utilization efficiency of FDM and OFDM is compared in Fig. 1.1.

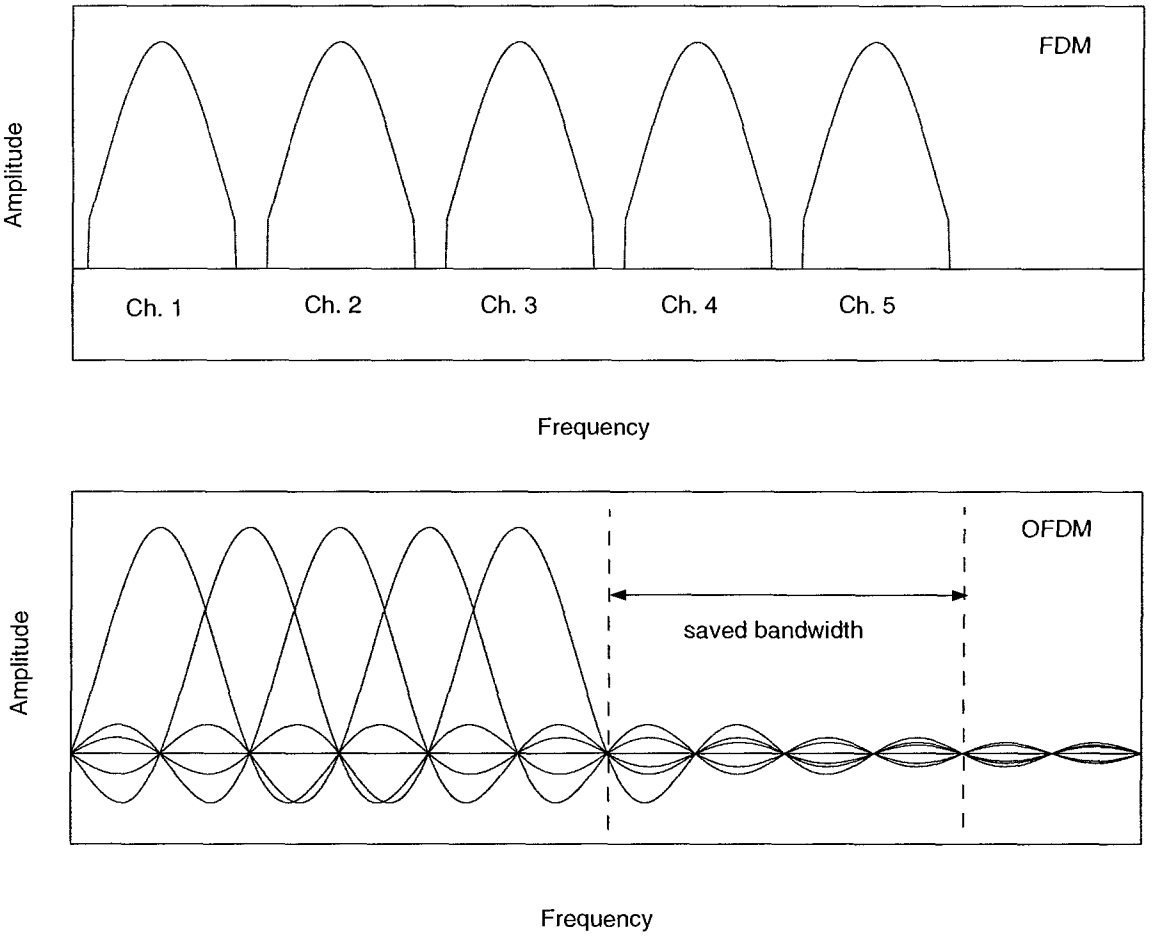

Figure 1.1. *Comparison of the spectral uitilization efficiency of FDM and OFDM.*

In the 1970s, a practical implementation of OFDM was proposed by Weinstein and Ebert [6], where the discrete Fourier transform (DFT) and inverse discrete Fourier transform (IDFT) were applied as part of the modulation and demodulation process. In addition to eliminating the banks of subcarrier oscillators and coherent demodulators required by FDM, a completely digital implementation could be built on special-purpose hardware that performs the fast Fourier transform (FFT) [7]. Recent advances in very large-scale intergration (VLSI) technology allow implementation of

large-size FFTs at affordable price, which further increase the popularity of OFDM systems.

Compared with single-carrier transmission, OFDM offers several key adavantages [1][2][8]. The first advantage is its robustness to multipath fading. In an OFDM system, a high-rate data stream is split into several low-rate streams that are transmitted simultaneously through orthogonal subcarriers. As the symbol duration of low-rate parallel subcarriers is increased, the relative amount of dispersion in time caused by multipath delay spread is decreased. Therefore, with the use of a cyclic prefix (CP) [9], the intersymbol interference (ISI) between successive OFDM symbols can almost completely be eliminated. Another adavantage of OFDM is its resistance to narrowband interference. Since the OFDM waveform is composed of many narrowband tones, a narrowband interference degrades the performance in a portion of the spectrum but has limited effect on the remaining part of the spectrum. Through the use of forward error correction coding [10]-[12], information lost to interference can be recovered. Because of these good properties, OFDM has been widely used as a transmission technique in a variety of communication systems. Well-known examples include digital audio broadcasting (DAB) [13], digital video broadcasting (DVB) [14], and the IEEE 802.11a and 802.11g standards for wireless local area networks (WLAN) [15].

Unfortunately, two major drawbacks are associated with OFDM. The first is its large peak-to-average power-ratio (PAPR) which makes system performance very sensitive to distortion introduced by nonlinear devices such as power amplifiers (PAs) [1][2][8][16][17]. In practice, linear PAs with a wide dynamic range are required to mitigate nonlinear distortion but such PAs are power inefficient. The second drawback of OFDM is its sensitivity to loss of orthogonality of subcarriers, which may be caused by carrier frequency offset (CFO) [18] or Doppler spread in a time-varying channel [1][2][8][19]-[22]. Loss of orthogonality of subcarriers leads to ICI, which, in turn, degrades the bit error rate (BER) performance of the system. While the ICI caused

by CFO can be easily estimated and compensated [23]-[28], the Doppler-induced ICI is more challenging to deal with. If not compensated for, ICI will result in an error floor that increases with Doppler frequency.

In an attempt to reduce the nonlinear distortion caused by PAs, a number of techniques and algorithms have been proposed to reduce the PAPR of the OFDM signal before it enters a PA. Generally, these techniques and algorithms can be classified into four major categories. First, a straightforward way would be to limit the signal strength at the transmitter to a desired level through clipping but the technique degrades the BER of the system and increases the out-of-band radiation [29][30] due to the increased harmonic content unless additional coding techniques and bandpass filtering are used [31]. Second, several PAPR-reduction algorithms have been proposed in [32]-[37] where PAPR reduction are combined with error-control coding. Very low PAPR can be achieved by these algorithms but at the cost of a significant reduction of data transmission rate. Moreover, these algorithms require large look-up tables and, therefore, are more suitable for OFDM systems with a small number of subcarriers. Third, a multiple signal representation approach has been proposed in [38][39] where a set of OFDM signals are generated at the OFDM transmitter and the transmit signal with the lowest peak power is selected. This approach is computationally efficient but it requires the transmission of a small amount of side information. The use of the selective mapping (SLM) algorithm [38] together with other PAPR-reduction algorithms has also been proposed in [40]. Fourth, several PAPR-reduction algorithms have been proposed in [41]-[44] where the extension of modulation constellation is exploited to reduce the PAPR of the OFDM signals. These algorithms are all distortionless PAPR-reduction algorithms and do not require the transmission of any side information. The algorithms differ from each other in the way they modify the modulation constellation. In [41], a tone reservation algorithm has been developed where several subcarriers are set aside for PAPR reduction. Since the subcarriers are orthogonal, the additive signal on unused subcarriers causes no distortion to the

data-bearing subcarriers. In [42][43], an active set extension (ASE) algorithm has been proposed where PAPR reduction is achieved by modifying the exterior modulation constellation over active subcarriers in a way that will not degrade the BER performance. In [44], a symmetric constellation extension (SCE) algorithm has been proposed for PAPR reduction whereby the subsymbols for each subcarrier can be represented by two symmetric constellation points and an optimal representation has been derived by using a de-randomization algorithm. Since for each constellation point there is one bit that is not used to transmit any information, the transmit power of OFDM systems using constellation extension is much larger than that of OFDM systems with no constellation extension.

Recently, ICI reduction for OFDM systems in fast time-varying channels has drawn a lot of attention [45]-[47]. Based on the maximum likelihood (ML) criterion, the ICI reduction problem can be formulated as an integer least-square (LS) problem whose solution requires computational complexity that grows exponentially with the number of variables. In attempts to reduce the computational complexity required by ML detection, several linear and nonlinear detection algorithms have been proposed for obtaining suboptimal solutions of the problem [45]-[47]. In [45], a linear minimum mean-square error (MMSE) detection algorithm has been proposed where signals on all subcarriers are used to suppress the ICI for a particular subcarrier. Since the number of subcarriers for OFDM systems is generally quite large, this algorithm requires intensive computation. In attempts to reduce the computational complexity, an MMSE detection algorithm has been derived in [46] where only signals on several neighbouring subcarriers are used in order to suppress the ICI for a particular subcarrier. Since the ICI for a particular subcarrier is mainly caused by the signals on its neighbouring subcarriers, the degradation in performance introduced by such simplification is not significant. Based on this MMSE algorithm, a decision feedback (DF) algorithm has been proposed in [46] to further improve the performance. In [47], the ICI reduction for multiple-input multiple-output (MIMO) OFDM systems

has been considered. An optimal linear pre-filtering algorithm has been developed where improved performance was achieved at the cost of increased computational complexity.

This thesis is primarily concerned with PAPR and ICI reduction for OFDM systems. The scope and specific contributions of the thesis are described below.

1.2 Scope and Contributions of This Thesis

This thesis is composed of six chapters. In Chapter 2, a preliminary study on wireless communication channels, OFDM systems, and several important PAPR-reduction and ICI-reduction algorithms is presented. Chapters 3 to 5 constitute the main part of the thesis where several new PAPR-reduction and ICI-reduction algorithms are proposed. Chapter 6 provides concluding remarks and suggestions for future study.

In Chapter 3, two new PAPR-reduction algorithms for OFDM systems are developed by continuously modifying the modulation constellation at active subcarriers and the modulation symbols at unused subcarriers. First, for OFDM systems with real-valued time-domain signals, it is shown that the PAPR-reduction problem can be formulated as a linear programming (LP) problem and its solution is obtained by using a new Newton method [48]. Since the feasible region associated with the LP problem obtained is always larger than that associated with the LP problem given in [41], the performance of the proposed algorithm is guaranteed to be better than that of the tone reservation algorithm [41]. Computer simulations are then presented which demonstrate that the proposed algorithm yields optimal PAPR-reduction solutions and considerable performance improvement can be achieved with the proposed algorithm relative to that achieved with the tone reservation algorithms [41] and the ASE algorithm [42]. Second, for OFDM systems with complex-valued time-domain signals, it is shown that the PAPR-reduction problem can be formulated as an unconstrained minimax optimization problem and its solution is obtained by using an

accelerated *least-pth* algorithm [49]. Computer simulations show that the proposed algorithm outperforms the ASE algorithm [42] and that improved PAPR reduction can be obtained when the proposed algorithm is combined with the SLM algorithm [38].

In Chapter 4, a new constellation extension technique is developed whereby the data are represented either by points in the original constellation or by extedned points. Since the constellation is extended in a discrete way, it is shown that the problem of finding an optimal representation of the OFDM signal is an integer programming problem. By applying the so called method of conditional probability (MCP) [50], two de-randomization algorithms are proposed to achieve suboptimal solutions of the problem. First, a Chernoff-bound based pessimistic estimator is derived and a de-randomization algorithm is constructed. Second, a polynomial-bound based pessimistic estimator is derived to approximate the Chernoff-bound based pessimistic estimator and then a corresponding de-randomization algorithm is developed. It is shown that the performance of the polynomial-bound based algorithm is quite close to that of the Chernoff-bound based algorithm but the former requires much less computational complexity. Next, selective rotation (SR) and coordinate descent optimization (CDO) algorithms [51] are proposed to further improve the performance. Computer simulations show that significant improvement in PAPR reduction is achieved by the proposed algorithms over the SLM algorithm [38] and the SCE algorithm [44]. In addition, it is shown that the increase in the average transmit power for the proposed algorithms, which is caused by the constellation extension, is much less than that for the SCE algorithm [44].

Chapter 5 is devoted to ICI reduction for OFDM systems in fast time-varying channels. For the algorithms proposed in [45][46], their detection performance becomes unsatisfactory when the Doppler shift of the channel is high. Therefore, more robust ICI-reduction algorithms are needed. In this chapter, two new ICI-reduction algorithms based on the ML criterion are proposed for obtaining a suboptimal solu-

tion of the associated integer LS problem. First, a low-complexity algorithm based on an iterative optimization scheme is proposed for OFDM systems where 4-quadrature-amplitude-modulation (4-QAM) is assumed for all subcarriers. Second, an algorithm based on the sphere decoding (SD) method [52] is proposed for OFDM systems using 4-QAM modulation or higher-order QAM modulations. Since the computational compelxity of the conventional SD algorithms [53][54] is still high, a scheme that can reduce the complexity of the SD algorithm is needed. By taking into account the available channel information, a new search strategy for the reduction of the compelxity of the SD algorithm is developed. Computer simulations are presented to demonstrate that the proposed iterative optimization algorithm removes the BER floor suffered by the MMSE algorithm [46] and outperforms the DF algorithms [46] in terms of BER performance and computational complexity. It is also shown that the performance can be further improved by using the proposed SD algorithm. Furthermore, because of the frequency diversity introduced by channel variations [55][56], improved performance can be achieved by the proposed algorithms at higher Doppler frequencies.

Chapter 2

PAPR and ICI Reduction in OFDM Systems

2.1 Introduction

In OFDM systems, the design of PAPR- and ICI-reduction algorithms depends on many considerations such as the bandwidth available, number of subcarriers, modulation scheme for each subcarrier, and the characteristics of the wireless communication channel involved. In this chapter, some background knowledge, concepts, and terminology for the wireless communication channel, the OFDM system, PAPR and ICI reduction are discussed, and several existing algorithms for PAPR and ICI reduction are reviewed. The chapter provides a basis on which the subsequent chapters are developed in a unified framework for various PAPR- and ICI-reduction algorithms.

2.2 Wireless Communication Channel

In a wireless communication system, a transmission channel is referred to as a propagation path over which radio signals travel from a base station to a terminal (forward link), or from a terminal to a base station (reverse link) [57]. Typical wireless communication channels vary from simple line-of-sight (LOS) transmission channels to very complicated ones that may be blocked by vehicles, mountains, and high-rise build-

ings. In addition, due to the relative motion of terminals and other radio propagation media with respect to the base station, the received signals often exhibit a great deal of randomness. Consequently, wireless communication channels are often modeled using statistical methods.

Two important parameters associated with wireless communication channels are *time dispersion* and *time variation.* Time dispersion is due to multiple reflections during signal propagation which travel along different paths of varying lengths and arrive at the receiver at different times. Time variation is due to varying radio signal propagation environment from the transmitter to the receiver such as movement of the transmitter, receiver, or other media. As a result of the relative movement of transmitters and receivers, the power level of the received signal often exhibits fluctuations and variations. This phenomenon is called *fading.*

2.2.1 Delay Spread: Frequency Selective Fading

Delay spread is a measurement used to describe the time dispersion of a wireless communication channel. The parameters frequently used in quantifying the delay spread of a wireless communication channel are the *mean excess delay, root-mean-square (rms) delay spread,* and *excess delay spread* [58]. In a typical wireless communication channel, the delay separation between adjacent propagation paths increases exponentially and the path amplitudes decay exponentially with respect to path delay [59][60]. Delay spread often leads to *frequency selective fading,* i.e., the fading effect of the received signal depends on frequency.

Coherence bandwidth is a measurement of the range of frequencies over which propagation channels can pass all spectral components with approximately equal gain and linear phase. This implies that the power levels of two signal frequencies are potentially correlated within the coherence bandwidth. If the coherence bandwidth is defined as the bandwidth over which the frequency correlation function is greater

than 0.9, then it can be roughly computed as

$$f_c = \frac{1}{50\sigma_t} \tag{2.1}$$

where σ_t denotes the *rms* delay spread [58]. A channel is said to be *frequency-flat fading* if the channel coherence bandwidth is greater than that of the transmitted baseband signal. In such a case, the delay spread is insignificant relative to the symbol duration and its effect at the receiver can be neglected. On the other hand, if the coherence bandwidth is smaller than the bandwidth of the transmitted baseband signal, the channel is said to be a *frequency-selective fading* channel and the effects of delay spread at the receiver can be considerable.

2.2.2 Doppler Spread: Time-Selective Fading

Doppler spread is a measurement often used to describe the time-varying nature of a wireless communication channel. When a pure tone signal is transmitted through a time-varying wireless communication channel, the received signal may spread over a finite spectral bandwidth. Doppler spread is defined as the range of frequencies over which the spectrum of the received signal assumes non-zero values. In wireless communications, Doppler spread is related to the velocity of moving objects such as mobiles and other propagation media, and the angle between the direction of movement and the direction of arrival (DOA) of scattered electromagnetic signals [58].

Coherence time is a measurement used to describe the frequency dispersion nature of a wireless communication channel in the time domain. It represents the time duration over which the power levels of two received signals have strong correlation. This implies that the channel condition is essentially invariant within the coherent time. Numerically, coherence time is inversely proportional to the Doppler spread. In wireless communication systems, coherence time is usually defined as the time duration over which the time correlation function is greater than 0.5, which can be

roughly computed as

$$T_c = \frac{9}{16\pi f_m} \tag{2.2}$$

In (2.2), $f_m = v/\lambda$ denotes the *maximum Doppler shift* with v and λ being the velocity of the mobile relative to the base station and the wave length of the radio signal, respectively. A channel is said to be *slow fading* if the coherence time is much longer than the symbol duration of the transmitted signal. In such a case, the effect of Doppler spread at the receiver is negligible. On the other hand, if the coherence time is shorter than or comparable with the symbol duration of the transmitted signal, the channel is said to be a *fast fading* channel in which the effect of Doppler spread cannot be ignored.

2.2.3 Discrete-Time Baseband Channel Model

In general, a wireless communication channel is often modeled as a wide-sense-stationary uncorrelated-scattering (WSSUS) channel [58][61]. The impulse response of such a channel is given by

$$h_c(t,\tau) = \sum_{m=0}^{M-1} h_c(t,\tau_m)\delta(\tau - \tau_m) \tag{2.3}$$

where $\delta(\tau)$, M, $h_c(t,\tau_m)$, and τ_m denote the unit impulse function, the number of resolvable propagation paths, the path gain, and the excess path delay of the mth propagation path, respectively. The input-output relationship is given by

$$y_c(t) = \int_{-\infty}^{\infty} x_c(t-\tau)h_c(t,\tau)d\tau \tag{2.4}$$

where $x_c(t)$ and $y_c(t)$ are the channel excitation and response, respectively. It is assumed that the bandwidth of the channel excitation is W and it can be correctly sampled at a sampling interval $T_p = 1/(2W)$. Using the generalized sampling-interpolation [62] theorem, we have

$$x_c(t) = \sum_k x_c(kT_p + t_0)\text{sinc}\left[\frac{t-(kT_p+t_0)}{T_p}\right] \tag{2.5}$$

This equation holds for any t_0. Using (2.5), (2.4) can be rewritten as

$$y_c(t) = \sum_l x_c(t - lT_p) \int_{-\infty}^{\infty} h_c(t, \tau)\text{sinc}\left(\frac{\tau}{T_p} - l\right) d\tau \tag{2.6}$$

where the substitution $t - (kT_p + t_0) = lT_p$ is used. It can be seen from (2.6) that the channel can be modelled as a tapped delay line (TDL) as shown in Fig. 2.1, where the time-varying TDL coefficients are

$$h(t, l) = \int_{-\infty}^{\infty} h_c(t, \tau)\text{sinc}\left(\frac{\tau}{T_p} - l\right) d\tau \quad \text{for} \quad l = 0, \ldots, L-1 \tag{2.7}$$

where $L = \lfloor \tau_M / T_p \rfloor + 1$, and the input-output relationship is

$$y(t) = \sum_{l=0}^{L-1} h(t, l)x(t - lT_p) \tag{2.8}$$

Based on (2.7) and (2.8), the discrete-time channel coefficients can be obtained as

$$h_d(n, l) = h(nT_p, l) \tag{2.9}$$

and the discrete-time received signal is given by

$$y_d(n) = y(nT_p) = \sum_{l=0}^{L-1} h_d(n, l)x_d(n - l) \tag{2.10}$$

where $x(n)$ and $y(n)$ are discrete-time channel excitation and response, respectively. The effects of time variation and time dispersion in wireless communication channels are represented by using variable path gain $h_d(n, l)$ and path delay l in the channel model. In the rest of the dissertation, the discrete-time channel model is adopted, unless otherwise mentioned, and the subscript d is dropped for the sake of convenience.

2.3 OFDM System

In an OFDM system, the available bandwidth W is divided into N orthogonal sub-carriers whose center frequencies are seperated by W/N. A high-rate data stream

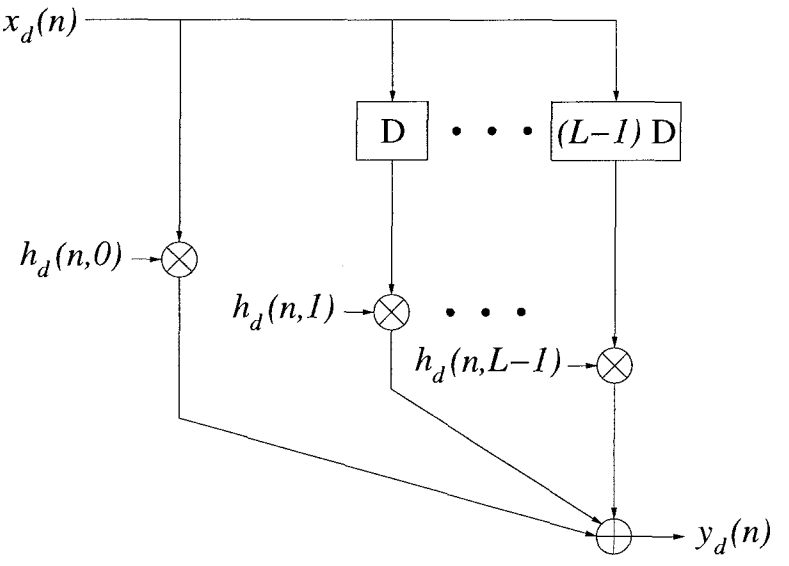

Figure 2.1. *A tap-delayed model for multipath propagation channels.*

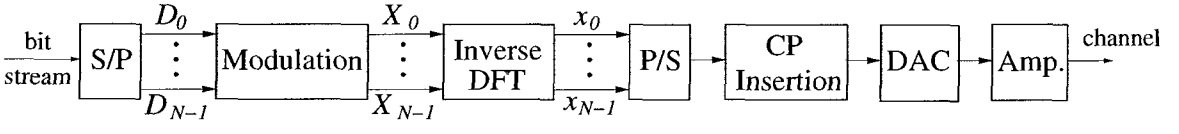

Figure 2.2. *An OFDM transmitter.*

is split into N low-rate streams that are transmitted simultaneously through these subcarriers. Each of the subcarriers is independently modulated using phase-shift keying (PSK) or quadrature amplitude modulation (QAM). The modulated signals for each subcarrier are transformed by an IDFT in order to generate the time-domain OFDM signal. A CP is inserted at the beginning of each OFDM symbol before it is enventually sent into the channel. The generation process of the OFDM signal is illustrated in Fig. 2.2 where S/P, P/S, and DAC represent serial-to-parallel, parallel-to-serial, and digital-to-analog converter, respectively, and the block labeled as "Amp." represents a PA. The information bits D_k and the modulated symbol X_k are referred to as the *data point* and *subsymbol* for the kth subcarrier, respectively. Vectors $\mathbf{X} = [X_0 \cdots X_{N-1}]^T$ and $\mathbf{x} = [x_0 \cdots x_{N-1}]^T$ are referred to as the frequency-domain and the time-domain *OFDM symbol*s, respectively.

Mathmetically, the OFDM symbol $\mathbf{x}$ can be obtained by using the IDFT as

$$x_n = \frac{1}{N}\sum_{k=0}^{N-1} X_k e^{j2\pi kn/N} \quad \text{for } n = 0, \ldots, N-1 \tag{2.11}$$

where x_n represents the nth element of $\mathbf{x}$. In matrix form, (2.11) can be expressed as

$$\mathbf{x} = \mathbf{QX} \tag{2.12}$$

where $\mathbf{Q}$ is the IDFT matrix whose elements are $q_{n,k} = (1/N)e^{j2\pi kn/N}$. A cyclic prefix with length equal to that of the channel impulse response (CIR) is inserted in the beginning of the OFDM symbol before it is transmitted into the multipath channel. Denoting the transmitted signal, received signal, and the CIR as $\mathbf{x}_{CP} = [x_{N-L+1} \cdots x_{N-1}\ x_0 \cdots x_{N-1}]^T$, $\mathbf{y} = [y_0 \cdots y_{N-1}]^T$, and $\mathbf{h}(n) = [h(n,0)\ h(n,1) \cdots h(n,L-1)]^T$, respectively, the received signal can be written as

$$\mathbf{y} = \mathbf{H}_{CP}\mathbf{x}_{CP} + \mathbf{n} \tag{2.13}$$

where $\mathbf{n} = [n_0 \cdots n_{N-1}]^T$ is a vector of additive white Guassian noise (AWGN) variables with zero mean and covariance matrix $\mathcal{E}\left[\mathbf{nn}^H\right] = \sigma^2\mathbf{I}$, and the channel matrix $\mathbf{H}_{CP}$ is given by

$$\mathbf{H}_{CP} = \begin{bmatrix} h(0,L-1) & h(0,L-2) & \cdots & h(0,0) & \cdots & 0 & 0 \\ 0 & h(1,L-1) & \cdots & h(1,1) & \cdots & 0 & 0 \\ \vdots & \vdots & \ddots & \vdots & \ddots & \vdots & \vdots \\ 0 & 0 & \cdots & 0 & \cdots & h(N-1,1) & h(N-1,0) \end{bmatrix}$$

It can be seen from (2.13) that if the length of the CP is equal to or longer than that of the CIR, then ISI can be avoided. Since the CP is only a copy of part of the OFDM symbol $\mathbf{x}$, (2.13) can be rewritten as

$$\mathbf{y} = \mathbf{Hx} + \mathbf{n} \tag{2.14a}$$

where

$$\mathbf{H}=\begin{bmatrix} h(0,0) & 0 & \cdots & h(0,2) & h(0,1) \\ h(1,1) & h(1,0) & \cdots & h(1,3) & h(1,2) \\ \vdots & \vdots & \ddots & \vdots & \vdots \\ h(L-1,L-1) & h(L-1,L-2) & \cdots & 0 & 0 \\ \vdots & \vdots & \ddots & \vdots & \vdots \\ 0 & 0 & \cdots & h(N-2,0) & 0 \\ 0 & 0 & \cdots & h(N-1,1) & h(N-1,0) \end{bmatrix} \tag{2.14b}$$

If the channel is time-invariant within one OFDM symbol duration, then the time indices in the expression of the CIR can be omitted, i.e., $\mathbf{h} = [h(0)\ h(1)\ \cdots\ h(L-1)]^T$, and (2.14b) can be simplified as

$$\mathbf{H}=\begin{bmatrix} h(0) & 0 & \cdots & h(2) & h(1) \\ h(1) & h(0) & \cdots & h(3) & h(2) \\ \vdots & \vdots & \ddots & \vdots & \vdots \\ h(L-1) & h(L-2) & \cdots & 0 & 0 \\ \vdots & \vdots & \ddots & \vdots & \vdots \\ 0 & 0 & \cdots & h(0) & 0 \\ 0 & 0 & \cdots & h(1) & h(0) \end{bmatrix} \tag{2.15}$$

At the receiver, after the removal of the CP, the received signal is transformed to $\mathbf{Y} = [Y_0\ \cdots\ Y_{N-1}]^T$ by using the DFT as

$$\mathbf{Y} = \mathbf{Q}^H\mathbf{y} \tag{2.16}$$

where $(\cdot)^H$ represents the Hermitian of $(\cdot)$. From (2.12), (2.14a), and (2.16), $\mathbf{Y}$ can be expressed as

$$\mathbf{Y} = \mathbf{A}\mathbf{X} + \mathbf{N} \tag{2.17a}$$

where

$$\mathbf{A} = \mathbf{Q}^H\mathbf{H}\mathbf{Q} \tag{2.17b}$$

and $\mathbf{N} = [N_0 \ \cdots \ N_{N-1}]^T = \mathbf{Q}^H\mathbf{n}$. Since the DFT matrix $\mathbf{Q}^H$ is unitary, $\mathbf{N}$ in (2.17a) is still white Gaussian noise. The task for now is to recover the transmitted signal $\mathbf{X}$ from the intermediate signal $\mathbf{Y}$. If the assumption in the derivation of (2.15) is valid, then it can be shown that $\mathbf{A}$ is a diagonal matrix with elements $A_{k,k} = H_k = (\mathbf{Qh})_k$ where $(\cdot)_k$ represents the kth element of a vector. In such a case, signal $\mathbf{Y}$ is ICI-free and the relationship in (2.17a) can be rewritten as

$$Y_k = H_k X_k + N_k \quad \text{for } k = 0, \ldots, N-1 \tag{2.18}$$

This relationship is illustrated in Fig. 2.3. It can be observed that the frequency-selective multipath channel is partitioned into N independent AWGN channels. As a consequence, a simple one-tap equalizer can be employed to recover the transmitted signal for each subcarrier [63]. The demodulation process of the OFDM signal is illustrated in Fig. 2.4 where function $\Phi[\cdot]$ represents the hard detection operation based on Eucliean distances between the output of the equalizer and the modulation constellation points.

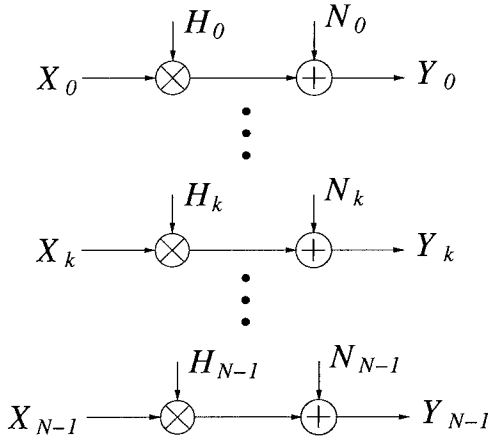

Figure 2.3. *Channel partition in OFDM system.*

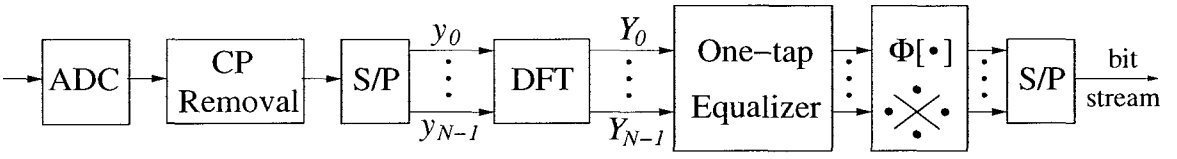

Figure 2.4. *An OFDM receiver.*

2.4 PAPR Reduction in OFDM Systems

A major drawback of OFDM signals is that they have a large envelope fluctuation. The reason behind this phenomenon is simple. Since an OFDM signal consists of a number of independently modulated subcarriers, when the subsymbols for each subcarrier are added up coherently, the maximum instantaneous power of the OFDM signal could be much larger than its average power. Typically, PAPR is used to quantify the envelope excursions of OFDM signals. For the system shown in Fig. 2.2, the PAPR of signal $\mathbf{x}$ is defined as

$$\text{PAPR}_0 = \frac{\|\mathbf{x}\|_\infty^2}{\mathcal{E}[\|\mathbf{x}\|_2^2]/N} \tag{2.19}$$

where $\mathcal{E}[\cdot]$, $\|\mathbf{x}\|_\infty$, and $\|\mathbf{x}\|_2$ denote the expectation of $[\cdot]$, the infinity-norm, and 2-norm of vector $\mathbf{x}$, respectively.

In attempt to investigate the distribution of PAPR of OFDM signals, we consider an OFDM system with N subcarriers where QPSK is adopted as the modulation scheme for each subcarrier, i.e., $X_k \in \{-1, 1, j, -j\}$. From the central limit theorem it follows that for large values of N, the values of the real and imaginary components of the OFDM signal x_n become Gaussian distributed, each with a mean of zero and variance of 0.5. The power distribution of x_n becomes a central chi-square distribution with two degrees of freedom and zero mean, with a cumulative distribution given by

$$\text{F}(\delta) = 1 - e^{-\delta} \tag{2.20}$$

Assuming that the samples are mutually uncorrelated, the probability that the PAPR

is less than some threshold level can be written as

$$\Pr(\text{PAPR} < \delta) = \mathrm{F}^N(\delta) = (1 - e^{-\delta})^N \tag{2.21}$$

For oversampled OFDM signals, however, the assumption made in deriving (2.21) is invalid. In this case, we assume that the distribution of oversampled OFDM signals of N subcarriers can be approximated by the distribution of OFDM signals of αN subcarriers without oversampling. Thus, the cumulative distribution function (CDF) of the PAPR is given by [2]

$$\Pr(\text{PAPR} < \delta) = (1 - e^{-\delta})^{\alpha N} \tag{2.22}$$

In Fig. 2.5, the theoretical CDF of the random variable PAPR is plotted as dashed curves for various values of N where α is set to 4.5 based on empirical experience. The simulated values of CDF are plotted in the same figure as solid curves as a reference. It can be observed that the CDF derived in (2.22) is a close approximation to the real CDF. Furthermore, based on (2.22), it can be shown that: 1) the probability of having a large PAPR increases with the growth of subcarrier number N; 2) large PAPR occurs with a small probability. For example, for the system with $N = 64$ subcarriers, the PAPR of more than 90% of all OFDM symbols is less than 9 dB, i.e., $\Pr(\text{PAPR} \leq 9) \geq 0.9$.

It is known that when signals with a large dynamic range are passed through nonlinear devices, they may suffer from severe nonlinear distortion [64]. The effect of nonlinear PAs on the OFDM signals will now be investigated. For the purpose of simplicity, a soft limiter (SL) model is used to approximate the nonlinearity of a PA, where its input and output signals are denoted as $x = |x|e^{j\phi}$ and $\mathrm{g}(x)$, respectively. The nonlinear characteristic of the SL can be obtained as

$$\mathrm{g}(x) = \begin{cases} x, & |x| \leq A \\ Ae^{j\phi}, & |x| > A \end{cases} \tag{2.23}$$

Since the amount of distortion introduced by the SL depends only on the ratio $A^2 / \{\mathcal{E}[\|\mathbf{x}\|_2^2]/N\}$ where A^2 is the maixmum output power of the SL, we can define

the parameter input back-off (IBO) as

$$\text{IBO} = 10 \log_{10} \left(\frac{A^2}{\mathcal{E}[\|\mathbf{x}\|_2^2]/N} \right) \quad \text{(dB)} \tag{2.24}$$

The power spectral density of the input and output signals of the SL are plotted in Fig. 2.6 for various values of IBO. It can be observed that when the nonlinearity is high, i.e., IBO is small, the in-band distortion and out-of-band radiation are quite severe. For example, the -25 dB bandwidth at IBO = 5 dB is almost twice as wide as that at IBO = 20 dB.

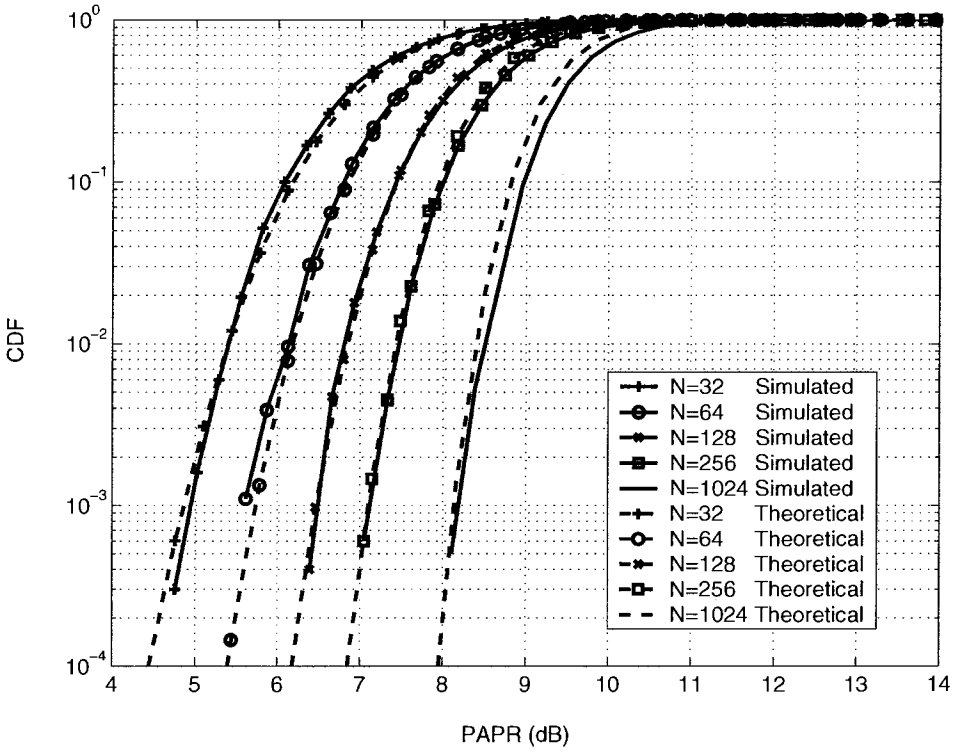

Figure 2.5. *Theoretical and simulated CDFs of the PAPR of OFDM signals.*

It is clear that although the high PAPR of OFDM signals only occurs with a small probability, the distortion caused by passing OFDM signals through a highly nonlinear PA is still quite severe and needs to be suppressed. In an attempt to mitigate nonlinear distortion, linear PAs with a wide dynamic range are required but

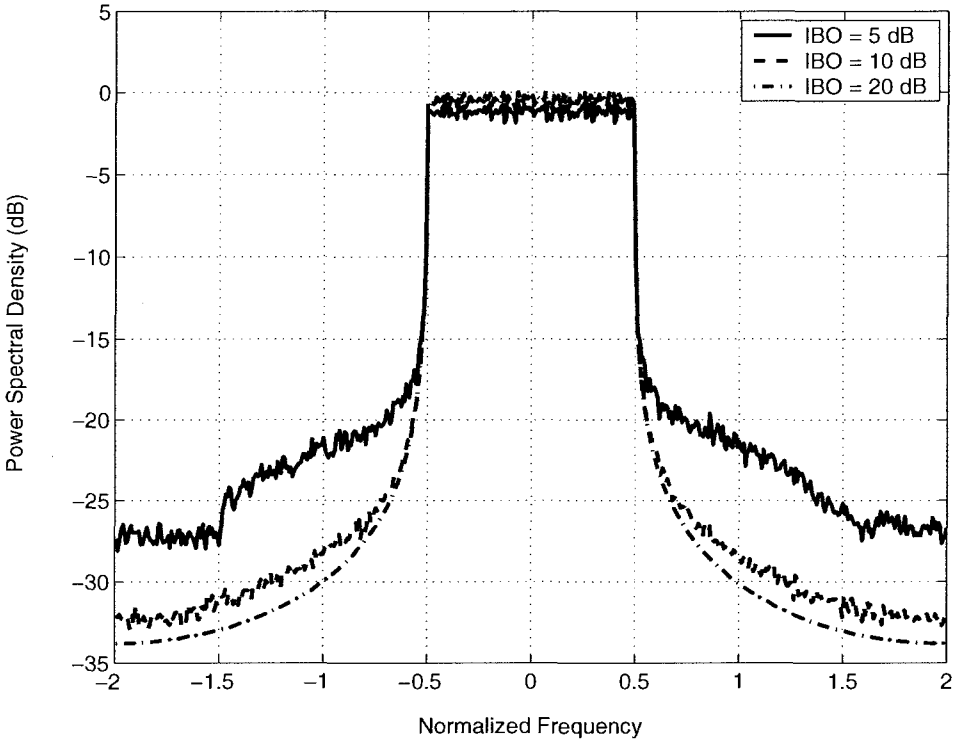

Figure 2.6. *PSD degradation of OFDM signals passed through an SL.*

such PAs are power inefficient. Recently, a number of PAPR-reduction techniques and algorithms have been proposed to reduce the PAPR of the OFDM signal before it enters a PA [29]-[44]. In what follows, we present a brief review of some of these algorithms.

2.4.1 Tone Reservation Algorithm

In [41], OFDM systems with real-valued transmit signals are considered where the input signal to the IDFT processor satisfies the conjugate symmetry conditions [65]. A distortionless algorithm has been proposed for PAPR reduction, referred to as the tone reservation algorithm, where an additive signal is inserted on the unused subcarriers. Analytically, one seeks to find an additive correction vector $\mathbf{c}$ (equivalently, vector $\mathbf{C}$ in the frequency domain) that modifies $\mathbf{x}$ to $\mathbf{x}+\mathbf{c}$ such that the PAPR for the

modified signal, i.e.,

$$\text{PAPR}(\mathbf{c}) = \frac{\|\mathbf{x}+\mathbf{c}\|_\infty^2}{\mathcal{E}[\|\mathbf{x}\|_2^2]/N} \tag{2.25}$$

is minimized without significant BER degradation. The PAPR-reduction problem can be addressed by minimizing the peak power of the modified signal $\mathbf{x}+\mathbf{c}$. It turns out that the increase of average power in the optimally modified signal is fairly moderate and the BER performance degradation due to such signal modification is usually insignificant. For the sake of fair comparisons with other PAPR-reduction algorithms, the peak power of the transmit signal will be used as a performance measure in the computer simulations presented in the following chapters.

In [41], the PAPR-reduction problem is addressed by calculating a real-valued vector $\mathbf{c}$ that solves the optimization problem

$$\underset{\mathbf{c}}{\text{minimize}} \ \|\mathbf{x}+\mathbf{c}\|_\infty = \underset{\mathbf{C}}{\text{minimize}} \ \|\mathbf{x}+\mathbf{QC}\|_\infty \tag{2.26}$$

If there are n_u unused subcarriers whose indices form the set $\mathcal{I}_u$, then the components X_k for $k \in \mathcal{I}_u$ are set to zero and the components C_k are nonzero only if $k \in \mathcal{I}_u$. Therefore, the optimization problem can be formulated as

$$\underset{\mathbf{C}}{\text{minimize}} \ \|\mathbf{x}+\mathbf{QC}\|_\infty \tag{2.30a}$$

$$\text{subject to:} \quad C_k = 0 \text{ for } k \notin \mathcal{I}_u. \tag{2.30b}$$

Given an even N, vector $\mathbf{c}$ is real-valued if the index set has the structure $\mathcal{I}_u = \{j_1, j_2, \ldots, j_{n_u/2}, N-j_{n_u/2}, \ldots, N-j_2, N-j_1\}$ and $\mathbf{C}$ satisfies the conjugate symmetry conditions, i.e., $C_k = C_{N-k}^H$ with C_0 and $C_{N/2}$ real-valued. To simplify the notation, the cases where k is equal to 0 or $N/2$ will be excluded. Let $\hat{\mathbf{Q}} = [\mathbf{q}_1 \ \mathbf{q}_2 \ \cdots \ \mathbf{q}_N]^T$ where $\mathbf{q}_k = [\cos(2\pi j_1 k/N) \ \cdots \ \cos(2\pi j_{n_u/2} k/N) \ -\sin(2\pi j_1 k/N) \ \cdots \ -\sin(2\pi j_{n_u/2} k/N)]^T$ and $\hat{\mathbf{C}} = [C_{rj_1} \ \cdots \ C_{rj_{n_u/2}} \ C_{ij_1} \ \cdots \ C_{ij_{n_u/2}}]^T$ where $C_{rk} = \text{Re}(C_k)$ and $C_{ik} = \text{Im}(C_k)$. It can be shown that $\mathbf{c} = \mathbf{QC} = \hat{\mathbf{Q}}\hat{\mathbf{C}}$. Thus, the problem in (30) can be converted to the problem

$$\underset{\mathbf{C}}{\text{minimize}} \ \|\mathbf{x}+\hat{\mathbf{Q}}\hat{\mathbf{C}}\|_\infty \tag{2.31}$$

where all variables in (2.31) are real-valued. This problem can be easily formulated as a linear programming (LP) problem [41][66].

2.4.2 Active Set Extension Algorithm

In [42], a PAPR reduction algorithm has been proposed, referred to as the active set extension algorithm, whereby the modulation constellation over active subcarriers is modified in such a way as not to degrade the BER performance. It is assumed that all subcarriers are active and the peak-reduction vector $\mathbf{C}$ is generated through a re-assignment of the constellation points as illustrated below. Let us consider a specific case of OFDM with 4-QAM modulation assumed for each subcarrier. As shown in Fig. 2.7, the conventional 4-QAM constellation points are located at the corners of the shaded regions. Each of these regions is a *feasible region* for the reason that if a conventional constellation point is reassigned to a point inside the corresponding shaded region, the minimum Euclidean distance between the newly assigned constellation point and any constellation point located in other feasible regions is guaranteed not to be less than the minimum distance among the conventional constellation points. As demonstrated in [42], the increase in the average transmit power due to the constellation modification is fairly small and, consequently, the BER performance will not be degraded significantly. A constellation point is said to be *feasible* if it is located within the associated feasible region.

Let $\mathbf{X}^{(0)}$ be the original OFDM symbol obtained using 4-QAM modulation of a given data stream. The time-domain vector $\mathbf{x}^{(0)}$ is obtained as the IDFT of $\mathbf{X}^{(0)}$. For the components of $\mathbf{x}^{(0)}$ whose magnitudes exceed a certain target peak level, clipping is used to limit their magnitudes to the target peak level. Denoting the modified time-domain vector as $\mathbf{x}^{(1)}$, we compute the DFT of $\mathbf{x}^{(1)}$ to obtain the OFDM symbol $\mathbf{X}^{(1)}$. Due to clipping, some subsymbols of $\mathbf{X}^{(1)}$ may lie outside their feasible regions. In order to avoid BER degradation, these subsymbols need to be modified. Suppose subsymbol $X_k^{(0)}$ is at corner point 1 as illustrated in Fig. 2.7, which becomes $X_k^{(1)}$ at

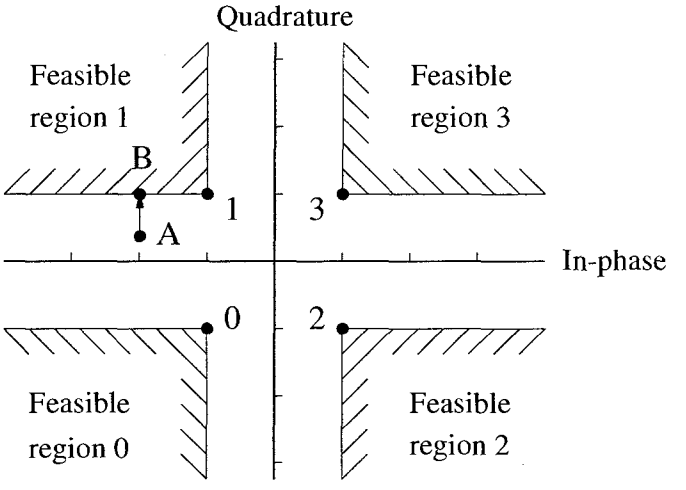

Figure 2.7. *Modification of a 4-QAM constellation point in an active subcarrier.*

point A after the application of IDFT, clipping, and DFT. Denoting the point that is feasible and nearest to point A as B, we modify $X_k^{(1)}$ such that it is represented by point B. If necessary, this IDFT/clipping/DFT/reassignment procedure is repeated for another $K-1$ times until the maximum magnitude of $\mathbf{x}^{(K)}$ is not larger than the target peak value.

2.4.3 Symmetric Constellation Extension Algorithm

In [44], a constellation extension algorithm has been proposed for PAPR reduction, referred to as the symmetric constellation extension algorithm where the subsymbols for each subcarrier are represented by two symmetric constellation points. Consider, for example, an OFDM system where 32-QAM modulation is adopted for each subcarrier and the constellation extension scheme is shown in Fig. 2.8. It can be observed that the constellation is divided into two sets, i.e., the upper and lower sets, and any data point can be represented by either a point from the upper set or a symmetric point from the lower set. Based on this constellation extension scheme, one seeks to reduce the PAPR of transmit signals by selecting the optimal representation of subsymbols by either a point from the upper set or a point from the lower set. It has been shown

that the PAPR-minimization problem is an integer programming problem and a sub-optimal solution can be obtained by using the *method of conditional probabilities* (MCP) [44].

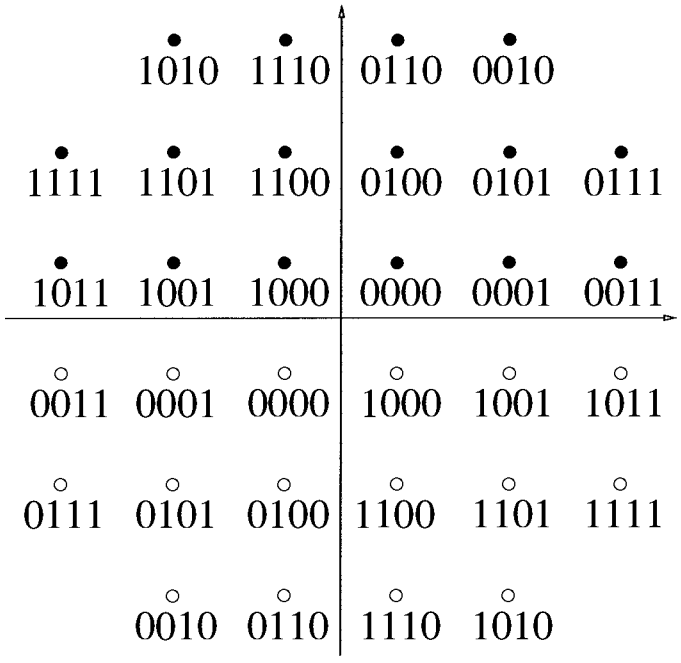

Figure 2.8. *A constellation extension scheme for 32-QAM modulation.*

2.5 ICI Reduction in OFDM Systems

In a fast-fading environment, the assumption of channel stationarity within an OFDM symbol duration may not be valid. In such a case, channel variations destroy the orthogonality in the OFDM subcarrier waveforms and cause ICI at the receiver [19][20]. Mathematically, the output signal of the DFT processor can be obtained by using (2.17) where matrix $\mathbf{A}$ is no longer a diagonal matrix due to channel variations. In particular, the signal for the kth subcarrier can be written as

$$Y_k = A_{k,k}X_k + \sum_{i=0,\ i\neq k}^{N-1} A_{k,i}X_i + N_k \quad \text{for } k = 0, \ldots, N-1 \tag{2.32}$$

where $A_{k,i}$ represents the (k,i)th element of matrix $\mathbf{A}$. It can be seen that for the kth subcarrier the received signal depends not only on the transmitted signal for this particular subcarrier but also on the transmitted signals for other subcarriers. The first and second terms on the right-hand side (r.h.s.) of (2.32) represent the attenuated signal and the ICI for the kth subcarrier, respectively.

To examine the effect of ICI at the receiver, we define the signal-to-intercarrier-interference ratio (SIR) for the kth subcarrier as

$$\mathrm{SIR}_k = \frac{\mathcal{E}\left[|S_k|^2\right]}{\mathcal{E}\left[|I_k|^2\right]} \quad \text{for } k = 0, \ldots, N-1 \tag{2.33a}$$

where

$$S_k = A_{k,k} X_k \quad \text{for } k = 0, \ldots, N-1 \tag{2.33b}$$

and

$$I_k = \sum_{i=0,\ i \neq k}^{N-1} A_{k,i} X_i \quad \text{for } k = 0, \ldots, N-1 \tag{2.33c}$$

Assume that each subsymbol X_k is a zero-mean random variable with variance $\mathrm{Var}(X_k) = E_s$. It has been shown [22] that the signal power for the kth subcarrier can be obtained as

$$\mathcal{E}\left[|S_k|^2\right] = E_s \quad \text{for } k = 0, \ldots, N-1 \tag{2.34a}$$

and, for a sufficient large N, I_k can be approximated by a zero-mean Gaussian random process with variance bounded as follows

$$\mathrm{Var}(I_k) \leq \frac{1}{12}(2\pi f_d T_s)^2 E_s \quad \text{for } k = 0, \ldots, N-1 \tag{2.34b}$$

where f_D and T_s represent the Doppler frequency and symbol duration, respectively. From (2.33) and (2.34), a lower bound of the SIR for the kth subcarrier can be obtained as

$$\mathrm{SIR}_k \geq \frac{12}{(2\pi f_d T_s)^2} \quad \text{for } k = 0, \ldots, N-1 \tag{2.35}$$

For an OFDM system with $N = 64$ subcarriers and a bandwidth equal to 200 kHz, the theoratical lower bound of SIR in (2.35) is plotted in Fig. 2.9 as a dash curve for various Doppler frequency. The actual SIR obtained by simulations is plotted as a solid curve in the same figure for reference, where a two-ray Rayleigh fading channel [46] is assumed. It can be observed that the lower bound in (2.35) is a close approximation of the actual SIR. It follows from (2.35) that the SIR degradation caused by ICI increases significantly when the Doppler frequency increases. For example, the theoratical SIR is 32 dB at a Doppler frequency of 50 Hz, but it reduces to 18 dB at a Doppler frequency of 200 Hz.

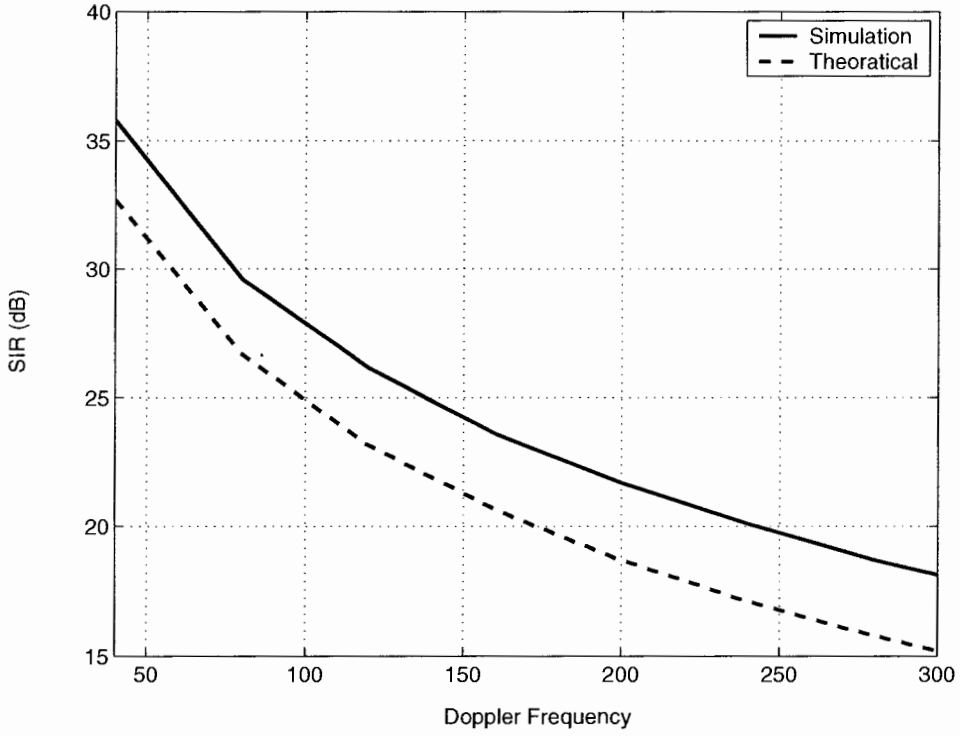

Figure 2.9. *The effect of channel variations on the SIR at receivers.*

Since the received signal for a particular subcarrier is corrupted by ICI which involves the transmitted signals of other subcarriers, the performance of the traditional one-tap equalizer [63] degradates as the Doppler frequency grows. In order to mitigate the effect of the ICI, a joint-detection (JD) algorithm is required at the receiver.

It has been shown in [46] that the performance of OFDM systems can be significantly improved if the signals for all subcarriers are utilized to identify the transmitted information bits. This can be done by inserting immediately after the DFT a processor that implements a JD algorithm. A general structure for the OFDM receiver that implements a JD algorithm is illustrated in Fig. 2.10.

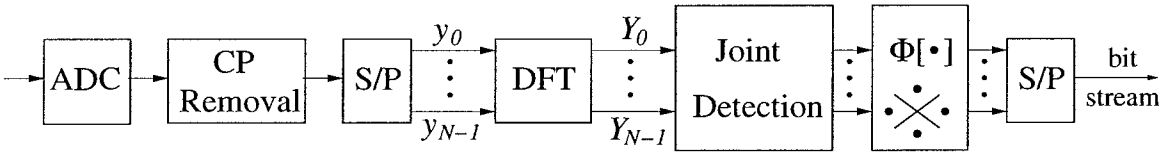

Figure 2.10. *An OFDM receiver that implements a joint-detection algorithm.*

In what follows, we examine several linear and nonlinear detection algorithms. This will help establish the necessary background for JD and offer a basis on which several new JD algorithms can be developed.

2.5.1 Maximum Likelihood Joint Detection

ML detection involves maximizing the *joint a posteriori probability* by selecting the information-bearing waveform that is closest to the observed waveform in terms of Euclidean distance [67]. For the signal detection problem in (2.17), ML detection can be carried out by solving the optimization problem

$$\text{minimize} \quad \|\mathbf{Y} - \mathbf{AX}\|_2^2 \tag{2.36a}$$

$$\text{subject to} : X_k \in \mathcal{M} \quad \text{for } k = 0, 1, \ldots, N-1 \tag{2.36b}$$

where $\mathcal{M}$ is the set of the constellation points associated with the modulation scheme of the OFDM system. The problem in (2.36) is a combinatorial optimization problem whose solution requires computational complexity that grows exponentially with the number of variables. In addition, in OFDM systems over frequency-selective fading channels, complete information on the CIR is required for ML detection.

In attempts to reduce the computational complexity required by ML detection, several linear and nonlinear JD algorithms have been proposed [46]. In the following, the MMSE detection and the DF detection algorithms proposed in [46] are briefly reviewed.

2.5.2 Linear MMSE Detection Algorithm

In [46], an MMSE algorithm has been proposed for ICI reduction, which is referred to as the linear MMSE detection algorithm. In this algorithm, a linear transformation is applied between the outputs of the DFT processor and the decision making devices, where the coefficients of the transformation are determined by minimizing the minimum-square-error (MSE) between the known binary information bits and the transformed outputs, i.e.,

$$\text{minimize} \quad \mathcal{E}\left[\|\mathbf{X} - \mathbf{W}^H\mathbf{Y}\|_2^2\right] \tag{2.37}$$

The closed-form solution of this problem is given by

$$\mathbf{W} = \left(E_s\mathbf{A}\mathbf{A}^H + \sigma^2 \cdot \mathbf{I}\right)^{-1}\mathbf{A} \tag{2.38}$$

Hence, the information bits can be determined as

$$\hat{\mathbf{X}} = \Phi\left[\mathbf{A}^H\left(E_s\mathbf{A}\mathbf{A}^H + \sigma^2 \cdot \mathbf{I}\right)^{-1}\mathbf{Y}\right] \tag{2.39}$$

It can be shown that the kth column of $\mathbf{W}$ is the solution of the following minimization problem

$$\text{minimize} \quad \mathcal{E}\left[\|X_k - \mathbf{W}_k^H\mathbf{Y}\|_2^2\right] \tag{2.40}$$

Therefore, the MMSE detection described above can be implemented in a decentralized form to reduce the complexity in case that multiple users share the frequency spectrum of the OFDM system, i.e., orthogonal frequency-division multiple access (OFDMA) system [68].

In [46], it has been shown that the ICI for a particular subcarrier is mainly contributed by its neighbouring subcarriers. Based on this observation, the detection process can be further simplified. Suppose that subsymbol X_k is to be detected. Let $K = 2M + 1$ where M is a positive integer, and define a $K \times 1$ vector $\mathcal{I}_k$ with the ith element $\mathcal{I}_k(i) = [k - M - 1 + i]_N + 1$ where $[\cdot]_N$ represents the modulus N operation. Let $\mathbf{Y}_k = \mathbf{Y}(\mathcal{I}_k)$, $\mathbf{A}_k = \mathbf{A}(:, \mathcal{I}_k)$, and $\mathbf{N}_k = \mathbf{N}(\mathcal{I}_k)$. From (2.17), we have

$$\mathbf{Y}_k = \mathbf{A}_k \mathbf{X} + \mathbf{N}_k \quad \text{for } k = 0, \ldots, N-1 \tag{2.41}$$

The linear transmformation for detection X_k can be obtained by solving the optimization problem

$$\text{minimize} \quad \mathcal{E}\left[\|X_k - \mathbf{W}_k^H \mathbf{Y}_k\|_2^2\right] \quad \text{for } k = 0, \ldots, N-1 \tag{2.42}$$

The closed-form solution of (2.42) can be found as

$$\mathbf{W}_k = \left(E_s \mathbf{A}_k \mathbf{A}_k^H + \sigma^2 \cdot \mathbf{I}\right)^{-1} \mathbf{A}_k \quad \text{for } k = 0, \ldots, N-1 \tag{2.43}$$

and the information bits can be determined as

$$\hat{X}_k = \Phi\left[\mathbf{A}_k^H \left(E_s \mathbf{A}_k \mathbf{A}_k^H + \sigma^2 \cdot \mathbf{I}\right)^{-1} \mathbf{Y}_k\right] \quad \text{for } k = 0, \ldots, N-1 \tag{2.44}$$

It can be shown that if M is selected properly, there is no significant performance degradation between the solution in (2.44) with respect to that in (2.39).

2.5.3 Decison-Feedback Detection Algorithm

In [46], the DF detection algorithm has been proposed based on the MMSE detection algorithm reviewed above. The detection order of all subsymbols is determined in such a way that first the subsymbol with the largest energy at the receiver is found and then the detection order for other subsymbols is arranged either in a forward way or a backward way. For example, assume that subsymbol X_l has the largest energy at the receiver, then the detection order can be arranged in a forward way

as $\mathcal{I}_d = \{l, \ldots, N-1, 0, \ldots, l-1\}$. Based on the established detection order, the detection of all subsymbols can be implemented successively. For the detection of subsymbol $X_{\mathcal{I}_d(1)}$, it can be achieved directly by using the MMSE detection characterized in (2.44) where the signal model in (2.41) is applied. For the detection of other subsymbols, first the signal vectors of the previous detected subsymbols are reconstructed and substracted from the received signal vectors, and then the detection algorithm described in Sec. (2.5.2) can be applied based on the updated signal model. For example, if we let $\hat{X}_m$ be the detected subsymbol of X_m, we have $\tilde{\mathbf{Y}}_k = \mathbf{Y}_k - \sum_{i=1}^{n_k} \mathbf{A}_k(:, \mathcal{I}_d(i)+1)\hat{X}_{\mathcal{I}_d(i)}$ where $k = \mathcal{I}_d(1), \mathcal{I}_d(2), \ldots, \mathcal{I}_d(N), n_k = k-m$ for $k > m$ or $n_k = N+k-m$ for $k < m$. Assuming that all previous subsymbols have been detected correctly, i.e., $\hat{X}_m = X_m$, then the signal model for the detection of X_k can be found as $\tilde{\mathbf{Y}}_k = \tilde{\mathbf{A}}_k\tilde{\mathbf{X}}_k + \tilde{\mathbf{w}}_k$ where $\tilde{\mathbf{A}}_k = \mathbf{A}_k(:, \mathcal{I}_d(n_k+1:N)+1)$, $\tilde{\mathbf{X}}_k = \mathbf{X}(\mathcal{I}_d(n_k+1:N)+1)$, and $\tilde{\mathbf{w}}_k = \mathbf{w}(\mathcal{I}_d(n_k+1:N)+1)$. The subsymbol $\hat{X}_k$ can be obtained by using the MMSE detection algorithm. It has been shown that an improved performance can be achieved by using this DF detection algorithm with respect to the MMSE detection algorithm in Sec. (2.5.2) at the cost of a slight increase of computational complexity.

Chapter 3

PAPR Reduction via Continous Constellation Extension

3.1 Introduction

In this chapter, new PAPR-reduction algorithms are developed for OFDM systems with real and complex signals. For the case of OFDM systems with real signals, the PAPR-reduction problem is formulated as an LP problem and its solution is obtained by using a new Newton algorithm [48]. Computer simulations show that the proposed LP-based algorithm yields optimal PAPR-reduction solutions and considerable performance improvement can be achieved relative to that achieved by using the tone reservation algorithm [41] and the ASE algorithm [42]. For the case of OFDM systems with complex signals, the PAPR-reduction problem is formulated as an unconstrained minimax optimization problem and its solution is obtained by using an accelerated *least-pth* algorithm [49]. Computer simulations show that the proposed *least-pth* algorithm outperforms the ASE algorithm [42] and that improved PAPR reduction can be obtained when the *least-pth* algorithm is combined with the SLM algorithm [38].

The chapter is organized as follows. The proposed LP-based and *least-pth* algorithms are developed in Sec. 3.2 and Sec. 3.3, respectively. The simulation results are then presented in Sec. 3.4. Conclusions are drawn in Sec. 3.5.

3.2 PAPR Reduction in OFDM Systems with Real Signals

3.2.1 System Configuration

We consider an N-subcarrier OFDM system with real signals and assume that the system has a certain number of unused subcarriers. A modulation scheme that can be either 4-QAM or 16-QAM [41][66] is assumed for active subcarriers. The number and index set of unused subcarriers are denoted as n_u and $\mathcal{I}_u = \{j_1, j_2, \ldots, j_{n_u/2}, N - j_{n_u/2}, \ldots, N-j_2, N-j_1\}$, respectively. The number and index set of active subcarriers that are chosen for PAPR reduction are denoted as n_a and $\mathcal{I}_a = \{l_1, l_2, \ldots, l_{n_a/2}, N - l_{n_a/2}, \ldots, N - l_2, N - l_1\}$, respectively. The index numbers are arranged such that $j_1 < j_2 < \cdots < j_{n_u/2} < N/2$ and $l_1 < l_2 < \cdots < l_{n_a/2} < N/2$ and sets $\mathcal{I}_u$ and $\mathcal{I}_a$ do not intersect. In the development of suitable algorithms for PAPR reduction, the concept of feasible region will be frequently used and it needs to be clarified. For 4-QAM modulation, the feasible region was defined in Sec. 2.4.2 and is illustrated in Fig. 2.7. For 16-QAM modulation, the feasible regions are shown in Fig. 3.1. As can be seen, for each of the interior constellation points (i.e., points 5, 7, 13, 15), the feasible region is reduced to the point itself, meaning that the interior constellation point is not allowed to change. For each of the exterior constellation points that are located at the corners (i.e., points 0, 2, 8, 10), the feasible region is the corresponding shaded region. For each of the non-corner exterior constellation points (i.e., points 1, 3, 4, 6, 9, 11, 12, 14), the feasible region is a line which starts at the constellation point and extends to infinity.

3.2.2 Algorithm

Based on the definition of PAPR in (2.19), our objective is to obtain a conjugate symmetric vector $\mathbf{C}$ such that the PAPR of the OFDM symbol $\boldsymbol{X} + \boldsymbol{C}$ is minimized,

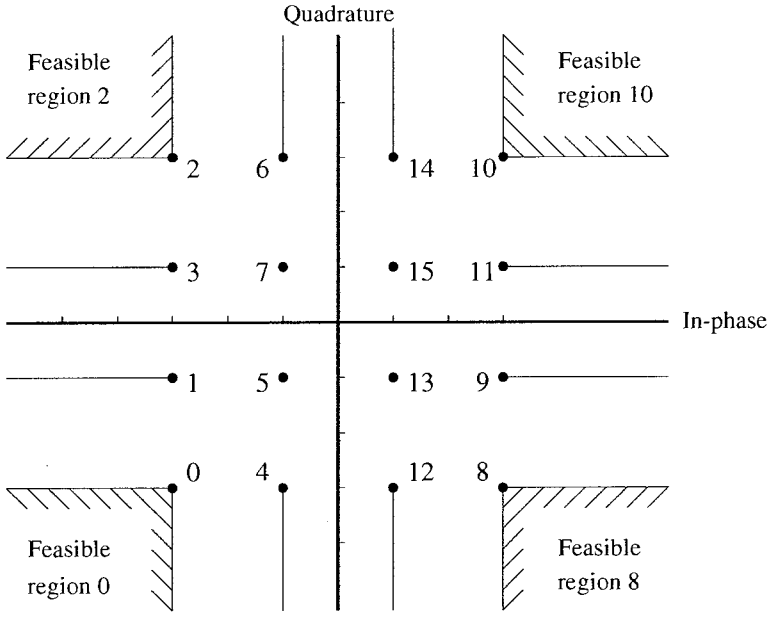

Figure 3.1. *Feasible region for 16-QAM constellation points.*

where vector $\mathbf{C}$ has non-zero values in the selected subcarriers whose indices are in either set $\mathcal{I}_u$ or $\mathcal{I}_a$ and the modified subsymbols in the active subcarriers remain feasible. The PAPR-reduction problem can be addressed by minimizing the peak power of the transmit signal $\mathbf{x} + \mathbf{QC}$. It turns out that the increase of average power in the transmit signal by constellation extension is fairly moderate and the BER performance degradation due to such constellation extension is usually insignificant. The PAPR-reduction problem is a constrained optimization problem that can be formulated as

$$\underset{\mathbf{C}}{\text{minimize}} \ \|\mathbf{x} + \mathbf{QC}\|_\infty \tag{3.1a}$$

$$\text{subject to:} \quad X_k + C_k \text{ be feasible for } k \in \mathcal{I}_a \tag{3.1b}$$

$$C_k = 0 \text{ for } k \notin \mathcal{I}_u \text{ and } k \notin \mathcal{I}_a \tag{3.1c}$$

By allowing point $X_k + C_k$ ($k \in \mathcal{I}_a$) to move within the feasible region, a solution of (3.1) can be obtained which is expected to outperform that of the optimization problem in (2.30).

Let $\tilde{\mathbf{Q}} = [\mathbf{q}_1\ \mathbf{q}_2\ \cdots\ \mathbf{q}_N]^T$ where $\mathbf{q}_k = [\cos(2\pi j_1 k/N)\ \cdots\ \cos(2\pi j_{n_u/2} k/N)\ \cos(2\pi l_1 k/N)\ \cdots\ \cos(2\pi l_{n_a/2} k/N)\ -\sin(2\pi j_1 k/N)\ \cdots\ -\sin(2\pi j_{n_u/2} k/N)\ -\sin(2\pi l_1 k/N)\ \cdots\ -\sin(2\pi j_{n_a/2} k/N)]^T$ and $\tilde{\mathbf{C}} = [C_{rj_1}\ \cdots\ C_{rj_{n_u/2}}\ C_{rl_1}\ \cdots\ C_{rl_{n_u/2}}\ C_{ij_1}\ \cdots\ C_{ij_{n_u/2}}\ C_{il_1}\ \cdots\ C_{il_{n_u/2}}]^T$. It can be verified that $\mathbf{QC} = \tilde{\mathbf{Q}}\tilde{\mathbf{C}}$ where $\tilde{\mathbf{Q}}$ and $\tilde{\mathbf{C}}$ are real-valued and the problem in (3.1) can be converted to

$$\underset{\tilde{\mathbf{C}}}{\text{minimize}}\ \|\mathbf{x} + \tilde{\mathbf{Q}}\tilde{\mathbf{C}}\|_\infty \tag{3.2a}$$

$$\text{subject to: } X_k + C_k \text{ be feasible for } k \in \mathcal{I}_a \tag{3.2b}$$

By including an upper bound τ for the objective function in (3.2a) as an additional design variable, the constrainted optimization problem in (3.2) can be formulated as

$$\text{minimize}\quad \tau \tag{3.3a}$$

$$\text{subject to:}\quad \left|x_k + (\tilde{\mathbf{Q}}\tilde{\mathbf{C}})_k\right| \le \tau \tag{3.3b}$$

$$X_k + C_k \text{ be feasible for } k \in \mathcal{I}_a \tag{3.3c}$$

where $(\tilde{\mathbf{Q}}\tilde{\mathbf{C}})_k$ denotes the kth element of $\tilde{\mathbf{Q}}\tilde{\mathbf{C}}$. The constraints in (3.3b) can be expressed in matrix form as

$$\begin{bmatrix} \tilde{\mathbf{Q}} & \mathbf{e} \\ -\tilde{\mathbf{Q}} & \mathbf{e} \end{bmatrix} \begin{bmatrix} \tilde{\mathbf{C}} \\ \tau \end{bmatrix} \ge \begin{bmatrix} -\mathbf{x} \\ \mathbf{x} \end{bmatrix} \tag{3.4}$$

where $\mathbf{e} = [1\ 1\ \cdots\ 1]^T \in \mathcal{R}^{N\times 1}$, and the optimization problem in (3.3) becomes

$$\text{minimize}\quad \tau \tag{3.5a}$$

$$\text{subject to}: \begin{bmatrix} \tilde{\mathbf{Q}} & \mathbf{e} \\ -\tilde{\mathbf{Q}} & \mathbf{e} \end{bmatrix} \begin{bmatrix} \tilde{\mathbf{C}} \\ \tau \end{bmatrix} \ge \begin{bmatrix} -\mathbf{x} \\ \mathbf{x} \end{bmatrix} \tag{3.5b}$$

$$X_k + C_k \text{ be feasible for } k \in \mathcal{I}_a \tag{3.5c}$$

In what follows, we convert the problem in (3.5) into explicit LP problems for different modulation schemes.

3.2.2.1 4-QAM Modulation Case

For 4-QAM modulation, all constellation points are exterior points and each is associated with a large feasible region, as shown in Fig. 3.7. By defining vectors $\mathbf{d} = [0 \cdots 0\ 1]^T \in \mathcal{R}^{n_u+n_a+1}$ and $\mathbf{y} = [\tilde{\mathbf{C}}\ \tau]^T$, the objective function in (3.5a) becomes $\mathbf{d}^T\mathbf{y}$ and the constraints in (3.5b) assume the form

$$\begin{bmatrix} \tilde{\mathbf{Q}} & \mathbf{e} \\ -\tilde{\mathbf{Q}} & \mathbf{e} \end{bmatrix} \mathbf{y} \geq \begin{bmatrix} -\mathbf{x} \\ \mathbf{x} \end{bmatrix} \tag{3.6}$$

If we denote $\tilde{\mathbf{X}}$ as a subvector of $\mathbf{X}$ composed of the elements with indices in $\mathcal{I}_u$ or $\mathcal{I}_a$, then the constraints in (3.5c) can be expressed as

$$S_{rk}C_{rk} \geq 0 \quad \text{for } k \in \mathcal{I}_a \text{ and } k < N/2 \tag{3.7a}$$

$$S_{ik}C_{ik} \geq 0 \quad \text{for } k \in \mathcal{I}_a \text{ and } k < N/2 \tag{3.7b}$$

where $S_{rk} = \text{sgn}[\text{real}(X_k)]$ and $S_{ik} = \text{sgn}[\text{imag}(X_k)]$. The constraints in (3.7) can be put together in matrix form as

$$\begin{bmatrix} \mathbf{S}_r & \mathbf{0} & \mathbf{0} \\ \mathbf{0} & \mathbf{S}_i & \mathbf{0} \end{bmatrix} \mathbf{y} \geq \begin{bmatrix} \mathbf{0} \\ \mathbf{0} \end{bmatrix} \tag{3.8}$$

where $\mathbf{S}_r$ and $\mathbf{S}_i$ are $(n_a/2) \times (N/2)$ matrices that can be generated by replacing the $(k, i_k)th$ component of the zero entry of each matrix by S_{rk} and S_{ik}, respectively, for $k = 1, 2, \ldots, n_u/2$. Furthermore, the linear constraints in (3.6) and (3.8) can be combined and the optimization problem in (3.5) can be formulated as

$$\text{minimize } \mathbf{d}^T\mathbf{y} \tag{3.9a}$$

$$\text{subject to: } \mathbf{A}\mathbf{y} \geq \mathbf{b} \tag{3.9b}$$

with

$$\mathbf{A} = \begin{bmatrix} \tilde{\mathbf{Q}} & & \mathbf{e} \\ -\tilde{\mathbf{Q}} & & \mathbf{e} \\ \mathbf{S}_r & \mathbf{0} & \mathbf{0} \\ \mathbf{0} & \mathbf{S}_i & \mathbf{0} \end{bmatrix}, \quad \mathbf{b} = \begin{bmatrix} -\mathbf{x} \\ \mathbf{x} \\ \mathbf{0} \\ \mathbf{0} \end{bmatrix} \tag{3.9c}$$

The problem in (3.9) is an LP problem with $n_a + n_u + 1$ variables and $2N + n_a$ constraints. Since N > n_u, the number of constraints in (3.9) is always greater than the number of design variables. This LP problem can be solved using a recently proposed Newton method [48] which is more efficient than the standard methods for LP problems, especially when the number of constraints is considerably greater than the number of design variables.

3.2.2.2 Other Modulation Cases

In the 16-QAM modulation case, the feasible region for each constellation point is illustrated in Fig. 3.1. For each selected active subcarrier k ($k \in \mathcal{I}_a$), if the modulated subsymbol X_k belongs to index set $\mathcal{G}_0 = \{5,\ 7,\ 13,\ 15\}$, then the corresponding C_k is set to zero; if X_k belongs to $\mathcal{G}_2 = \{0,\ 2,\ 8,\ 10\}$, then C_k is constrained exactly in the same way as in the QPSK case; if X_k belongs to $\mathcal{G}_1 = \{1,\ 3,\ 9,\ 11\}$ or $\mathcal{G}_{12} = \{4,\ 6,\ 12,\ 14\}$, then the *imaginary* or *real* component of C_k is set to zero, as appropriate. Under these circumstances, it can be verified that the optimization problem at hand can be formulated as an LP problem of the form in (3.9).

For other modulation schemes such as K-QAM with K > 16, feasible regions similiar to that in Fig. 3.1 can be defined and with straightforward modification of the data set $\{\mathbf{A}, \mathbf{y}, \mathbf{b}\}$, the corresponding PAPR-reduction problem can be formulated as a standard LP problem. In practical applications, channel coding might be required to improve system performance, e.g., a standard binary code is combined with QAM modulation [2][69]. In such applications, a soft decision decoding scheme can be combined with the proposed algorithm to obtain the transmitted information. We conclude this section with two remarks.

1. In the proposed LP-based algorithm, the number of active subcarriers involved in the optimization can vary. Therefore, the algorithm offers a tradeoff between computational complexity and performance.
2. For the sake of simplicity, only the Nyquist sampling rate has been considered

in the derivation of the above algorithm. However, with straightforward modifications, the algorithm can be extended to systems where the time-domain signals are oversampled.

3.3 PAPR Reduction in OFDM Systems with Complex Signals

3.3.1 System Configuration

We consider an N-subcarrier OFDM system with complex signals and assume that there are no unused subcarriers in the system. A modulation scheme that can be either 4-QAM or 16-QAM [41][66] is assumed for all subcarriers [41][66]. The number and index set of active subcarriers that are chosen for PAPR reduction are denoted as n_a and $\mathcal{I}_a = \{j_1, j_2, \ldots, j_{n_a}\}$, respectively.

3.3.2 Algorithm

For OFDM systems with complex signals, the peak-reduction vector $\mathbf{C}$ is modified in selected active subcarriers so as to minimize $\|\mathbf{x} + \mathbf{QC}\|_\infty$ subject to the modified subsymbols in the active subcarriers remaining feasible. Denote $\tilde{\mathbf{C}}$ as the subvector of $\mathbf{C}$ composed of the elements with indices in $\mathcal{I}_a$ and $\tilde{\mathbf{Q}}$ as the submatrix of $\mathbf{Q}$ composed of columns with indices in $\mathcal{I}_a$. The problem can be formulated as

$$\underset{\tilde{\mathbf{C}}}{\text{minimize}} \quad \|\mathbf{x} + \tilde{\mathbf{Q}}\tilde{\mathbf{C}}\|_\infty \tag{3.10a}$$

$$\text{subject to :} \quad X_k + C_k \text{ be feasible for } k \in \mathcal{I}_a \tag{3.10b}$$

If we denote the kth row of $\tilde{\mathbf{Q}}$ as $\tilde{\mathbf{q}}_k^T$ and the kth component of $\mathbf{x}$ as x_k, then the objective function in (3.10a) is the infinity norm of an N-dimensional vector whose kth component is $x_k + \tilde{\mathbf{q}}_k^T\tilde{\mathbf{C}}$, and the problem in (3.10) can be formulated as the

minimax problem

$$\underset{\tilde{\mathbf{C}}}{\text{minimize}} \quad \max_{1 \le k \le N} \|x_k + \tilde{\mathbf{q}}_k^T \tilde{\mathbf{C}}\| \tag{3.11a}$$

$$\text{subject to:} \quad X_k + C_k \text{ be feasible} \quad \text{for } k \in \mathcal{I}_a \tag{3.11b}$$

Note that in general x_k and vectors $\tilde{\mathbf{q}}_k^T$ and $\tilde{\mathbf{C}}$ are complex-valued. If we let $x_k = x_{r,k} + jx_{i,k}$, $\tilde{\mathbf{q}}_k = \tilde{\mathbf{q}}_{r,k} + j\tilde{\mathbf{q}}_{i,k}$, and $\tilde{\mathbf{C}} = \tilde{\mathbf{C}}_r + j\tilde{\mathbf{C}}_i$, then the norm in (3.11a) assumes the form

$$\|\hat{\mathbf{x}}_k + \mathbf{P}_k \hat{\mathbf{C}}\| \tag{3.12a}$$

where

$$\hat{\mathbf{x}}_k = \begin{bmatrix} x_{r,k} \\ x_{i,k} \end{bmatrix}, \quad \mathbf{P}_k = \begin{bmatrix} \tilde{\mathbf{q}}_{r,k}^T & -\tilde{\mathbf{q}}_{i,k}^T \\ \tilde{\mathbf{q}}_{i,k}^T & \tilde{\mathbf{q}}_{r,k}^T \end{bmatrix}, \quad \hat{\mathbf{C}} = \begin{bmatrix} \tilde{\mathbf{C}}_r \\ \tilde{\mathbf{C}}_i \end{bmatrix} \tag{3.12b}$$

and the problem in (3.11) can be expressed as

$$\underset{\tilde{\mathbf{C}}}{\text{minimize}} \quad \max_{1 \le k \le N} \|\hat{\mathbf{x}}_k + \mathbf{P}_k \hat{\mathbf{C}}\| \tag{3.13a}$$

$$\text{subject to:} \quad X_k + C_k \text{ be feasible} \quad \text{for } k \in \mathcal{I}_a \tag{3.13b}$$

In what follows, we show that for several important modulation schemes, the problem in (3.13) can be converted to an unconstrained optimization problem.

3.3.2.1 4-QAM Modulation Case

As in Sec. 3.2, the constraints in (3.12b) can be formulated as the inequalities in (3.8). Essentially, these constraints require that the signs of C_{rk} and C_{ik} be identical to those of S_{rk} and S_{ik}, respectively. If we define a sign vector $\mathbf{s}$ as

$$\mathbf{s} = \begin{bmatrix} s_1 & \cdots & s_{n_a} & s_{n_a+1} & \cdots & s_{2n_a} \end{bmatrix}^T = \begin{bmatrix} S_{r1} & \cdots & S_{rn_a} & S_{i1} & \cdots & S_{in_a} \end{bmatrix}^T \tag{3.14}$$

then the constraints in (3.13b) can be eliminated by assuming vector $\hat{\mathbf{C}}$ to be of the form

$$\hat{\mathbf{C}} = \begin{bmatrix} s_1 y_1^2 & \cdots & s_{n_a} y_{n_a}^2 & s_{n_a+1} y_{n_a+1}^2 & \cdots & s_{2n_a} y_{2n_a}^2 \end{bmatrix}^T \tag{3.15}$$

where y_i is the ith component of an unconstrained parameter vector $\mathbf{y} = [y_1 \ \cdots \ y_{2n_a}]^T$, and the problem in (3.15) is converted to

$$\underset{\mathbf{y}}{\text{minimize}} \quad \max_{1 \le k \le N} \|\hat{\mathbf{x}}_k + \hat{\mathbf{P}}_k \mathbf{y}^2\| \tag{3.16}$$

where $\hat{\mathbf{P}}_k$ is obtained by multiplying each column of $\mathbf{P}_k$ by the corresponding component of vector $\mathbf{s}$, and $\mathbf{y}^2$ denotes the vector obtained by squaring the components of vector $\mathbf{y}$. Efficient optimization algorithms are available in the literature that can be used to solve the minimax problem in (3.16), see, for example, [49], where an accelerated *least-pth* approach is proposed for minimax optimization.

3.3.2.2 Other Modulation Cases

As may be expected, other modulation schemes such as 16-QAM can also be handled in a way similar to that in Sec. 3.2.2.2. With appropriate modifications to the sign vector, the corresponding PAPR problem can be formulated as an unconstrained minimax optimization problem. The following remarks can be made at this point.

1. The proposed *least-pth* algorithm does not require transmission of any side information.
2. If a small amount of side information is available, the SLM algorithm in [38] is a promising technique since it provides a considerable PAPR reduction without explicit side information. In such a system, the proposed *least-pth* algorithm can be smoothly integrated with the SLM algorithm to achieve more PAPR reduction without any difficulties.

3.4 Simulations

The proposed PAPR-reduction algorithms were applied to several OFDM systems and the performance achieved was evaluated and compared with that of the algorithms

proposed in [41][42] for the OFDM systems with real signals and that of the algorithms proposed in [38][42] for the OFDM systems with complex signals.

In our simulations, 4-QAM modulation was assumed in all active subcarriers. The OFDM signal was oversampled by a factor of 2 using zero padding in the frequency domain before the application of the PAPR-reduction algorithms. In order to approximate the analog signal accurately [70], the sampling rate was increased to 8 times the Nyquist rate by a root-raised cosine (RRC) filter with a rolloff factor of 0.12. The output signal of the RRC filter, $s(t)$, was measured to evaluate the PAPR-reduction performance. The configuration of the OFDM transmitter under consideration is shown in Fig. 3.2.

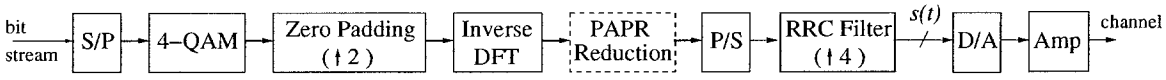

Figure 3.2. *Implementation of an OFDM transmitter for PAPR reduction.*

A commonly used performance measure for PAPR-reduction algorithms is the clipping probability which is defined as the probability that the peak power of the OFDM signal exceeds a given power threshold s_0^2, i.e., $Pr\{\max[s^2(t)] > s_0^2\}$. The abscissa was normalized with respect to the average power of the OFDM signal before PAPR reduction, denoted by δ_0^2, and is given in decibels.

3.4.1 OFDM Systems with Real Signals

The OFDM system in our simulations had $N = 512$ subcarriers where $n_u = 16$ subcarriers (about 3% of the total subcarriers) in the highest frequency range were unused.

Example 1: The LP-based algorithm proposed in Sec. 3.3.2.2 was applied to reduce the peak power of the transmit signal. Various values of n_a were used to obtain the peak-reduction vector $\mathbf{C}^*$, and the clipping probability versus various power threshold values associated with vector $\mathbf{C}^*$ is plotted as the solid curves in Fig. 3.3. For the sake

of comparison, the clipping probability obtained using the tone reservation algorithm [41] and for the original OFDM signal is also plotted in the same figure as dashed and dot-dashed curves, respectively. It is evident that, after a small number of iterations, the proposed LP-based algorithm resulted in significant performance improvement over that of the tone reservation algorithm. For example, for a clipping probability of 10^{-3}, the LP-based algorithm with $n_a = 240$ offers a 0.88-dB improvement over the tone reservation algorithm after 8 iterations.

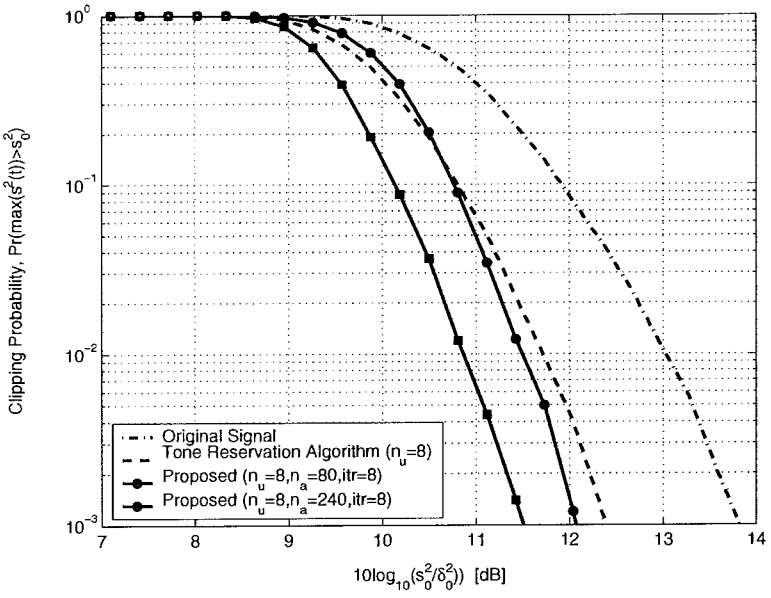

Figure 3.3. *Performance comparison of the proposed LP-based and the tone reservation algorithms.*

The clipping probability obtained using the proposed LP-based algorithm was also compared with that obtained using the ASE algorithm [42] for various numbers of iterations, i.e., $itr = 5$, 10, and 100 and the target PAPR was set to be 9 dB. The results obtained are plotted in Fig. 3.4. For the sake of comparison, the clipping probability for the original OFDM signals is also plotted as the dot-dashed curve. It can be observed that although the ASE algorithm is capable of reducing the peak power in a small number of iterations, better performance can be achieved using the

proposed LP-based algorithm. For example, for a clipping probability of 10^{-3}, the proposed LP-based algorithm with $n_a = 240$ offers a 0.57-dB improvement over the ASE algorithm with $itr = 10$.

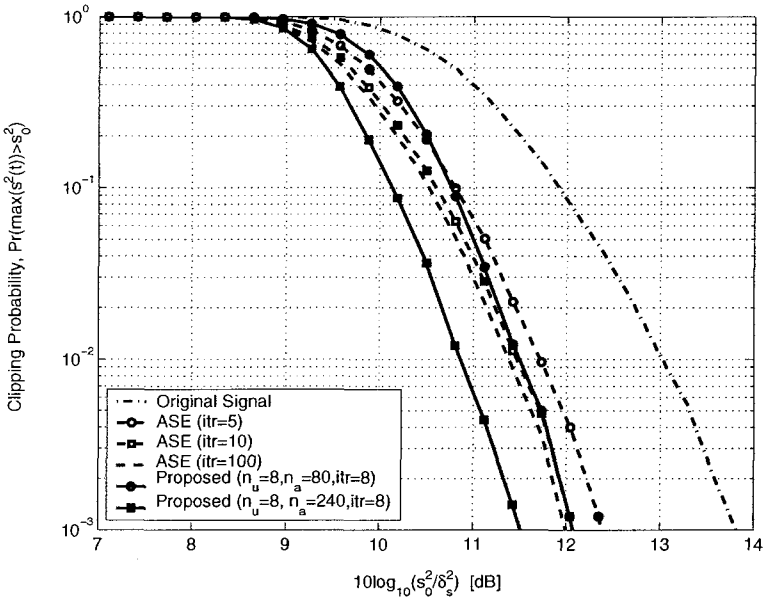

Figure 3.4. *Performance comparison of the proposed LP-based and the ASE algorithms.*

The performance difference can be illustrated more explicitly using constellation-point patterns in the frequency domain as described below. The proposed LP-based algorithm with $n_a = 240$, $itr = 8$ and the ASE algorithm with $itr = 100$ were applied to an arbitrarily chosen OFDM symbol $\mathbf{X}$ to obtain the corresponding peak-reduction vectors $\mathbf{C}^*$ and $\bar{\mathbf{C}}^*$, respectively. The 120 constellation points obtained using the proposed LP-based algorithm in active subcarriers with index $j \leq N/2$ and 8 constellation points in unused subcarriers with index $j \leq N/2$ are shown in Figs. 3.5a and b, respectively; the corresponding results obtained using the ASE algorithm are shown in Figs. 3.5c and d, respectively. It is observed that the distributions of the optimal constellation points are very different from those obtained with the ASE algorithm. Note that since an optimal solution of a constrained optimization

problem is usually on the boundary of its feasible region, most of the constellation points obtained by the proposed algorithm are located on or are very close to the lines that define the feasible regions as shown in Figs. 3.5a and c. Also note that, as a result of superposition of the peak-reduction signal and the original signal, the signal power for this OFDM symbol increases. For the system considered in our simulation, the average power increase was 0.368 and 0.624 dB, respectively, for $n_a = 80$ and 240. Considering the significant PAPR reduction achieved, the small BER degradation caused by the power increase appears to be acceptable.

It is of interest to compare the computational complexity of the proposed LP-based algorithm with those of the existing algorithms [41][42] and this is done in Tables 3.1 and 3.2 where the performance of each algorithm is quantified in terms of its PAPR-reduction improvement in dB over the original data for a clipping probability of 10^{-3}. The computational complexity of PAPR-reduction algorithms is measured in terms of the ratio of the CPU time for each algorithm to that of the proposed PAPR-reduction algorithm with $n_a = 240$, for which the CPU time [1] was normalized to unity.

From Table 3.1, the following conclusions can be drawn:

- The proposed LP-based algorithm leads to improved performance and requires less computation than the tone reservation algorithm in [41].
- A tradeoff is offered by the proposed LP-based algorithm between performance and computational complexity. Selecting fewer active subcarriers for peak-power reduction can dramatically reduce the complexity of the proposed LP-based algorithm at the cost of a moderate performance degradation.

From Table 3.2, it can be observed that

- To achieve a similar performance, the amount of computation required by the proposed LP-based algorithm is much less than that required by the ASE algorithm.

[1] The CPU time was calculated by using MATLAB command 'cputime'. The command returns the total CPU time (in seconds) used by MATLAB from the time it was started.

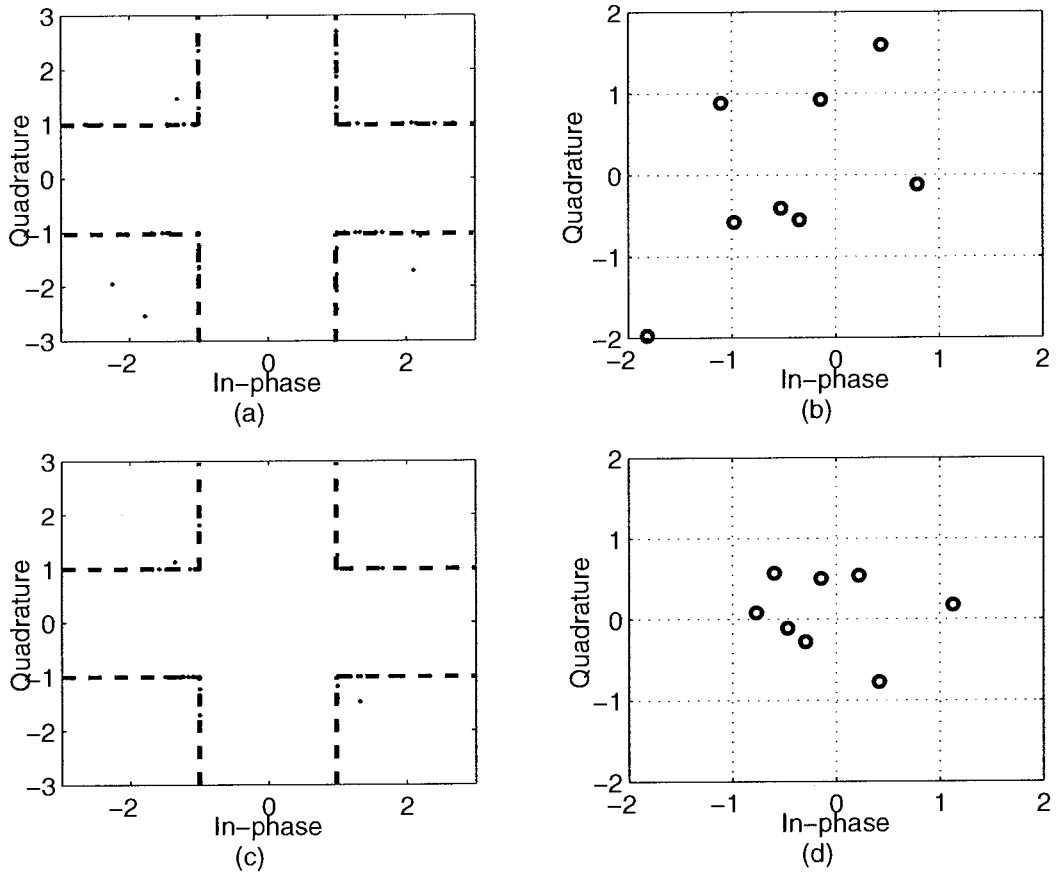

Figure 3.5. *Distributions of the modified constellation points using the proposed LP-based and the ASE algorithms. (a) in active subcarriers by the proposed LP-based algorithm, (b) in unused subcarriers by the proposed LP-based algorithm, (c) in active subcarriers by the ASE algorithm, (d) in unused subcarriers by the ASE slgorithm.*

Table 3.1. *Comparison of PAPR-Reduction Algorithms*

PAPR-reduction algorithms		Proposed LP		Tone Researvation Algorithm
		$n_a = 240,\ itr = 8$	$n_a = 80,\ itr = 8$	
Performance gain (dB)		2.34	1.78	1.46
Computational Complexity	Normalized CPU Time	1	0.13	1.5

- The performance of the ASE algorithm reaches its limit after a certain number of iterations, but the proposed LP-based algorithm can still improve its performance by using more active subcarriers for peak-power reduction.

Table 3.2. *Comparison of PAPR-Reduction Algorithms*

PAPR-reduction algorithms		ASE Algorithm			Proposed LP (itr = 8)	
		$itr = 5$	$itr = 10$	$itr = 100$	$n_a = 80$	$n_a = 240$
Performance gain (dB)		1.47	1.78	1.82	1.78	2.34
Computational Complexity	Normalized CPU Time	0.18	0.35	3.5	0.13	1

3.4.2 OFDM Systems with Complex Signals

For OFDM systems with complex signals where all subcarriers are active, the tone reservation algorithm in [41] cannot be used but the ASE algorithm in [42], the SLM algorithm in [38], and the proposed *least-pth* algorithm are applicable. The example presented below consists of two parts. In the first part, the *least-pth* algorithm proposed in Sec. 3.3.2 is simulated and compared with that of the ASE algorithm. In the second part, it is demonstrated that if the side information required by the SLM algorithm is available, the application of the proposed *least-pth* algorithm with the OFDM signal selected by the SLM algorithm as an initial point can reduce the PAPR by a substantial amount.

Example 2:

(a) We considered an OFDM transmitter with $N = 64$ subcarriers. First, the proposed *least-pth* algorithm was applied with various values of n_a to obtain an optimal peak-reduction vector $\mathbf{C}^*$, and the clipping probability is plotted as a solid curve in Fig. 3.6. Then, the performance of the ASE algorithm in [42] was evaluated with the target PAPR set to 6 dB, and the clipping probability for various numbers of

iterations, i.e., $itr = 20$ and 100, is plotted in Fig. 3.6 as dashed curves. It is observed that performance improvement can be achieved by the ASE algorithm with 20 iterations, but the algorithm's capability reaches its limit after 100 iterations. For example, for a clipping probability of 10^{-3}, a 1-dB improvement can be achieved by the ASE algorithm using 20 iterations, but only 1.2-dB improvement can be achieved using 100 iterations. On the other hand, for the same clipping probability, the proposed *least-pth* algorithm with $n_a = 28$ and $itr = 4$ offers a 1-dB gain over the ASE algorithm with $itr = 100$. As for computational complexity, the proposed *least-pth* algorithm with $n_a = 10$ and $itr = 4$ achieves a performance similar to that of the ASE algorithm with 100 iterations as can be seen in Fig. 3.6 but the amount of computation required by the proposed *least-pth* algorithm is 20% less than that required by the ASE algorithm. In this system, the average power increase of the proposed *least-pth* algorithm is 0.534 and 0.706 dB, respectively, for $n_a = 10$ and 28.

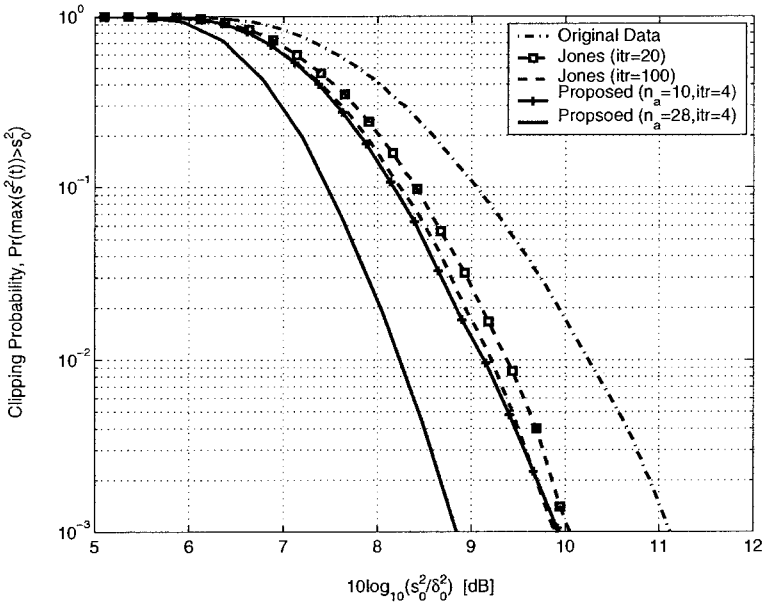

Figure 3.6. *Performance comparison of the proposed least-pth and the ASE algorithms.*

(*b*) We also considered an OFDM transmitter with 64 subcarrier where the side

information required by the SLM algorithm in [38] is available. The performance of the SLM algorithm with the number of candidate sequences, $U = 4$ and 16, was evaluated and plotted in Figs. 3.7 and 3.8, respectively, as the dashed curves. In each case, the proposed *least-pth* algorithm with the best OFDM signal selected by the SLM algorithm as an initial point was then applied. The performance achieved after 1 and 2 iterations is shown in the same figures as solid lines. For the case of $U = 4$, the performance gain was 0.9 dB after 1 iteration and 1.5 dB after 2 iterations. The average power increase is 0.098 and 0.535 dB, respectively, after 1 and 2 iterations. For the case of $U = 16$, the performance gain was 0.2 dB after 1 iteration and 0.7 dB after 2 iterations. The average power increase is 0.031 and 0.396 dB, respectively, after 1 and 2 iterations.

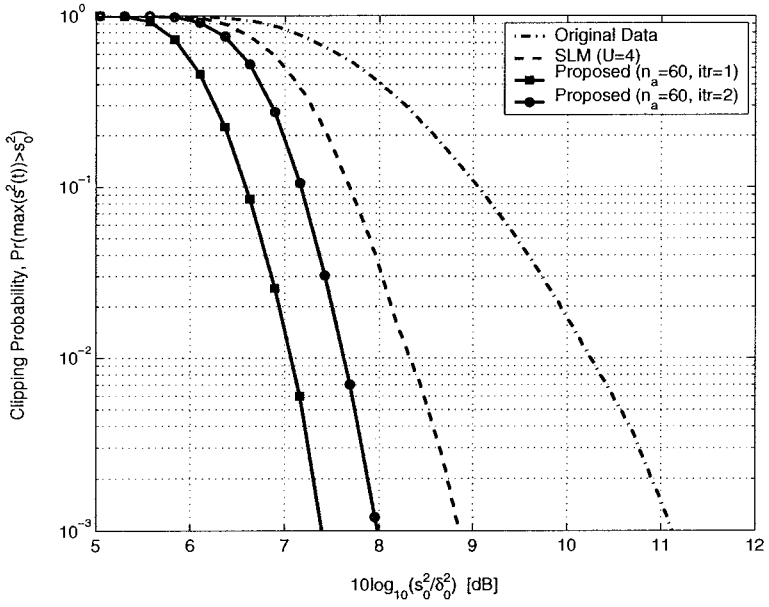

Figure 3.7. *Performance of the proposed least-pth algorithm combined with the SLM algorithm.*

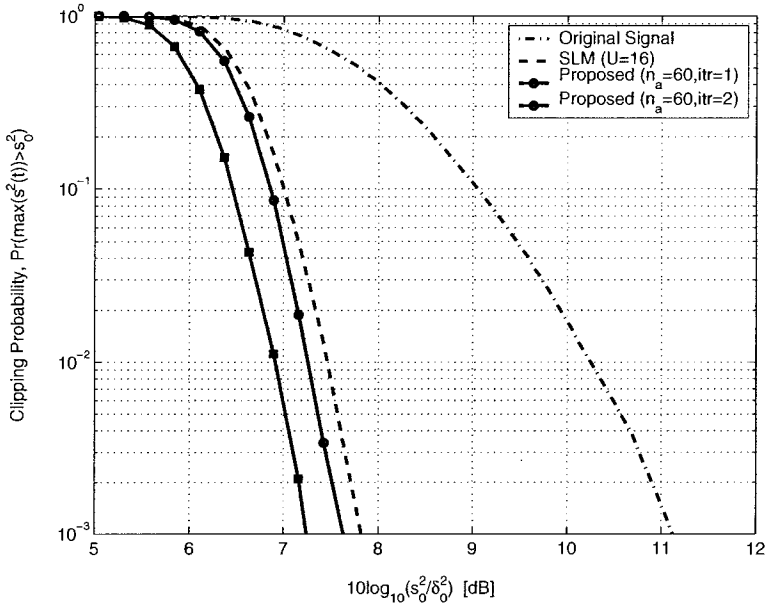

Figure 3.8. *Performance of the proposed least-pth algorithm combined with the SLM algorithm.*

3.5 Conclusions

Two new PAPR-reduction algorithms, one for OFDM systems with real signals and the other for OFDM systems with complex signals, have been proposed. For OFDM systems with real signals, a new LP-based algorithm has been proposed where all the subsymbols in unused subcarriers and the exterior constellation points in active subcarriers are optimized simultaneously. For OFDM systems with complex signals where all subcarriers are active, a new algorithm has been proposed using an accelerated *least-pth* approach. Our simulations have demonstrated that the proposed PAPR-reduction algorithms offer considerable performance improvement in many practical situations over several existing algorithms. Furthermore, the proposed algorithms offer a tradeoff between performance and computational complexity, which can often be used to advantage in a number of applications.

Chapter 4

PAPR Reduction via Discrete Constellation Extension

4.1 Introduction

In this chapter, PAPR reduction for OFDM systems with complex signals is investigated in a probabilistic framework [44][71]. A new constellation extension technique is developed whereby the data are represented either by points in the original constellation or by extended points. In an attempt to find the optimal representation of the OFDM signal, two de-randomization algorithms are proposed by applying the so called conditional probablity method. The performance of the proposed de-randomization algorithms can be further improved by the combining the de-randomization, SR, and CDO algorithms. Design examples are presented which demonstrate that a significant improvement of PAPR reduction can be achieved by the proposed algorithms over several existing algorithms [38][44].

The chapter is organized as follows. In Sec. 4.2, a brief description of the system is given, and the proposed constellation extension scheme is described and the problem is formulated; then new PAPR-reduction algorithms for the solution of the problem are described. In Sec. 4.3, various PAPR-reduction algorithms are compared though simulations. Conclusions are drawn in Sec. 4.4.

4.2 PAPR Reduction in OFDM Systems with Complex Signals

4.2.1 System Configuration

A 16-QAM modulation is assumed for each subcarrier in which case the constellation assume the form shown in Fig. 4.1a. The constellation extension scheme for this type of modulation is illustrated in Fig. 4.1b where any data point with a value greater than or equal to 4 can be represented by a pair of two possible constellation points. For example, data point $D_k = 15$ (or 1111 in binary form) can be represented either by $X_k^0 = -3 - 3j$ or by $X_k^1 = -3 + 5j$ where the superscripts of X_k^0 and X_k^1 are used to identify which constellation point is selected to represent D_k, i.e., X_k^0 indicates that an exterior point of the conventional constellation is used to represent D_k; on the other hand, X_k^1 indicates that a corresponding extended point is used to represent D_k. Based on this constellation extension technique, one seeks to reduce the PAPR of the transmit signals by selecting the optimal representation of data points by either the exterior or the extended points. The minimum Euclidean distance between the extended constellaton point and any conventional constellation point is guaranteed not to be less than the minimum distance among the conventional constellation points. As will be demonstrated later, the increase of average transmit power due to the constellation extension is fairly small and, consequently, the BER performance of the system will not be degraded significantly.

4.2.2 Problem Formulation

Based on the definition of PAPR in (2.19), our objective is to obtain an optimal representation of the data points such that the PAPR of the OFDM symbol $\boldsymbol{X}$ is minimized. The PAPR-reduction problem can be addressed by minimizing the peak power of the transmit signal $\mathbf{x}$. It turns out that the increase of average power

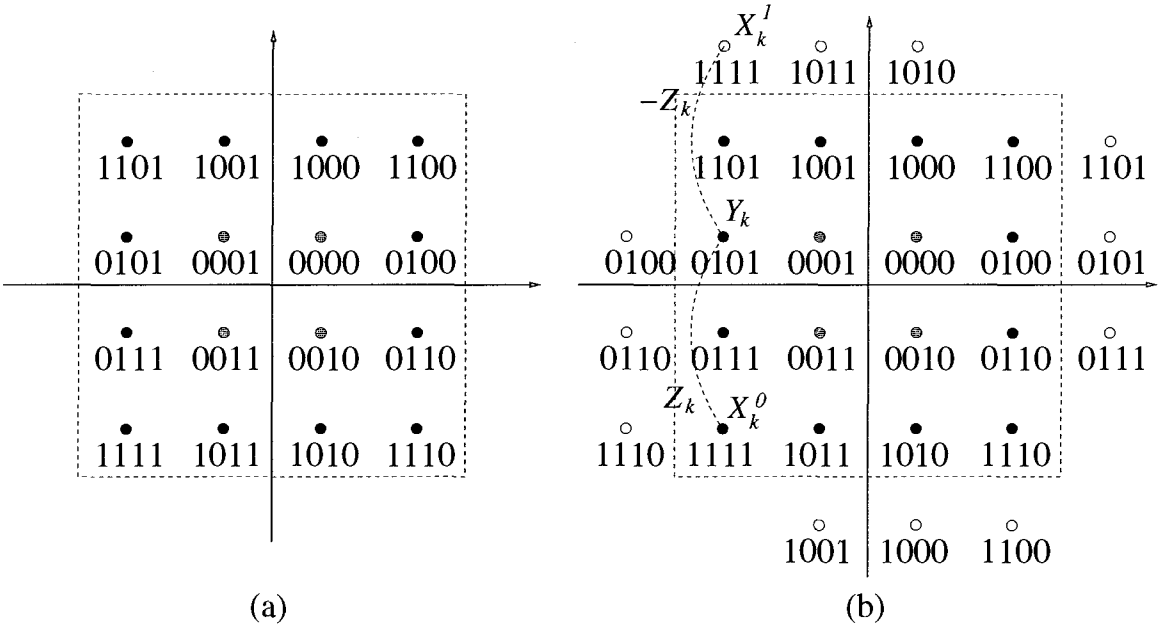

Figure 4.1. *(a) 16-QAM constellation with Gray code bit mapping. (b) extension of 16-QAM constellation.*

in the transmit signal by constellation extension is fairly moderate and the BER performance degradation due to such constellation extension is usually insignificant. For the sake of fair comparison with other PAPR-reduction algorithms, the peak power of the transmit signal will be used as a performance measure in the computer simulations presented in Sec. 4.3. Denoting the number and index set of subcarriers where constellation extension is applied as K and $\mathcal{I} = \{i_1, i_2, \ldots, i_K\}$, respectively, and letting $\bar{\boldsymbol{X}} = [X_{i_1} \cdots X_{i_K}]^T$, the PAPR-reduction problem can be formulated as

$$\underset{\bar{\boldsymbol{X}}}{\text{minimize}} \quad \max_{0 \le n \le N-1} \left| \sum_{k=0}^{N-1} X_k e^{\frac{j2\pi kn}{N}} \right| \tag{4.1a}$$

$$\text{subject to: } X_k \in \{X_k^0, X_k^1\} \quad \text{for } k \in I \tag{4.1b}$$

If we let

$$Y_k = \frac{X_k^0 + X_k^1}{2} \text{ and } Z_k = \frac{X_k^0 - X_k^1}{2} \quad \text{for } k \in I \tag{4.2a}$$

then we have

$$X_k^0 = Y_k + Z_k \text{ and } X_k^1 = Y_k - Z_k \quad \text{for } k \in I \tag{4.2b}$$

The problem in (4.1) can thus be reorganized as

$$\underset{\boldsymbol{s}}{\text{minimize}} \quad \max_{0 \le n \le N-1} \left| \sum_{k=0,\ k \notin I}^{N-1} X_k e^{\frac{j2\pi kn}{N}} + \sum_{k=1}^{K} Y_{i_k} e^{\frac{j2\pi i_k n}{N}} + \sum_{k=1}^{K} s_k Z_{i_k} e^{\frac{j2\pi i_k n}{N}} \right| \tag{4.3a}$$

$$\text{subject to: } s_k \in \{1, -1\} \quad \text{for } k = 1, \ldots, K \tag{4.3b}$$

where vector $\boldsymbol{s} = [s_1 \ \cdots \ s_K]^T$ is referred to as the *sign vector*. The variables in (4.3) are complex-valued. If we define

$$c_n = \begin{cases} \text{Re}\left[\sum_{k=0,k\notin I}^{N-1} X_k e^{\frac{j2\pi kn}{N}} + \sum_{k=1}^{K} Y_{i_k} e^{\frac{j2\pi i_k n}{N}}\right] & 0 \le n \le N-1 \\ \text{Im}\left[\sum_{k=0,k\notin I}^{N-1} X_k e^{\frac{j2\pi k(n-N)}{N}} + \sum_{k=1}^{K} Y_{i_k} e^{\frac{j2\pi i_k (n-N)}{N}}\right] & N \le n \le 2N-1 \end{cases} \tag{4.4a}$$

and

$$d_{nk} = \begin{cases} \text{Re}\left[Z_{i_k} e^{\frac{j2\pi i_k n}{N}}\right] & 0 \le n \le N-1 \\ \text{Im}\left[Z_{i_k} e^{\frac{j2\pi i_k (n-N)}{N}}\right] & N \le n \le 2N-1 \end{cases} \tag{4.4b}$$

where $\text{Re}(\cdot)$ and $\text{Im}(\cdot)$ represent the real and imaginary components of the variable, respectively, then the objective function in (4.3) can be written as

$$\left| c_n + \sum_{k=1}^{K} s_k d_{nk} + j c_{n+N} + j \sum_{k=1}^{K} s_k d_{n+N,k} \right| \tag{4.5}$$

Since the magnitude of a complex number is always no less than the maximum of the magnitudes of its real and imaginary components, i.e.,

$$\begin{aligned} &\left| c_n + \sum_{k=1}^{K} s_k d_{nk} + j c_{n+N} + j \sum_{k=1}^{K} s_k d_{n+N,k} \right| \\ &\ge \max\left\{ \left| c_n + \sum_{k=1}^{K} s_k d_{nk} \right|, \ \left| c_{n+N} + \sum_{k=1}^{K} s_k d_{n+N,k} \right| \right\} \end{aligned} \tag{4.6}$$

we can write

$$\begin{aligned} &\max_{0 \le n \le N-1} \left| c_n + \sum_{k=1}^{K} s_k d_{nk} + j c_{n+N} + j \sum_{k=1}^{K} s_k d_{n+N,k} \right| \\ &\ge \max_{0 \le n \le 2N-1} \left| c_n + \sum_{k=1}^{K} s_k d_{nk} \right| \end{aligned} \tag{4.7}$$

Hence, the problem in (4.3) can be relaxed to

$$\underset{\boldsymbol{s}}{\text{minimize}} \quad \max_{0\le n\le 2N-1} \left| c_n + \sum_{k=1}^{K} s_k d_{nk} \right| \tag{4.8a}$$

$$\text{subject to: } s_k \in \{1, -1\} \quad \text{for} \quad k = 1, \ldots, K \tag{4.8b}$$

where the variables involved are real. The relationship between the solutions of the problems in (4.3) and (4.8) will now be examined. If $\boldsymbol{s}^\star$ is the solution of the problem in (4.8), $n^\star$ is the index n at which the maximum of $\left|c_n + \sum_{k=1}^{K} s_k^\star d_{nk}\right|$ is achieved, $\tilde{\boldsymbol{s}}$ is the solution of the problem in (4.3), and $\tilde{n}$ is the index n at which the maximum of $\left|c_n + \sum_{k=1}^{K} \tilde{s}_k d_{nk} + jc_{n+N} + j\sum_{k=1}^{K} \tilde{s}_k d_{n+N,k}\right|$ is achieved, then it can be shown that

$$\begin{aligned} &\left| c_{n^\star} + \sum_{k=1}^{K} s_k^\star d_{n^\star k} \right| \\ \le &\left| c_n + \sum_{k=1}^{K} \tilde{s}_k d_{nk} + jc_{n+N} + j\sum_{k=1}^{K} \tilde{s}_k d_{n+N,k} \right| \\ \le &\sqrt{2} \left| c_{n^\star} + \sum_{k=1}^{K} s_k^\star d_{n^\star k} \right| \end{aligned} \tag{4.9}$$

It follows from (4.9) that the solution of the problem in (4.8) can be regarded as a good approximation of the solution of the problem in (4.3). For this reason, a good suboptimal solution of the ICI-reduction problem at hand can be obtained by solving the problem in (4.8) instead of that in (4.3). The proof of (4.9) is given in Appendix A.

4.2.3 Algorithms

The minimax optimization problem in (4.8) is an integer programming problem which can be solved by using the MCP [44][50][71].

4.2.3.1 De-Randomization Algorithm

Consider sign vectors $\boldsymbol{s} = [s_1 \cdots s_K]$ where $s_1, \ldots, s_K$ are treated as random variables that can assume values of 1 or -1 with equal probability. Let A_n^λ be the event that

$\left|c_n + \sum_{k=1}^{K} d_{nk}s_k\right| \geq \lambda$ and $\Pr\left(A_n^{\lambda}\right)$ be the probability that event A_n^{λ} occurs. Let us assume that λ is chosen such that

$$\sum_{n=0}^{2N-1} \Pr\left(A_n^{\lambda}\right) < 1 \tag{4.10}$$

If the first component of the optimal sign vector is taken to be $s_1^{\star} = 1$, then a suboptimal sign vector $\boldsymbol{s}^{\star}$ can be obtained sequentially as

$$s_j^{\star} = \arg\left[\min_{s_j \in \{1,-1\}} \sum_{n=0}^{2N-1} \Pr\left(A_n^{\lambda} | s_1^{\star}, \ldots, s_{j-1}^{\star}, s_j\right)\right] \quad \text{for } j = 2, \ldots, K \tag{4.11}$$

Consequently, we have

$$\begin{aligned} &\sum_{n=0}^{2N-1} \Pr\left(A_n^{\lambda} | s_1^{\star}, \ldots, s_{j-1}^{\star}, s_j^{\star}\right) \\ &\quad = \min_{s_j \in \{1,-1\}} \sum_{n=0}^{2N-1} \Pr\left(A_n^{\lambda} | s_1^{\star}, \ldots, s_{j-1}^{\star}, s_j\right) \\ &\quad \leq \mathrm{P}_{avg} \end{aligned} \tag{4.12a}$$

and

$$\begin{aligned} \mathrm{P}_{avg} &= \frac{\sum_{n=0}^{2N-1} \Pr\left(A_n^{\lambda} | s_1^{\star}, \ldots, s_{j-1}^{\star}, 1\right) + \sum_{n=0}^{2N-1} \Pr\left(A_n^{\lambda} | s_1^{\star}, \ldots, s_{j-1}^{\star}, -1\right)}{2} \\ &= \sum_{n=0}^{2N-1} \Pr\left(A_n^{\lambda} | s_1^{\star}, \ldots, s_{j-1}^{\star}\right) \end{aligned} \tag{4.12b}$$

which in conjunction with (4.10) imply that

$$\sum_{n=0}^{2N-1} \Pr\left(A_n^{\lambda} | s_1^{\star}, \ldots, s_K^{\star}\right) \leq \sum_{n=0}^{2N-1} \Pr\left(A_n^{\lambda}\right) < 1 \tag{4.12c}$$

With the entire vector $\boldsymbol{s}^{\star}$ known, the probability $\Pr\left(A_n^{\lambda} | s_1^{\star}, \ldots, s_K^{\star}\right)$ for each n is either zero or one. Hence, it can be inferred that the conditional probabilities in (4.11b) are all zero, i.e., $\Pr\left(A_n^{\lambda} | s_1^{\star}, \ldots, s_K^{\star}\right) = 0$ for $n = 0, \ldots, 2N-1$, which means that $\left|c_n + \sum_{k=1}^{K} s_k^{\star} d_{nk}\right| < \lambda$. In other words, the sign vector $\boldsymbol{s}^{\star} = [s_1^{\star} \cdots s_K^{\star}]$ obtained

using (4.11) can be regarded as a suboptimal solution for which the objective function in the problem in (4.8) is guaranteed to be smaller than λ. In the above method, the solution $\boldsymbol{s}^{\star}$ is obtained by first treating the elements of the sign vector $\mathbf{s}$ as random variables and then using a conditional probability argument in conjunction with the constraint in (4.10) to de-randomize the sign vector iteratively. For this reason, the solution method is referred to as a *de-randomization* method [50].

Although in principle the sign vector $\boldsymbol{s}^{\star}$ can be determined using the method of conditional probabilities as described in (4.11), numerical evaluation of the conditional probabilities is often difficult. A remedy to the problem is to derive easy-to-evaluate upper bounds on the conditional probability so that suboptimal solutions can be developed by working with the upper bounds instead of the conditional probabilities. For the problem in (4.8), we are interested in an upper bound $U_n(\lambda, s_1, \ldots, s_j)$ for the conditional probability known as *pessimistic estimator* [50] such that

$$\Pr\left(A_n^{\lambda} | s_1, \ldots, s_j\right) \leq U_n(\lambda, s_1, \ldots, s_j) \quad \text{for } j = 1, \ldots, K \tag{4.13a}$$

where the condition

$$\min_{s_j \in \{1,-1\}} \sum_{n=0}^{2N-1} U_n(\lambda, s_1, \ldots, s_{j-1}, s_j) \leq \sum_{n=0}^{2N-1} U_n(\lambda, s_1, \ldots, s_{j-1}) \tag{4.13b}$$

is satisfied. From (4.13a) and (4.13b), it is quite clear that if we impose the additional constraint

$$\sum_{n=0}^{2N-1} U_n(\lambda) < 1 \tag{4.13c}$$

where $U_n(\lambda)$ denotes the upper bound of $\Pr\left(A_n^{\lambda}\right)$ with all the components of $\mathbf{s}$, i.e., $s_1, \ldots, s_K$, treated as random variables, then the pessimistic estimator $U_n(\lambda, s_1, \ldots, s_j)$ can be used to replace the conditional probability $\Pr\left(A_n^{\lambda} | s_1, \ldots, s_j\right)$ in (4.11) to deduce a suboptimal solution $\boldsymbol{s}^{\star}$. In effect, working with a pessimistic estimator $U_n(\lambda, s_1, \ldots, s_j)$ satisfying the conditions in (4.13a)-(4.13c), a suboptimal sign vec-

tor $\boldsymbol{s}^\star$ can be determined sequentially as

$$\begin{aligned} s_j^\star &= \arg\left[\min_{s_j\in\{1,-1\}} \sum_{n=0}^{2N-1} U_p\left(\lambda,\, s_1^\star,\, \ldots,\, s_{j-1}^\star,\, s_j\right)\right] \\ &= -\operatorname{sign}\left[\sum_{n=0}^{2N-1} U_n\left(\lambda,\, s_1^\star,\, \ldots, s_{j-1}^\star,\, 1\right) - \sum_{n=0}^{2N-1} U_n\left(\lambda,\, s_1^\star,\, \ldots, s_{j-1}^\star,\, -1\right)\right] \end{aligned} \tag{4.14}$$

for $j = 2, \ldots, K$.

4.2.3.2 Chernoff-Bound-Based Algorithm

In what follows, a pessimistic estimator is derived based on the Chernoff bound [62] which can be described by the inequality

$$\Pr(Y \geq \delta) \leq e^{-\gamma\delta} E(e^{\gamma Y}) \tag{4.15}$$

where γ is a nonnegative parameter to be optimized. To see how the Chernoff bound can be applied to our problem, we write the conditional probability as

$$\begin{aligned} &\Pr\left(\left|c_n + \sum_{k=1}^{K} s_k d_{nk}\right| \geq \lambda | s_1,\, \ldots,\, s_j\right) \\ &\quad = \Pr\left(\sum_{k=j+1}^{K} s_k d_{nk} \geq \lambda - c_n - \sum_{k=1}^{j} s_k d_{nk}\right) \\ &\qquad + \Pr\left(-\sum_{k=j+1}^{K} s_k d_{nk} \geq \lambda + c_n + \sum_{k=1}^{j} s_k d_{nk}\right) \end{aligned} \tag{4.16}$$

where $\lambda + c_n + \sum_{k=1}^{j} s_k d_{nk}$ and $\lambda - c_n - \sum_{k=1}^{j} s_k d_{nk}$ can be treated as constants, just like δ in (4.15), since $s_1, \ldots, s_j$ are assumed to be known. By applying the Chernoff bound in (4.15) to (4.16), we obtain

$$\Pr\left(\left|c_n + \sum_{k=1}^{K} s_k d_{nk}\right| \geq \lambda | s_1,\, \ldots,\, s_j\right) \leq P_c \tag{4.17a}$$

where

$$\begin{aligned} P_c &= e^{-\gamma\lambda+\gamma c_n+\gamma\sum_{k=1}^{j} s_k d_{nk}} \mathcal{E}\left(e^{\gamma\sum_{k=j+1}^{K} s_k d_{nk}}\right) + e^{-\gamma\lambda-\gamma c_n-\gamma\sum_{k=1}^{j} s_k d_{nk}} \mathcal{E}\left(e^{-\gamma\sum_{k=j+1}^{K} s_k d_{nk}}\right) \\ &= 2e^{-\gamma\lambda}\cosh\left(\gamma c_n + \gamma\sum_{k=1}^{j} s_k d_{nk}\right) \prod_{k=j+1}^{N} \cosh(\gamma d_{nk}) \end{aligned} \tag{4.17b}$$

The last equality in (4.17b) follows from the fact that the random variables $s_{j+1}, \ldots, s_K$ are independent which assume values of 1 or -1 with equal probability. Using the above analysis, a pessimistic estimator can be derived as

$$U_n(\lambda^\star, s_1, \ldots, s_j) = 2e^{-\gamma^\star\lambda^\star}\cosh\left(\gamma^\star c_n + \gamma^\star\sum_{k=1}^{j} s_k d_{nk}\right)\prod_{k=j+1}^{N}\cosh(\gamma^\star d_{nk}) \quad (4.18a)$$

for $j = 1, \ldots, K$, where

$$\varepsilon = \max_{0\le n\le 2N-1}\left(c_n^2 + \sum_{k=1}^{K} d_{nk}^2\right),\ \lambda^\star = \sqrt{2\varepsilon\log(4N)} \text{ and } \gamma^\star = \lambda^\star/\varepsilon \quad (4.18b)$$

The derivation of (4.18) is given in Appendix B.

The Chernoff-bound based pessimistic estimator in (4.18) can be used in conjunction with (4.14) to obtain a suboptimal solution $\boldsymbol{s}^\star$ for the problem in (4.8). In fact, using (4.18a), Eq. (4.14) becomes

$$\begin{aligned} s_j^\star &= -\text{sign}\left[\sum_{n=0}^{2N-1} U_n\left(\lambda^\star, s_1^\star, \ldots, s_{j-1}^\star, 1\right) - \sum_{n=0}^{2N-1} U_n\left(\lambda^\star, s_1^\star, \ldots, s_{j-1}^\star, -1\right)\right] \\ &= -\text{sign}\left[\sum_{n=0}^{2N-1}\sinh\left(\gamma^\star c_n + \gamma^\star\sum_{k=1}^{j-1} s_k^\star d_{nk}\right)\sinh(\gamma^\star d_{nk})\prod_{k=j+1}^{K}\cosh(\gamma^\star d_{nk})\right] \quad (4.19) \end{aligned}$$

for $j = 2, \ldots, K$. It follows that the objective function in (4.8a) at $\boldsymbol{s} = \boldsymbol{s}^\star$ is smaller than $\lambda^\star$. Using (4.2b) and (4.19), the optimized OFDM symbol $\boldsymbol{X}^\star$ can be obtained as

$$\boldsymbol{X}_k^\star = \begin{cases} X_k & \text{for } k \notin I \\ Y_k + s_l^\star Z_k & \text{for } k \in I \end{cases} \quad (4.20)$$

where l is the index of element k in set I in the case that $k \in I$. From (4.1) and (4.9), we can write

$$\max_{0\le n\le N-1}\left|\sum_{k=0}^{N-1} X_k^\star e^{\frac{j2\pi kn}{N}}\right|^2 < 2\lambda^{\star 2}$$

In other words, the peak power of the optimized OFDM symbol $\boldsymbol{X}^\star$ is guaranteed to be smaller than $2\lambda^{\star 2}$. An algorithm based on the above solution method is summarized in Table 4.1.

Table 4.1. *A Chernoff-Bound Based Algorithm for PAPR Reduction*

Step 1
Input the OFDM symbol $\boldsymbol{X} = [X_1 \ \cdots \ X_N]$.
Step 2
For $k \in I$, compute Y_k and Z_k using (4.4a).
Compute c_n and d_{nk} using (4.6).
Evaluate parameters ε, $\lambda^\star$, and $\gamma^\star$ using (4.18b).
Step 3
Determine the sign vector $\boldsymbol{s}^\star = [s_1^\star \ \cdots \ s_K^\star]$ with $s_1^\star = 1$ sequentially using (4.19).
The optimized OFDM symbol $\boldsymbol{X}^\star$ can be obtained using (4.20).

4.2.3.3 Polynomial-Bound Based Algorithm

The most computation-intensive operation in the evaluation of upper bound $U_p(\lambda^\star, s_1, \ldots, s_j)$ in (4.18a) is the evaluation of the hyperbolic cosine functions involved. In what follows we derive a polynomial upper bound for the hyperbolic cosine function on a given interval that will eventually lead to a polynomial-bound based pessimistic estimator.

It follows from (4.17) that

$$\begin{aligned}
&\Pr\left(\gamma\left|c_n + \sum_{k=1}^{K} s_k d_{nk}\right| \geq \gamma\lambda\right) \\
&= \Pr\left(\left|c_n + \sum_{k=1}^{K} s_k d_{nk}\right| \geq \lambda\right) \\
&\leq 2e^{-\gamma\lambda}\cosh(\gamma c_n)\prod_{k=1}^{K}\cosh(\gamma d_{nk}) \\
&\leq 2e^{-\gamma\lambda}\max_{n=0,\ldots,2N-1}\left[\cosh(\gamma c_n)\prod_{k=1}^{K}\cosh(\gamma d_{nk})\right] \qquad (4.21)
\end{aligned}$$

For example, for $N = 64$, we have $\gamma = 20$ and $\gamma\lambda = 11$. In such a case, (4.21)

becomes

$$\Pr\left(\gamma\left|c_n+\sum_{k=1}^{K}s_k d_{nk}\right|\geq\gamma\lambda\right)\leq P_n \tag{4.22a}$$

where

$$P_n=2e^{-11}\max_{n=0,\ldots,2N-1}\left[\cosh\left(\gamma c_n\right)\prod_{k=1}^{K}\cosh(\gamma d_{nk})\right]=0.0025 \tag{4.22b}$$

We stress that the bound derived in (4.22) is not tight and computer simulations have indicated that the actual interval into which the value of $\gamma\left|c_n+\sum_{k=1}^{K}s_k d_{nk}\right|$ falls is considerably smaller than $[0,11]$. Based on these observations, we seek a polynomial upper bound $g(x)=1+k_1x^2+k_2x^4$ for $\cosh(x)$ with $0\leq x\leq M$, i.e.,

$$\cosh(x)\leq 1+k_1x^2+k_2x^4 \quad \text{for } 0\leq x\leq M \tag{4.23}$$

If we define

$$G_n\left(\lambda,\, s_1,\,\ldots,\,s_j\right)=2e^{-\gamma\lambda}g\left(\gamma c_n+\gamma\sum_{k=1}^{j}s_k d_{nk}\right)\prod_{k=j+1}^{K}g\left(\gamma d_{nk}\right) \tag{4.24}$$

then (4.18), (4.23), and (4.24) imply that

$$Pr\left(A_n^{\lambda}|s_1,\,\ldots,\,s_j\right)\leq G_n\left(\lambda,\,s_1,\,\ldots,\,s_j\right) \tag{4.25}$$

which is the condition in (4.13a) for $G_n\left(\lambda,\,s_1,\,\ldots,\,s_j\right)$. In addition, if we require that polynomial $g(x)$ satisfy the inequality

$$g(a)g(b)\geq\frac{g(a+b)+g(a-b)}{2} \tag{4.26}$$

for any a and b, then we have

$$\begin{aligned}
\sum_{n=0}^{2N-1}G_n\left(\lambda,\,s_1,\,\ldots,\,s_{j-1}\right) &= \sum_{n=0}^{2N-1}\left[2e^{-\gamma\lambda}g\left(\gamma c_n+\gamma\sum_{k=1}^{j-1}s_k d_{nk}\right)\prod_{k=j}^{K}g\left(\gamma d_{nk}\right)\right]\\
&\geq \sum_{n=0}^{2N-1}\left\{e^{-\gamma\lambda}\left[g\left(\gamma c_n+\gamma\sum_{k=1}^{j-1}s_k d_{nk}+\gamma d_{nj}\right)\right.\right.\\
&\quad \left.\left.+g\left(\gamma c_n+\gamma\sum_{k=1}^{j-1}s_k d_{nk}-\gamma d_{nj}\right)\right]\prod_{k=j+1}^{K}g(\gamma d_{nk})\right\}\\
&\geq \min_{s_j\in\{1,-1\}}\sum_{n=0}^{2N-1}G_n\left(\lambda,\,s_1,\,\ldots,\,s_{j-1},s_j\right)
\end{aligned} \tag{4.27}$$

which is the condition in (4.13b) for $G_n(\lambda, s_1, \ldots, s_j)$. It can be verified that polynomial bound $g(x)$ satisfies (4.26) if its coefficients are chosen such that

$$k_1^2 - 6k_2 \geq 0 \tag{4.28}$$

To identify the optimal values of parameters k_1 and k_2, we introduce an upper bound for the difference $g(x) - \cosh(x)$ as

$$g(x) - \cosh(x) \leq \delta \quad \text{for } 0 \leq x \leq M \tag{4.29}$$

and k_1 and k_2 are determined by minimizing δ subject to the constraints in (4.23), (4.28), (4.29), $k_1 \geq 0$ and $k_2 \geq 0$. The nonlinear constraint in (4.28) in conjuction with the nonnegativity constraints $k_1 \geq 0$ and $k_2 \geq 0$ defines the shaded region in Fig. 4.2. This nonconvex region can be approximated by the triangular region defined by a tangent line of the parabola $k_2 = k_1^2/6$ and the k_1-axis where the triangular region is convex and can be described by the constraint

$$\frac{ck_1}{3} - k_2 - \frac{c^2}{6} \geq 0 \tag{4.30}$$

Replacing the nonlinear constraint in (4.28) by the linear constraint in (4.30), the optimal parameters k_1 and k_2 for polynomial $g(x)$ can be determined by solving the linear progamming problem

$$\begin{aligned}
& \text{minimize } \delta && \text{(4.31a)}\\
\text{subject to: } & k_1 \geq 0,\ k_2 \geq 0, && \text{(4.31b)}\\
& k_1 x^2 + k_2 x^4 - \cosh(x) + 1 \geq 0 \quad \text{for } 0 \leq x \leq M && \text{(4.31c)}\\
& -k_1 x^2 - k_2 x^4 + \cosh(x) - 1 - \delta \geq 0 \quad \text{for } 0 \leq x \leq M && \text{(4.31d)}\\
& \frac{ck_1}{3} - k_2 - \frac{c^2}{6} \geq 0 && \text{(4.31e)}
\end{aligned}$$

where the parameter vector of the LP problem is $[\delta\ k_1\ k_2]^T$ and variable x assumes values on interval $[0, M]$. For example, with $M = 6$ and $c = 0.88$, solving the LP problem in (4.31) gives $k_1 = 0.8844$ and $k_2 = 0.1303$.

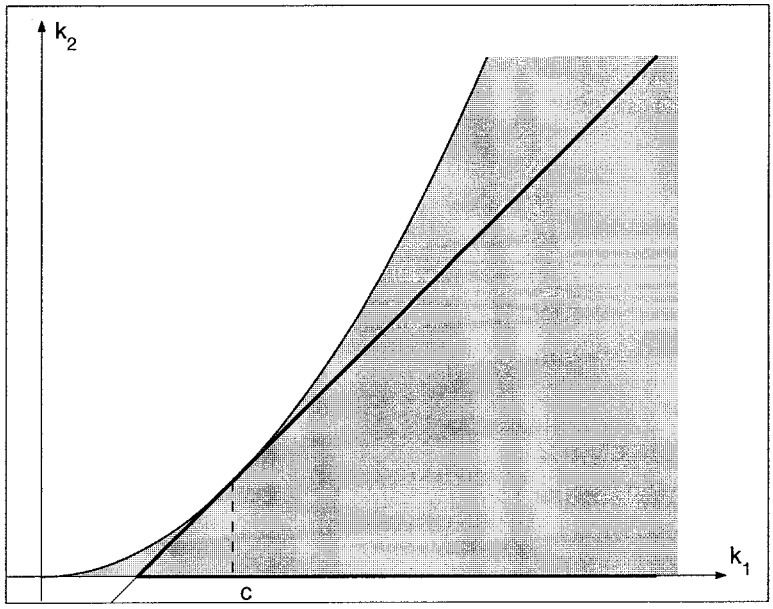

Figure 4.2. *An approximation of the nonconvex constraint.*

For $M = 6$, it can be shown that if the values of γ and λ in (4.24) are chosen such that

$$\varepsilon = \max_{0 \le n \le 2N-1} \sum_{k=1}^{K} \left(c_n^2 + d_{nk}^2\right), \ \lambda^\star = \sqrt{3.538\varepsilon \log(4N)} \text{ and } \gamma^\star = 0.565\lambda^\star/\varepsilon \tag{4.32}$$

then

$$G_n\left(\lambda^\star, s_1, \ldots, s_j\right) = 2e^{-\gamma^\star\lambda^\star} g\left(\gamma^\star c_n + \gamma^\star \sum_{k=1}^{j} d_{nk}\right) \prod_{k=j+1}^{K} g\left(\gamma^\star d_{nk}\right) \tag{4.33}$$

satisfies the condition in (4.13c) and, therefore, $G_n\left(\lambda^\star, s_1, \ldots, s_j\right)$ can be used as a pessimistic estimator. See Appendix C for a proof.

The polynomial-bound based pessimistic estimator in (4.33) can be used in conjunction with (4.14) to obtain a suboptimal solution $\boldsymbol{s}^\star$ for problem (4.8). Using (4.33), Eq. (4.14) becomes

$$s_j^\star = -\text{sign}\left[\sum_{n=0}^{2N-1} G_n\left(\lambda^\star, s_1^\star, \ldots, s_{j-1}^\star, 1\right) - \sum_{n=0}^{2N-1} G_n\left(\lambda^\star, s_1^\star, \ldots, s_{j-1}^\star, -1\right)\right] \tag{4.34}$$

for $j = 2, \ldots, K$. Using (4.2b) and (4.34), the optimized OFDM symbol $\boldsymbol{X}^\star$ can be obtained as in (4.20). By using an argument similar to that in Sec. 4.2.3.2, the peak power of optimized OFDM symbol $\boldsymbol{X}^\star$ is guaranteed to be smaller than $2\lambda^{\star 2}$. An algorithm based on the above solution method is summarized in Table 4.2.

Table 4.2. *A Polynomial-Bound Based Algorithm for PAPR Reduction*

Step 1
Input the OFDM symbol $\boldsymbol{X} = [X_1 \ \cdots \ X_N]$.
Step 2
For $k \in I$, compute Y_k and Z_k using (4.4a).
Compute c_n and d_{nk} using (4.6).
Evaluate parameters ε, $\lambda^\star$, and $\gamma^\star$ using (4.33).
Step 3
Determine the sign vector $\boldsymbol{s}^\star = [s_1^\star \ \cdots \ s_K^\star]$ with $s_1^\star = 1$ sequentially using (4.34).
The optimized OFDM symbol $\boldsymbol{X}^\star$ can be obtained using (4.20).

4.2.4 Enhancement for the Proposed Algorithms

The performance of the proposed de-randomization algorithms can be improved further through several enhancement techniques as described below.

4.2.4.1 Selective Rotations Algorithm

The objective function in (4.3a) remains unchanged if all complex-valued terms are rotated by an angle θ since

$$\left| \sum_{k=0,k\notin I}^{N-1} X_k e^{\frac{j2\pi kn}{N}} + \sum_{k=1}^{K} Y_{i_k} e^{\frac{j2\pi i_k n}{N}} + \sum_{k=1}^{K} s_k Z_{i_k} e^{\frac{j2\pi i_k n}{N}} \right|$$
$$= \left| e^{j\theta} \left(\sum_{k=0,k\notin I}^{N-1} X_k e^{\frac{j2\pi kn}{N}} + \sum_{k=1}^{K} Y_{i_k} e^{\frac{j2\pi i_k n}{N}} + \sum_{k=1}^{K} s_k Z_{i_k} e^{\frac{j2\pi i_k n}{N}} \right) \right|$$

On the other hand, this rotation leads to a different set of d_{nk} which can be obtained using (4.4) with X_k, Y_{i_k}, and Z_{i_k} replaced by $e^{j\theta}X_k$, $e^{j\theta}Y_{i_k}$, and $e^{j\theta}Z_{i_k}$, respectively. If we use the parameters d_{nk} generated by K different rotation angles θ_0, θ_1, ..., θ_{K-1} with $\theta_0 = 0$, then we can obtain K suboptimal sign vectors $\boldsymbol{s}_0^\star$, $\boldsymbol{s}_1^\star$, ..., $\boldsymbol{s}_{K-1}^\star$ from which the best sign vector can be identified by comparing the performance of the corresponding suboptimal solutions. Since the set of rotation angles includes $\theta = 0$, the suboptimal solution obtained using the SR algorithm is always superior to the suboptimal solution of the de-randomization algorithm described in Table 4.1 or 4.2.

4.2.4.2 Coordinate Descent Optimization Algorithm

If we define

$$f(\mathbf{s}) = \max_{0\le n\le 2N-1} f_n(\mathbf{s}) \tag{4.35a}$$

where

$$f_n(\mathbf{s}) = \left| c_n + \sum_{k=1}^{K} s_k d_{nk} \right| \quad \text{for } n = 0, \ldots, 2N-1 \tag{4.35b}$$

with $\mathbf{s} = [s_1 \cdots s_K]$ and $s_k \in [1, -1]$ for $k = 1, \ldots, K$, then the idea of coordinate descent optimization [51] can be applied to reduce the value of $f(\mathbf{s})$ iteratively as follows. Suppose only one element of the sign vector $\mathbf{s}$ is allowed to switch at each iteration. First, the value of $f_n(\mathbf{s})$ after the sign switch of element s_{k_c} can be obtained

as

$$f_n(\mathbf{s}, k_c) = \left| c_n + \sum_{k=1, k\neq k_c}^{K} s_k d_{nk} - s_{k_c} d_{nk_c} \right| \tag{4.36}$$

for $n = 0, \ldots, 2N-1$ and $k_c = 1, \ldots, K$. Next, the change in value of f can be obtained as

$$\Delta_f(k_c) = f(\mathbf{s}) - \max_{0\leq n\leq 2N-1} f_n(\mathbf{s}, k_c) \quad \text{for } k_c = 1, \ldots, K \tag{4.37}$$

If we define

$$\hat{k}_c = \arg\left[\max_{1\leq k_c\leq K} \Delta_f(k_c) \right] \tag{4.38}$$

and $\Delta_f(\hat{k}_c) \leq \epsilon$, where ϵ is a predefined tolerance, then a local minimum of function $f(\mathbf{s})$ is achieved and the algorithm terminates. Otherwise, the steepest descent direction for function $f(\mathbf{s})$ can be found as $-s_{\hat{k}_c}$. Therefore, the sign vector can be updated as $\mathbf{s} = \left[s_1 \cdots s_{\hat{k}_c-1} \; -s_{\hat{k}_c} \; s_{\hat{k}_c+1} \cdots s_K\right]$. Since the value of $f(\mathbf{s})$ is constantly reduced at each iteration, the CDO technique can be applied to enhance the performance of the de-randomization algorithm proposed in Sec. 4.2.3. An algorithm based on the above algorithm is summarized in Table 4.3.

Note that the CDO algorithm described above can be generalized in a way that at each iteration, multiple elements of the sign vector $\mathbf{s}$ are allowed to change. In general, it can be expected that better performance can be obtained at the cost of increased computational complexity.

4.2.4.3 Improved Performance using SLM Algorithms

In the proposed algorithms, only one data set has been utilized for PAPR reduction. The performance can be improved by combining the proposed algorithms with the SLM algorithm as illustrated in Fig. 4.3. First, multiple candidate data sets are generated at the transmitter. Second, for each of the data sets the proposed de-randomization algorithm is applied and the one with the least PAPR is selected. Third, the proposed SR and CDO algorithms are applied to the data set selected in the second stage for further PAPR reduction.

Table 4.3. *A Coordinate Descent Optimization Algorithm for PAPR Reduction*

Step 1

Set the tolerance $\epsilon = 0.01$.

Input c_n and d_{nk} using (4.4).

Input the sign vector $\mathbf{s} = \mathbf{s}^\star$, where $\mathbf{s}^\star$ is obtained by using (4.19).

Step 2

Compute $f(\mathbf{s})$ using (4.35a).

Compute $f_n(\mathbf{s}, k_c)$ using (4.36).

Compute $\Delta_f(k_c)$ using (4.37).

Determine $\hat{k}_c$ using (4.38).

Step 3

If $\Delta_f(\hat{k}_c) \leq \epsilon$, then output sign vector $\mathbf{s}$ and algorithm terminates.

Otherwise, update sign vector as $\mathbf{s} = \left[s_1 \ \cdots \ s_{\hat{k}_c-1} \ -s_{\hat{k}_c} \ s_{\hat{k}_c+1} \ \cdots \ s_K\right]$ and go to **Step 2**.

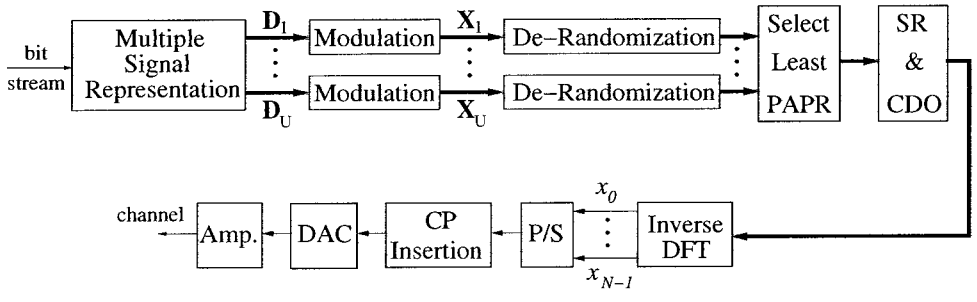

Figure 4.3. *Combination of the proposed and the SLM algorithms.*

4.3 Simulations

The proposed Chernoff-bound and polynomial-bound based derandomization algorithms were applied to an OFDM system with 64 subcarriers and the PAPR-reduction performance was evaluated and compared with those of the SLM and SCE algorithms proposed in [38] and [44], respectively. In order to approximate the analog signal ac-

curately, oversampling was applied and the same configuration as in Sec. 3.4 was used. For the SLM algorithm in [38], the number of candidate sequences is denoted as U. For the proposed SR algorithm, the number of rotations is denoted as K and the rotation angles θ was set to the values $0, \pi/K, \ldots, (K-2)\pi/K, (K-1)\pi/K$. For the proposed CDO algorithm, the number of elements of the sign vector that can be changed at each optimization iteration is denoted as *Bit*.

Example 1: The extended constellation adopted for the proposed Chernoff-bound and the polynomial-bound based algorithms is shown in Fig. 4.1b, and the clipping probabilities versus various power threshold values are plotted as the solid and dash curves in Fig. 4.4, respectively. For the SLM algorithm, a 16-QAM constellation was adopted. For the sake of comparison, the clipping probabilities obtained using the SLM algorithm and for the OFDM signal with no PAPR reduction are plotted in the same figure as dot-dashed curves. First, it can be observed from Fig. 4.4 that by combining each de-randomization algorithm with the SR algorithm, a significant PAPR reduction can be achieved. For example, for a clipping probability of 10^{-3}, a 1.7- and 3.1-dB improvement can be obtained by the Chernoff-bound based algorithm with $K = 1$ and $K = 4$, respectively, over the OFDM signal with no PAPR reduction. Note that the power increase associated with the Chernoff-bound based algorithm is approximately 0.45-dB over the average power of the OFDM signal with no PAPR reduction. Second, it can be observed from Fig. 4.5 that by combining each derandomization algorithm with the CDO algorithm, significant performance improvement can be achieved relative to that achieved with the SLM algorithm. For example, by using the Chernoff-bound based algorithm with CDO and assmuing a clipping probability of 10^{-3}, an improvement of 0.9 dB can be achieved relative to the performance achieved with the SLM algorithm with $U = 16$. Note that, in such a case, the power increase with respect to the average power is approximately 0.64 dB. Third, it can be observed from Figs. 4.4 and 4.5 that the performance of the polynomial-bound based algorithm is quite close to that of the Chernoff-bound based

algorithm. Fourth, it can be observed from Fig. 4.6 that the performance can be further improved by combining the proposed algorithms with the SLM algorithm. For example, a 1.4-dB improvement can be obtained by using the combined algorithm with $U = 4, K = 2, Bit = 1$ over the SLM algorithm with $U = 16$.

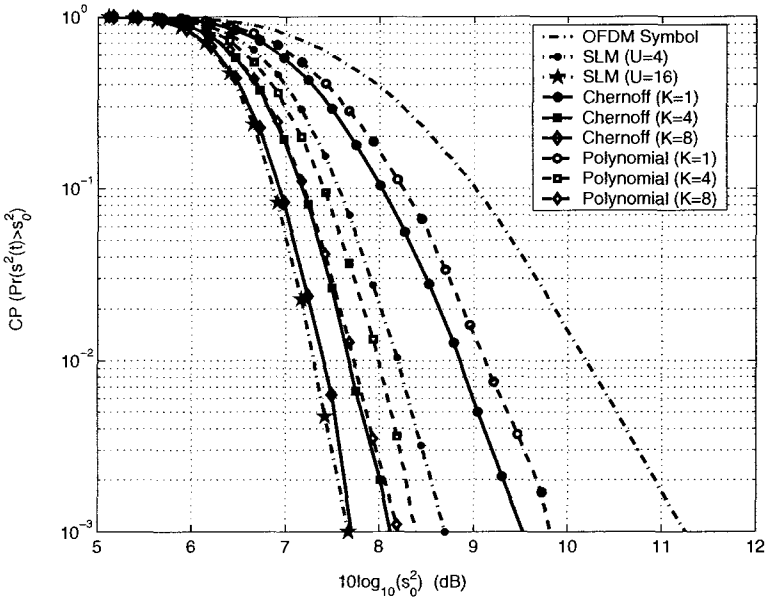

Figure 4.4. *Performance comparison of the SLM and the de-randomization algorithms.*

Example 2: The performance of PAPR-reduction algorithms using various constellation extension schemes was compared and the results are plotted in Fig. 4.7. The clipping probabilities for systems using the schemes in Fig. 4.1b and Fig. 2.8 [44] versus various power threshold values are plotted in Fig. 4.7 as dashed and solid curves, respectively. It can be observed that significant improvement can be achieved by the proposed algorithms using the scheme in Fig. 4.1b over the SCE algorithms using the scheme in Fig. 2.8. Note that because of the one-bit redundancy associated with the scheme in Fig. 2.8, the effective transmission rate of OFDM system is 4 bits per subcarrier for both schemes. On the other hand, compared with the average power of the OFDM system, a 3-dB power increase is associated with the scheme in Fig. 2.8.

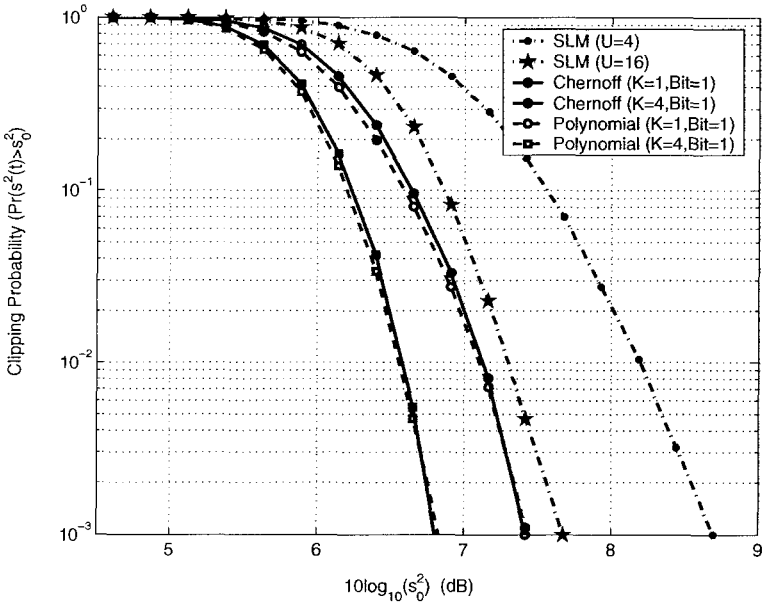

Figure 4.5. *Performance comparison of the SLM algorithm and the proposed algorithms.*

This power increase is much higher than that associated with the scheme in Fig. 4.1b, which is about 0.64 dB.

The computational complexity of the proposed algorithms are compared with those of existing algorithms in Tables 4.4 where the performance of each algorithm is quantified in terms of its PAPR-reduction improvement in dB over the OFDM signal with no PAPR reduction for a clipping probability of 10^{-3}. The computational complexity of the algorithms is measured in terms of the ratio of the CPU time (see footnote on p. 45) required for each algorithm to that of the SLM algorithm with $U = 16$, for which the CPU time was normalized to unity. It can be observed that by combining the proposed polynomial-bound based algorithm with the SR, CDO, and SLM algorithms, improved performance can be achieved with less computation with respect to the performance and computation required by some existing PAPR-reduction algorithms.

From Table 4.4, the following conclusions can be drawn:

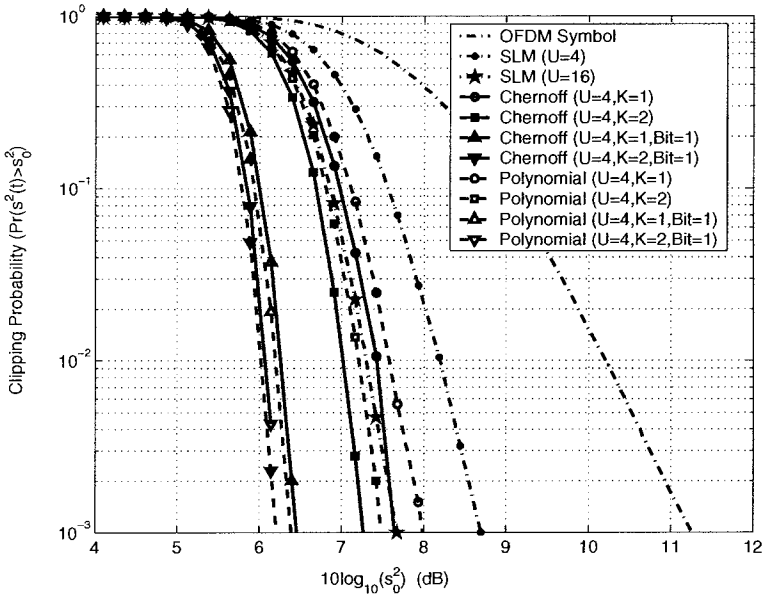

Figure 4.6. *Performance comparison of the SLM algorithms and the proposed algorithms which combine with the SLM algorithm.*

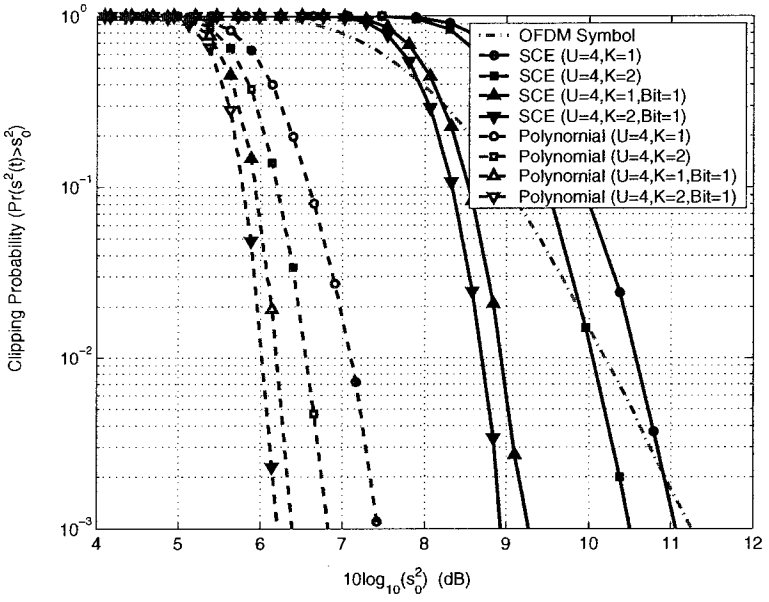

Figure 4.7. *Performance comparison of PAPR-Reduction algorithms using various constellation extension schemes.*

- By combining the proposed polynomial-bound based algorithm with the SR, CDO, and SLM algorithms, improved performance can be achieved for less computation with respect to the SLM algorithm in [38].
- The proposed algorithms offer a tradeoff between performance and computational complexity. For example, if the computational resources available are very limited, then the performance offered by the proposed polynomial-bound based algorithm is marginal; if additional computational resources are available, then improved performance can be achieved by using a combination of the proposed polynomial-bound based algorithm, SR algorithm, and CDO algorithm; if additional side information is available, then the performance can be further improved by also using the SLM algorithm.

Table 4.4. *Performance and Complexity of PAPR-Reduction Algorithms*

Algorithms	SLM Algorithm	Proposed Polynomial-Bound Based Algorithm					
		No SLM ($U = 1$) No CDO ($Bit = 0$)		No SLM ($U = 1$) CDO ($Bit = 1$)		SLM ($U = 4$) CDO ($Bit = 1$)	
	$U = 16$	SR ($K = 4$)	SR ($K = 8$)	SR ($K = 1$)	SR ($K = 4$)	SR ($K = 1$)	SR ($K = 2$)
Performance Gain (dB)	3.4	2.85	3.05	3.8	4.4	4.8	5
Normalized CPU Time	1	0.45	0.95	0.41	0.85	0.83	1.25

4.4 Conclusions

A new constellation extension technique has been developed. Based on a conditional probability method, two new de-randomization algorithms have been proposed for PAPR reduction. The performance of the de-randomization algorithms can be significantly improved by combining them with the selective rotation and coordinate descent optimization algorithms. Simulations have demonstrated that the proposed

algorithms outperform the SLM algorithm in [38] and the SCE algorithm in [44] in terms of PAPR reduction and computational complexity. The performance can be further improved by combining the proposed algorithms with the SLM algorithm.

Chapter 5

ICI Reduction in OFDM Systems

5.1 Introduction

While fast variations of wireless channel characteristics cause ICI in OFDM systems, they also introduce frequency diversity which can be exploited to improve system performance [56]. In this chapter, ICI reduction in OFDM systems is investigated and two new ICI-reduction algorithms for OFDM systems with complex signals are proposed. First, for an OFDM system where 4-QAM is assumed for all subcarriers, a low-complexity ICI-reduction algorithm based on an iterative optimization scheme is proposed. We also propose an ICI-reduction algorithm based on the SD algorithm [52]. By considering channel information, a new search strategy is developed to reduce the computational complexity of the SD algorithm. Design examples are presented, which demonstrate that the proposed iterative ICI-reduction algorithm outperforms several existing algorithms in terms of BER performance and computational complexity. It is also shown that the detection performance can be further improved by using the proposed SD algorithm. Furthermore, it is shown that the proposed algorithms can exploit the frequency diversity introduced by channel variations and, therefore, improved performance can be achieved at higher Doppler frequencies.

The chapter is organized as follows. In Sec. 5.2, following the description of the system configuration and problem formulation, new ICI-reduction algorithms to mitigate the effect of ICI are proposed. In Sec. 5.3, the performance of various ICI-

reduction algorithms are compared by simulations. Conclusions are drawn in Sec. 5.4.

5.2 ICI Reduction in OFDM Systems with Complex Signals

5.2.1 System Configuration

An N-subcarrier OFDM system with complex signals is considered where the modulation scheme for each subcarrier can be either 4-QAM or 16-QAM. A CP with length equal to 20% of the OFDM symbol duration is inserted at the beginning of each OFDM sumbol. The fast-fading channel described in Sec. 2.2.3 is assumed where the length of its impulse response is no longer than that of the CP. At the receiver, after the removal of the CP, the signal is transformed using the DFT before the ICI-reduction algorithms can be applied.

5.2.2 Problem Formulation

It follows from (2.17) and (2.32) that in a fast-fading environment the received signal at any particular subcarrier consists of both the signal component and the ICI component. In an attempt to mitigate the effect of ICI, advanced detection algorithms are required at the receiver. Based on the maximum likelihood detection criterion, the ICI-reduction problem can be formulated as in (2.36), which is essentially a combinatorial optimization problem whose solution requires computational complexity that grows exponentially with the number of variables. The variables in (2.36) are complex. If we let $\mathbf{Y} = \mathbf{Y}_r + j\mathbf{Y}_i$, $\mathbf{A} = \mathbf{A}_r + j\mathbf{A}_i$, and $\mathbf{X} = \mathbf{X}_r + j\mathbf{X}_i$, then the norm in (2.36a) assumes the form

$$\|\tilde{\mathbf{Y}} - \tilde{\mathbf{A}}\tilde{\mathbf{X}}\|_2^2 \tag{5.1a}$$

where

$$\tilde{\mathbf{Y}} = \begin{bmatrix} \mathbf{Y}_r \\ \mathbf{Y}_i \end{bmatrix}, \ \tilde{\mathbf{A}} = \begin{bmatrix} \mathbf{A}_r & -\mathbf{A}_i \\ \mathbf{A}_i & \mathbf{A}_r \end{bmatrix}, \ \tilde{\mathbf{X}} = \begin{bmatrix} \mathbf{X}_r \\ \mathbf{X}_i \end{bmatrix} \tag{5.1b}$$

and the problem in (2.36) can be expressed as

$$\text{minimize} \quad \|\tilde{\mathbf{Y}} - \tilde{\mathbf{A}}\tilde{\mathbf{X}}\|_2^2 \tag{5.2a}$$

$$\text{subject to} : \tilde{X}(i) \in \tilde{\mathcal{M}} \quad \text{for } i = 0, 1, \ldots, 2N-1 \tag{5.2b}$$

where $\tilde{\mathcal{M}}$ represents the set of points associated with the real or imaginary components of the modulation constellation. For the sake of simplicity, 4-QAM modulation is assumed for all subcarriers and, therefore, we have $\tilde{\mathcal{M}} = \{1, -1\}$.

5.2.3 Iterative Optimization Algorithm

For the optimization problem in (5.2) where 4-QAM is adopted for all subcarriers, we propose an ICI-reduction algorithm where the elements of vector $\tilde{X}$ are to be determined iteratively.

Assume that the number and the set of indices of the undetermined elements in vector $\tilde{X}$ during the kth iteration are denoted as N_k and $\mathcal{I}_k$, respectively. During the first iteration, we have $N_1 = 2N$ and $\mathcal{I}_1 = \{0, \ldots, 2N-1\}$. If we define

$$\tilde{\mathbf{X}}_1 = \tilde{\mathbf{X}}(\mathcal{I}_1), \ \tilde{\mathbf{A}}_1 = \tilde{\mathbf{A}}(:, \mathcal{I}_1), \ \tilde{\mathbf{Y}}_1 = \tilde{\mathbf{Y}}, \ \mathbf{B}_1 = 2\tilde{\mathbf{A}}_1^T\tilde{\mathbf{A}}_1, \ \mathbf{b}_1 = -2\tilde{\mathbf{A}}_1^T\tilde{\mathbf{Y}}_1 \tag{5.3}$$

and let $k = 1$, then the problem in (5.2) can be converted to

$$\text{minimize} \quad \frac{1}{2}\tilde{\mathbf{X}}_k^T\mathbf{B}_k\tilde{\mathbf{X}}_k + \tilde{\mathbf{X}}_k^T\mathbf{b}_k \tag{5.4a}$$

$$\text{subject to} : \tilde{X}_k(i) \in \{1, -1\} \quad \text{for } i = 0, \ldots, N_k - 1 \tag{5.4b}$$

If the constraints are satisfied, then $\tilde{\mathbf{X}}_k^T\tilde{\mathbf{X}}_k = N_k$ and the problem in (5.4) can be relaxed to

$$\text{minimize} \quad \frac{1}{2}\tilde{\mathbf{X}}_k^T\mathbf{B}_k\tilde{\mathbf{X}}_k + \tilde{\mathbf{X}}_k^T\mathbf{b}_k \tag{5.5a}$$

$$\text{subject to} : \tilde{\mathbf{X}}_k^T\tilde{\mathbf{X}}_k = N_k \tag{5.5b}$$

The matrix $\mathbf{B}_k$ in (5.5) is a positive definite matrix and, therefore, it can be diagonalized as

$$\mathbf{B}_k = \mathbf{U}_k^T \mathbf{S}_k \mathbf{U}_k \tag{5.6}$$

where $\mathbf{S}_k$ and $\mathbf{U}_k$ are diagonal and orthogonal matrices, respectively. If we let

$$\mathbf{Y}_k = \mathbf{U}_k \tilde{\mathbf{X}}_k \tag{5.7a}$$

$$\tilde{\mathbf{b}}_k = \mathbf{U}_k \mathbf{b}_k \tag{5.7b}$$

and

$$\tilde{\mathbf{X}}_k = \mathbf{U}_k^T \mathbf{Y}_k \tag{5.7c}$$

then the problem in (5.5) can be converted to

$$\text{minimize} \quad \frac{1}{2}\mathbf{Y}_k^T \mathbf{S}_k \mathbf{Y}_k + \mathbf{Y}_k^T \tilde{\mathbf{b}}_k \tag{5.8a}$$

$$\text{subject to :} \quad \mathbf{Y}_k^T \mathbf{Y}_k = N_k \tag{5.8b}$$

Here, we define the Lagrangian

$$L(\mathbf{Y}_k, \lambda_k) = \frac{1}{2}\mathbf{Y}_k^T \mathbf{S}_k \mathbf{Y}_k + \mathbf{Y}_k^T \tilde{\mathbf{b}}_k + \lambda_k (\mathbf{Y}_k^T \mathbf{Y}_k - N_k) \tag{5.9}$$

Using the first-order Karush-Kuhn-Tucker (KKT) conditions, we have

$$\frac{\partial L(\mathbf{Y}_k, \lambda_k)}{\partial \mathbf{Y}_k} = (\mathbf{S}_k + 2\lambda_k \mathbf{I}_k)\mathbf{Y}_k + \tilde{\mathbf{b}} = 0 \tag{5.10}$$

and we see from (5.8) and (5.10) that the solution of the problem in (5.8) can be obtained by solving the problem

$$\mathbf{Y}_k = -(\mathbf{S}_k + 2\lambda_k \mathbf{I}_k)^{-1} \tilde{\mathbf{b}}_k \tag{5.11a}$$

$$\text{subject to :} \quad \mathbf{Y}_k^T \mathbf{Y}_k = N_k \tag{5.11b}$$

On replacing vector $\mathbf{Y}_k$ in (5.11b) using the relationship in (5.11a), we have

$$\tilde{\mathbf{b}}_k^T (\mathbf{S}_k + 2\lambda_k \mathbf{I}_k)^{-2} \tilde{\mathbf{b}}_k = N_k \tag{5.12}$$

where $\mathbf{S}_k + 2\lambda_k \mathbf{I}_k$ is a diagonal matrix. Therefore, (5.12) can be expressed as

$$\sum_{i=0}^{N_k-1} \frac{\tilde{b}_k^2(i)}{[S_k(i) + 2\lambda_k]^2} = N_k \tag{5.13}$$

where $\tilde{b}_k(i)$ and $S_k(i)$ represent the ith element of vector $\tilde{\mathbf{b}}_k$ and the main diagonal of matrix $\mathbf{S}_k$, respectively. The only unknown variable in (5.12) is λ_k and its optimal value can be determined numerically by solving the following one-dimensional optimization problem

$$\text{minimize} \quad \left| \sum_{i=0}^{N_k-1} \frac{\tilde{b}_k^2(i)}{[S_k(i) + 2\lambda_k]^2} - N_k \right| \tag{5.14a}$$

$$\text{subject to :} \quad -\frac{1}{2} \min_{0 \le i \le N_k-1} S_k(i) + \epsilon \le \lambda_k \le \frac{1}{2} \max_{0 \le i \le N_k-1} |\tilde{b}_i| \tag{5.14b}$$

where ϵ is a small positive number. The solution of the problem in (5.13) can be found using, for example, a dichotomous search algorithm. Once λ_k is found, the ith element of vector $\mathbf{Y}_k$ can be computed as

$$Y_k(i) = -\frac{\tilde{b}_k(i)}{S_k(i) + 2\lambda_k} \quad \text{for } i = 0, \ldots, N_k - 1 \tag{5.15}$$

Using (5.7c), an estimation of the vector $\tilde{\mathbf{X}}_k$ can be obtained as

$$\bar{\mathbf{X}}_k = \mathbf{U}_k^T \mathbf{Y}_k \tag{5.16}$$

Binary values for $\hat{\mathbf{X}}_k$ are assigned as

$$\hat{X}_k(i) = \begin{cases} 1 & \text{if } \bar{X}_k(i) > \alpha \\ -1 & \text{if } \bar{X}_k(i) < -\alpha \\ \text{undetermined} & \text{otherwise} \end{cases} \tag{5.17}$$

where $i = 0, \ldots, N_k - 1$ and α is the decision threthold. If $\alpha = 0$, then the decision process in (5.17) becomes the hard decision

$$\hat{\mathbf{X}}_k = \text{sign}\left[\bar{\mathbf{X}}_k\right] \tag{5.18}$$

and all the elements of vector $\hat{\mathbf{X}}_k$ can be determined by using (5.18). If $\alpha > 0$, some of the elements of vector $\bar{\mathbf{X}}_k$ may fall in the region where $|\bar{X}_k(i)| \leq \alpha$, and, therefore, these elements cannot be determined in the current iteration. In such a case, more iterations are needed and a feedback scheme can be exploited. Denoting the set of indices of the elements of $\tilde{\mathbf{X}}$ that have been determined in the kth iteration as $\mathcal{I}_k^d$, we have $\mathcal{I}_{k+1} = \mathcal{I}_k - \mathcal{I}_k^d$ and

$$\begin{aligned} &\tilde{\mathbf{X}}_{k+1} = \tilde{\mathbf{X}}(\mathcal{I}_{k+1}),\ \tilde{\mathbf{A}}_{k+1} = \tilde{\mathbf{A}}(:, \mathcal{I}_{k+1}),\ \tilde{\mathbf{Y}}_{k+1} = \tilde{\mathbf{Y}}_k - \tilde{\mathbf{A}}(:, \mathcal{I}_k^d)\tilde{\mathbf{X}}(\mathcal{I}_k^d) \\ &\mathbf{B}_{k+1} = 2\tilde{\mathbf{A}}_{k+1}^T\tilde{\mathbf{A}}_{k+1},\ \mathbf{b}_{k+1} = -2\tilde{\mathbf{A}}_{k+1}^T\tilde{\mathbf{Y}}_{k+1} \end{aligned} \tag{5.19}$$

Based on the updated variables in (5.19), a similar optimization problem of reduced size can be formulated as in (5.2) for the $(k+1)$th iteration, which can be solved following the same procedure. When all the elements of vector $\tilde{\mathbf{X}}$ are determined, i.e., set $\mathcal{I}_{k+1}$ is empty, the algorithm terminates. A step-by-step description of the above algorithm is listed in Table 5.1.

5.2.4 Sphere Decoding Algorithm

SD algorithms have been widely used to solve integer least-squares (LS) problems [52]-[54]. One technical difficulty associated with SD algorithms is the high computational complexity, i.e., its solution requires computational complexity that grows exponentially with the number of variables. In what follows, we describe an enhanced sphere decoding algorithm for the ICI-reduction problem in (5.2), where a new search strategy for the reduction of the complexity of the SD algorithm is developed. Note that although the proposed algorithm is developed for ICI reduction in OFDM systems where 4-QAM is assumed for all subcarriers, the algorithm can be easily extended and applied to OFDM systems using other modulation schemes.

In an attempt to improve the detection performance, vector $\tilde{\mathbf{X}}$ is re-ordered according to the asymptotic effective energy of each element [73] and the columns of matrix $\tilde{\mathbf{A}}$ are re-ordered accordingly. Let $\mathbf{s} = \text{order}(\tilde{\mathbf{X}})$ and $\mathbf{G} = \text{order}(\tilde{\mathbf{A}})$ represent

Table 5.1. *An Iterative Optimization Algorithm for ICI Reduction*

Step 1

Set $k = 1$ and input the decision threthold α.

Initialize the variables N_k, $\mathcal{I}_k$, $\tilde{\mathbf{X}}_k$, $\tilde{\mathbf{A}}_k$, $\tilde{\mathbf{Y}}_k$, $\mathbf{B}_k$, and $\mathbf{b}_k$ as in (5.3).

Step 2

Formulate the optimization problem as in (5.4).

Find λ_k by solving the problem in (5.14).

Compute $\bar{\mathbf{X}}_k$ using (5.15) and (5.16).

Compute $\hat{\mathbf{X}}_k$ using (5.17).

Find $\mathcal{I}_k^d$ and compute $\mathcal{I}_{k+1}$.

Step 3

If $\mathcal{I}_{k+1}$ is empty, then output the detected vector $\hat{\mathbf{X}}$ and stop; otherwise, compute the variables N_{k+1}, $\mathcal{I}_{k+1}$, $\tilde{\mathbf{X}}_{k+1}$, $\tilde{\mathbf{A}}_{k+1}$, $\tilde{\mathbf{Y}}_{k+1}$, $\mathbf{B}_{k+1}$, and $\mathbf{b}_{k+1}$ using (5.19).

Set $k = k + 1$, and repeat from Step 2.

the re-ordered vector $\tilde{\mathbf{X}}$ and matrix $\tilde{\mathbf{A}}$, respectively. The objective function in (5.2a) becomes

$$\|\tilde{\mathbf{Y}} - \tilde{\mathbf{A}}\tilde{\mathbf{X}}\|_2^2 = \|\tilde{\mathbf{Y}} - \mathbf{G}\mathbf{s}\|_2^2 \tag{5.20}$$

and the problem in (5.2) can be written as

$$\text{minimize} \quad \|\tilde{\mathbf{Y}} - \mathbf{G}\mathbf{s}\|_2^2 \tag{5.21a}$$

$$\text{subject to} : s_i \in \{1, -1\} \quad \text{for } i = 0, 1, \ldots, 2N - 1 \tag{5.21b}$$

where s_i represents the ith element of vector $\mathbf{s}$. By applying the QR-decomposition to matrix $\mathbf{G}$, we write

$$\mathbf{G} = \mathbf{Q}\mathbf{R} \tag{5.22}$$

where $\mathbf{Q}$ and $\mathbf{R}$ are orthogonal and upper triangular matrices, respectively. If we let

$$\mathbf{p} = \mathbf{Q}^T\tilde{\mathbf{Y}} \tag{5.23}$$

then the objective function in (5.21a) can be obtained as

$$\|\tilde{\mathbf{Y}} - \mathbf{Gs}\|_2^2 = \|\mathbf{Q}^T \left(\tilde{\mathbf{Y}} - \mathbf{Gs}\right)\|_2^2 = \|\mathbf{p} - \mathbf{Rs}\|_2^2 \tag{5.24}$$

and the problem in (5.21) can be reformulated as

$$\text{minimize} \quad \|\mathbf{p} - \mathbf{Rs}\|_2^2 \tag{5.25a}$$

$$\text{subject to} : s_i \in \{1, -1\} \quad \text{for } i = 0, 1, \ldots, 2N-1 \tag{5.25b}$$

The solution of the integer LS problem in (5.25) can be obtained by applying an SD algorithm [52] that takes into account the special structure of $\mathbf{R}$.

The basic idea of an SD algorithm is to search only lattice points that lie in a certain hypersphere of radius r around the given vector $\mathbf{p}$ so as to reduce the search space compared with that of the exhaustive search algorithms. Note that a necessary and sufficient condition for a point $\mathbf{Rs}$ to lie within the hypersphere of radius r is that the modulus of distance vector between the point $\mathbf{Rs}$ and the center point $\mathbf{p}$ is less than the radius, i.e.,

$$\|\mathbf{p} - \mathbf{Rs}\|_2^2 \leq r^2 \tag{5.26a}$$

which can also be written as

$$\sum_{i=0}^{2N-1} \left(p_i - \sum_{j=i}^{2N-1} R_{ij} s_j \right)^2 \leq r^2 \tag{5.26b}$$

where p_i and R_{ij} represent the ith element of $\mathbf{p}$ and the (i,j)th element of $\mathbf{R}$, respectively. The left-hand side (l.h.s.) of (5.26b) can be expanded as

$$(p_{2N-1} - R_{2N-1,2N-1} s_{2N-1})^2 + (p_{2N-2} - R_{2N-2,2N-1} s_{2N-1} - R_{2N-2,2N-2} s_{2N-2})^2 + \ldots \leq r^2 \tag{5.27}$$

By considering only the first term on the l.h.s. of (5.27), a necessary condition for $\mathbf{Rs}$ to lie within the hypersphere can be obtained as

$$(p_{2N-1} - R_{2N-1,2N-1} s_{2N-1})^2 \leq r^2 \tag{5.28}$$

and the feasible region for s_{2N-1} can be obtained as

$$\left\lceil \frac{-r + p_{2N-1}}{R_{2N-1,2N-1}} \right\rceil \leq s_{2N-1} \leq \left\lfloor \frac{r + p_{2N-1}}{R_{2N-1,2N-1}} \right\rfloor \tag{5.29}$$

where $\lceil \cdot \rceil$ and $\lfloor \cdot \rfloor$ represent the ceiling and floor functions, respectively. Note that if we let

$$r_{2N-1} = r, \; p_{2N-1,2N} = p_{2N-1} \tag{5.30a}$$

then (5.29) can be expressed as

$$\left\lceil \frac{-r_{2N-1} + p_{2N-1,2N}}{R_{2N-1,2N-1}} \right\rceil \leq s_{2N-1} \leq \left\lfloor \frac{r_{2N-1} + p_{2N-1,N}}{R_{2N-1,2N-1}} \right\rfloor \tag{5.30b}$$

By considering the first two terms on the l.h.s. of (5.27), an improved necessary condition can be obtained as

$$(p_{2N-2,2N-1} - R_{2N-2,2N-2} s_{2N-2})^2 \leq r_{2N-2}^2 \tag{31a}$$

where

$$\begin{aligned} r_{2N-2}^2 &= r_{2N-1}^2 - (p_{2N-2} - R_{2N-1,2N-1} s_{2N-1})^2 \\ p_{2N-2,2N-1} &= p_{2N-1} - R_{2N-2,2N-1} s_{2N-1} \end{aligned} \tag{31b}$$

Thus, the feasible region of s_{2N-2} can be obtained as

$$\left\lceil \frac{-r_{2N-2} + p_{2N-2,2N-1}}{R_{2N-2,2N-2}} \right\rceil \leq s_{2N-2} \leq \left\lfloor \frac{r_{2N-2} + p_{2N-2,2N-1}}{R_{2N-2,2N-2}} \right\rfloor \tag{5.32}$$

In a similar fashion, the remaining elements of $\mathbf{s}$ can be obtained successively as

$$\left\lceil \frac{-r_k + p_{k,k+1}}{R_{k,k}} \right\rceil \leq s_k \leq \left\lfloor \frac{r_k + p_{k,k+1}}{R_{k,k}} \right\rfloor \tag{5.33a}$$

for $k = 2N-3, \ldots, 1$, where

$$\begin{aligned} p_{k,k+1} &= p_k - \sum_{i=k+1}^{2N-1} R_{k,i} s_i \\ r_k^2 &= r_{k+1}^2 - \left(p_{k+1} - \sum_{i=k+1}^{2N-1} R_{k+1,i} s_i \right)^2 \end{aligned} \tag{5.33b}$$

Based on the feasible region of s_k in (5.33a), one can determine the value of s_k accordingly. It can be observed that the above procedure actually constructs a binary tree, as illustrated in Fig. 5.1, where the branches at the kth level of the tree represent the possible values of the kth component of vector $\mathbf{s}$. Each path in the binary tree from top to bottom, i.e., level $2N-1$ to level 0, represents a vector $\mathbf{s}$ such that point $\mathbf{Rs}$ lies in the hypersphere. By using the above procedure, all lattice points in the hypersphere can be determined and the solution of the problem in (5.25) can be obtained by finding the path such that the distance between the corresponding point and the center point is minimized.

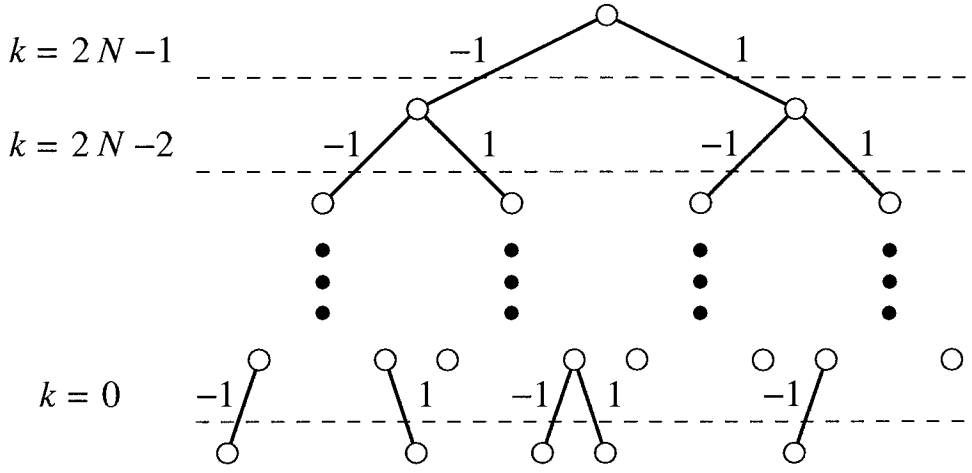

Figure 5.1. *A binary tree constructed for the search of lattice points in a 2N-dimensional hypersphere.*

Although the idea of an SD algorithm is quite simple, several key problems have to be considered in an attempt to design an efficient SD algorithm. First, we need to choose an appropriate initial radius of the $2N$-dimensional hypersphere. Several choices for the initialization of the radius have been proposed [53][54]. In our algorithm, the initial radius of the $2N$-demensional hypersphere is set to a very large value. Thus, it is guaranteed that a point inside the hypersphere can be found. Once this is done, the radius of the hypersphere can be replaced by the distance between

the newly found point and the center point.

Next, we need to determine the sequence of the binary tree search. A commonly used search strategy is the depth-first search [53][54][74] where the left subtree is always visited before the right subtree of the same parent node. In order to explain the tree search process, a $2N$-by-2 matrix $\mathbf{B}$ is defined to indicate the status of the branches along the search path, where $B(k,1)$ and $B(k,2)$ for $k = 2N-1, \ldots, 0$ indicate the status of the left and right branches at the kth level, respectively. For example, if $s_k = -1$ falls into the feasible region in (5.33a), then the left branch at the kth level is open and $B(k,1) = 1$. Otherwise, the left branch at the kth level is closed and $B(k,1) = 0$. A node at level k is said to be a *dead node* if its sub-branches are both closed, i.e., $B(k,1) = B(k,2) = 0$. In an attempt to avoid repetitions, the branches that have been visited are kept closed.

Since the initial radius is set to a very large value, the first point inside the hypersphere is found to be $\mathbf{s}_1^\star = [-1 \ -1 \ \cdots \ -1]^T$. In such a case, we have $B(k,1) = 0$ and $B(k,2) = 1$ for $k = 2N-1, \ldots, 0$. Once $\mathbf{s}_1^\star$ is found, the radius of the hypersphere can be updated as $r_{2N-1} = \|\mathbf{p} - \mathbf{R}\mathbf{s}_1^\star\|_2$. The feasible region for each element of $\mathbf{s}$ and matrix $\mathbf{B}$ can be updated accordingly. Next, we go up one level and check whether the right branch at level 1 is open. If so, the right branch is visited and another point inside the hypersphere is found to be $\mathbf{s}_2^\star = [-1 \ -1 \ \cdots \ -1 \ 1]^T$. Then the radius of the hypersphere, the feasible region for each element in $\mathbf{s}$, and matrix $\mathbf{B}$ can be updated accordingly. Otherwise, we go up one level and check whether the right branch at level 2 is open. The procedure is continued until a right branch is found to be open, and that branch is visited and its subtree is searched in a similar manner. The search continues until there are no open branch at all levels. At this point, the current point $\mathbf{s}^\star$ is the exact solution of the problem in (5.25). A step-by-step description of the above algorithm is described in Table. 5.2.

There are several drawbacks in the above SD algorithm. First, since the left subtree is always visited before the right subtree of the same parent node, the algorithm

Table 5.2. *A Sphere Decoding Algorithm Using Depth-First Search*

Step 1 Input $\mathbf{Y}$, $\mathbf{A}$, $\mathbf{X}$.

Calculate $\mathbf{p}$ and $\mathbf{R}$ using (5.22) and (5.23).

Set $l = 0$ (number of points inside the hypersphere), $r = \infty$.

Set $k = 2N - 1$ (branch level), $r_k = r$, $p_{k,k+1} = p_k$, $\mathbf{B} = \text{zeros}(2N, 2)$.

Step 2 Find the feasible region of s_k using (5.33) and update $B(k, :)$.

Step 3 If $k = 0$, then go to **Step 5**.

If $k = 2N - 1$ and $B(k, 1) = B(k, 2) = 0$, then go to **Step 6**.

Step 4 If $B(k, 1) = 1$, let $s_k^\star = -1$, $B(k, 1) = 0$, $k = k - 1$, and go to **Step 2**.

If $B(k, 2) = 1$, let $s_k^\star = 1$, $B(k, 2) = 0$, $k = k - 1$, and go to **Step 2**.

Let $B(0 : k, :) = \text{ones}(k + 1, 2)$, $k = k + 1$, and go to **Step 3**.

Step 5 If $B(k, 1) = 1$, then $s_k^\star = -1$, $l = l + 1$, save the solution $\mathbf{s}_l^\star = \mathbf{s}$.

Update the radius of the hypersphere as $r_{2N-1} = \|\mathbf{p} - \mathbf{R}\mathbf{s}_l^\star\|_2$.

Find the feasible region of s_k for $k = 2N - 1, \ldots, 0$ using (5.33).

Update matrix $\mathbf{B}$ while keeping the visited branches closed.

Go to **Step 3**.

If $B(k, 2) = 1$, then $s_k^\star = 1$, $l = l + 1$, save the solution $\mathbf{s}_L^\star = \mathbf{s}$.

Update the radius of the hypersphere as $r_{2N-1} = \|\mathbf{p} - \mathbf{R}\mathbf{s}_l^\star\|_2$.

Find the feasible region of s_k for $k = 2N - 1, \ldots, 0$ using (5.33).

Update matrix $\mathbf{B}$ while keeping the visited branches closed.

Let $B(k, :) = \text{ones}(1, 2)$, $k = k + 1$, and go to **Step 4**.

Let $B(k, :) = \text{ones}(1, 2)$, $k = k + 1$, and go to **Step 4**.

Step 6 Output $\mathbf{s} = \mathbf{s}_l^\star$ as the solution of the problem in (5.25) and stop.

may not achieve the current best solution. Second, if the exact solution is located in the most right side of the binary tree, then the efficiency of the algorithm becomes quite low. Third, even if the exact solution is found, the algorithm will not stop until the rest of the tree is checked. If there are many other solutions which give similar

values of the objective function to that given by the exact solution, then the complexity of the algorithm can be extremely high. In what follows, remedies to these technical drawbacks are proposed.

In an attempt to find the current best solution, say, at the kth level, we can choose the value that minimizes r_{k-1} as the first choice of s_k, i.e.,

$$s_k^\star = \arg\left(\min_{s_k\in\{-1,1\}} r_{k-1}\right) \tag{5.34a}$$

In other words, the branch which generates larger reduction in the value of the objective function in (5.25) is visited before the other branch of the same parent node. This scheme is a *greedy scheme* in that it always pursues the current best solution without considering the performance of the following steps.

In an attempt to improve the search efficiency of the algorithm, a probabilistic search strategy is proposed which maximizes the probability that the current solution be optimal. In a high signal-to-noise (SNR) region, the probability of detection error in two or more bits is much smaller than that of detection error in one bit. Therefore, our main concern is to increase the probability that a one-bit detection error is corrected. It can be shown [54] that if only one bit of vector $\mathbf{s}^\star$ is detected incorrectly, then the probability that the detection error occurs in $s_k^\star$ is inversely related to the absolute value of $R_{k,k}$. Let the elements on the main diagonal of $\mathbf{R}$ be ordered from smallest to largest according to their absolute values. For all the open branches along a path, the branch associated with the smallest absolute value of $R_{k,k}$ is visited first. Such a search strategy maximizes the probability that a one-bit detection error can be corrected.

In an attempt to reduce the complexity of the algorithm, a stopping criterion is proposed as follows. Once a point inside the hypersphere is found, we count the number of further search steps. If this number reaches a predefined threshold before a new point inside the hypersphere is found, then the algorithm is stopped and the current solution is taken to be the final solution to the problem. Our simulation studies have

demonstrated that if this pre-defined number is chosen carefully, the complexity of the algorithm can be reduced without significant degradation in performance.

An SD algorithm which incorporates the above idea is as follows. At the beginning of the tree search, a depth-first search strategy is used until the first point inside the hypersphere is found. The first solution and the path corresponding to this solution can be denoted as $\mathbf{s}_1^\star$ and P_1, respectively. The radius of the hypersphere can be updated as $r_{2N-1} = \|\mathbf{p} - \mathbf{R}\mathbf{s}_1^\star\|_2$. The matrix $\mathbf{B}_1$ is updated accordingly, where the subscript indicates that this matrix is used to represent the status of the branches characterized by path P_1. For all open branches described by path P_1, the one associated with the smallest absolute value of $R_{k,k}$ is visited, and its subtree is searched using the depth-first strategy until another point inside the hypersphere $\mathbf{s}_2^\star$ is found or a dead node is reached. This path is denoted as P_2. If $\mathbf{s}_2^\star$ is found, then the radius of the hypersphere is updated as $r_{2N-1} = \|\mathbf{p} - \mathbf{R}\mathbf{s}_2^\star\|_2$ and the matrix $\mathbf{B}$ can be updated accordingly. At this point we have two paths, P_1 and P_2. For all open branches along these two paths, the one associated with the smallest absolute value of $R_{k,k}$ is visited. The search continues until the stopping criterion is satisfied. A step-by-step description of the algorithm is listed in Table 5.3.

5.3 Simulations

The proposed ICI-reduction algorithms were applied to an OFDM system where the number of subcarriers was chosen to be 64 and 4-QAM was adopted as the modulation scheme for each subcarrier. The bandwidth of the OFDM system and the carrier frequency were set to $B = 200$ kHz and $f_c = 2$ GHz, respectively. The length of the CP was set to $N_p T_c = (N/8)T_c = T_s/8$, where T_s and T_c are the time durations of OFDM symbols and chips, respectively. A two-tap Rayleigh fading channel model [46] was assumed, where the Doppler frequency of the channel is denoted as f_D. While the delay of the first tap was zero, the delay of the second tap was randomly generated

Table 5.3. *A Sphere Decoding Algorithm for ICI Reduction*

Step 1 Input $\mathbf{Y}$, $\mathbf{A}$, $\mathbf{X}$.

Input L (maximum paths) and itr_{max} (maximum number ofsearches).

Calculate $\mathbf{p}$ and $\mathbf{R}$ using (5.22) and (5.23).

Set $l = 0$ (number of paths recorded) and $itr = 0$ (number of searches).

Set $k = 2N - 1$ (branch level), $r_k = \infty$, $p_{k,k+1} = p_k$, and $\mathbf{B} = \text{zeros}(2N, 2)$.

Step 2 Find the first solution $\mathbf{s}_1^\star$ using the depth-first search.

$l = l + 1$, update the radius of the hypersphere and matrix $\mathbf{B}_l$.

Step 3 For all recorded paths, find out the open branch with the smallest absolute value of $R_{k,k}$. Search the corresponding subtree using the depth-first search.

Step 4 If a solution is found, then set $itr = 0$, $l = l + 1$, and update the radius of the hypersphere. Update $\mathbf{B}_i$ for $i = 1, \ldots, l$.

If $l > L$, then for all paths calculate the smallest $R_{k,k}$ associated with its open branch and delete the path whose smallest absolute value of $R_{k,k}$ is most significant. Go to **Step 3**.

Otherwise, go to **Step 3**.

Otherwise, set $l = l + 1$, $itr = itr + 1$, update matrix $\mathbf{B}_l$.

If $itr > itr_{max}$, then go to **Step 5**.

If $l > L$, then for all paths calculate the smallest $R_{k,k}$ associated with its open branch and delete the path whose smallest absolute value of $R_{k,k}$ is most significant. Go to **Step 3**.

Otherwise, go to **Step 3**.

Step 5 Output $\mathbf{s} = \mathbf{s}_l^\star$ as the solution of the problem in (5.25) and stop.

with uniform distribution from $\{T_c, 2T_c, \ldots, N_pT_c\}$. The BER performance of the proposed algorithm was evaluated and compared with that of several existing algo-

rithms under a variety of system configurations. For the proposed SD algorithm, the maximum number of paths recorded and the maximum search steps allowed between two solutions were denoted as L and itr_{max}, respectively. For the DF algorithm in [46], the number of neighbouring subcarriers that were used to suppress the ICI at a particular subcarrier was taken to be $2K + 1$.

Example: First we considered an OFDM system where $f_D T_s = 0.1$. For the proposed SD algorithm with $L = 40$ and $itr_{max} = 10^5$, the BER versus the ratio of energy-per-bit to spectral noise density (Eb/N0) is plotted as the solid curve in Fig. 5.2. For the proposed iterative optimization algorithm with $\alpha = 0.9$ or $a = 1.0$, the BER versus Eb/N0 is plotted in Fig. 5.2 as the dash-dotted and dash curves, respectively. For the sake of comparison, the BER of the DF algorithm in [46] is plotted in the same figure for various values of K. It is shown that improved performance can be obtained by the proposed algorithms compared with that of the DF algorithm. For example, at the BER level of 10^{-3}, a 0.5-dB and 2-dB improvement of Eb/N0 can be achieved by the iterative optimization algorithm with $\alpha = 0.9$ and the SD algorithm, respectively, compared with the DF algorithm with $K = 15$. It was found out that the CPU time required by the iterative optimization algorithm with $\alpha = 0.9$ is only 80% that required by the DF algorithm with $K = 15$.

The performance of the ICI-reduction algorithms for the cases where $f_D T_s = 0.25$ is plotted in Fig. 5.3. As can be seen, the performance of the proposed algorithms improve with the increase in Doppler frequency. For example, for the proposed SD algorithm, while for the case of $f_D T_s = 0.1$ an $Eb/N0$ ratio of 27 dB is required to achieve the BER level of 10^{-3}, for the case of $f_D T_s = 0.25$ an $Eb/N0$ ratio of 24.5 dB is required to achieve the same BER level. This improvement with increasing f_D can be attributed to the increase in frequency diversity introduced by the higher Doppler frequency [56].

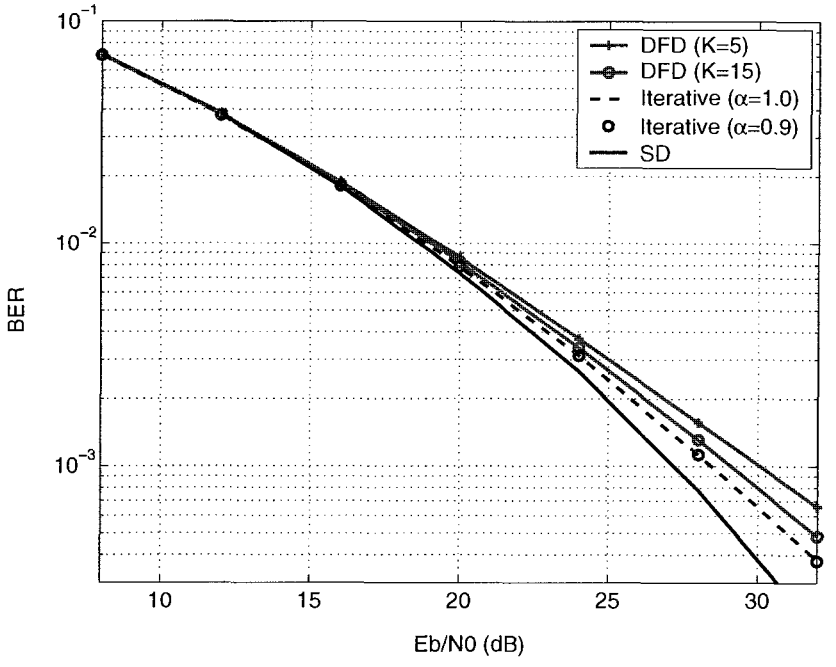

Figure 5.2. *Performance comparision of ICI-reduction algorithms.*

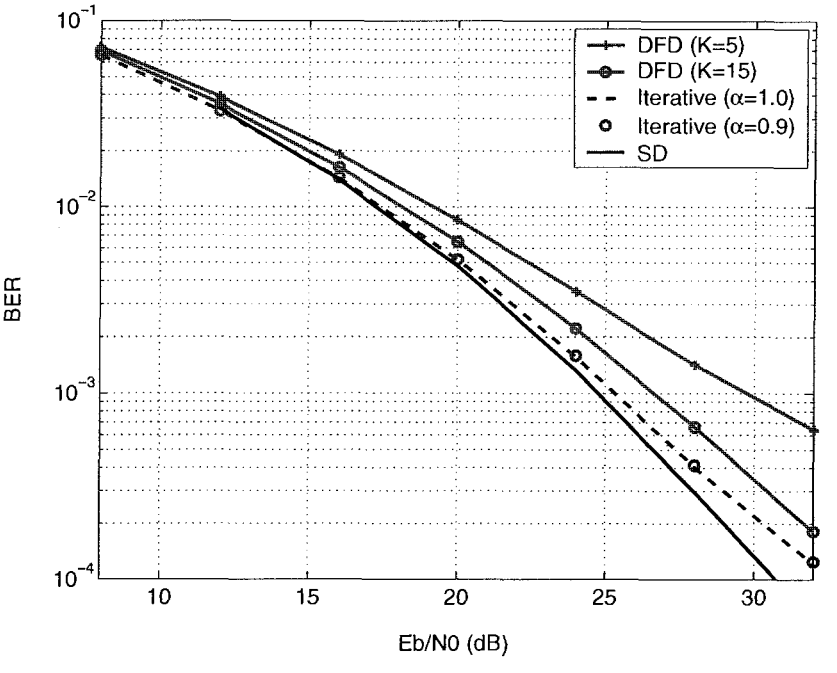

Figure 5.3. *Performance comparision of ICI-reduction algorithms.*

5.4 Conclusions

A new iterative optimization algorithm for ICI reduction has been proposed, which outperforms several existing algorithms in terms of bit-error-rate performance and computational complexity. The ICI-reduction performance can be further improved by using the proposed SD algorithm. It has also been shown that the proposed algorithms can exploit the frequency diversity introduced by channel variations and, therefore, improved performance can be achieved at higher Doppler frequencies.

Chapter 6

Conclusions and Future Work

6.1 Conclusions

Several PAPR-reduction and ICI-reduction algorithms have been proposed in Chapters 3 to 5 for a variety of OFDM systems. Chapter 3 describes an LP-based algorithm for PAPR reduction in OFDM systems with real signals and the accelerated *least-pth* algorithm for PAPR reduction in OFDM systems with complex signals. Chapter 4 describes the de-randomization algorithm, the SR algorithm, and the CDO algorithm for PAPR reduction in OFDM systems with complex signals. Chapter 5 describes the iterative optimization algorithm and the SD algorithm for ICI reduction in OFDM systems with complex signals.

6.1.1 PAPR Reduction in OFDM Systems with Real Signals

In Sec. 3.2, a new constellation extension technique has been proposed for PAPR reduction, where the modulation constellation at active subcarriers and the modulation symbols in unused subcarriers are continuously modified. Using this technique, the PAPR-reduction problem for OFDM systems with real signals has been formulated as an LP problem where the number of constraints is much larger than that of the variables. The solution of the problem has been obtained by using a Newton algorithm [48].

Simulations have demonstrated that by using the proposed LP-based algorithm

considerable performance improvement can be achieved relative to that achieved with the algorithm in [41] and the ASE algorithm in [42]. The performance improvement is achieved at the cost of a slight increase in the transmit power.

6.1.2 PAPR Reduction in OFDM Systems with Complex Signals

In Sec. 3.3, the constellation extension technique proposed in Sec. 3.2 has been applied for PAPR reduction in OFDM systems with complex signals. The PAPR-reduction problem was formulated as a minimax optimization problem and an accelerated *least-pth* algorithm [49] has been proposed. Our simulations have demonstrated that the proposed algorithm offers considerable performance improvement over the ASE algorithm [42] in many practical situations. Improved PAPR reduction can be achieved when the accelerated *least-pth* algorithm is combined with the SLM algorithm [38]. Furthermore, the accelerated *least-pth* algorithm offers a tradeoff between performance and computational complexity, which can often be used to advantage in a number of applications.

In Chapter 4, a new constellation extension technique for PAPR reduction in OFDM systems with complex signals has been developed whereby the data are represented either by points in the original constellation or by extended points. In order to find the optimal representation of the OFDM signal, two de-randomization algorithms have been proposed by applying the so called conditional probablity method, i.e., the Chernoff-bound based and the polynomial-bound based algorithms. In an attempt to further improve the performance, the SR and CDO algorithms have been proposed.

It has been demonstrated by simulations that the de-randomization algorithms outperform the SLM algorithm [38] and the SCE algorithm [44] in terms of PAPR reduction and computational complexity. The polynomial-bound based algorithm

offers similar performance as the Chernoff-bound based algorithm with much less computation. It has also been shown that the performance can be further improved by combining the proposed de-randomization, SR, and CDO algorithms with the SLM algorithm [38].

6.1.3 ICI Reduction in OFDM Systems

Chapter 5 dealt with ICI reduction in OFDM systems with complex signals in fast time-varying channels. While fast variations of wireless channel characteristics cause ICI in OFDM systems, they also introduce frequency diversity which can be exploited to improve the detection performance [56]. Two new algorithms have been proposed for ICI reduction. For OFDM systems using 4-QAM for all subcarriers, a low-complexity ICI-reduction algorithm based on an iterative optimization algorithm was proposed. For OFDM systems using high-order modulation, an ICI-reduction algorithm based on the SD algorithm [52] was proposed. By considering channel information, a new search strategy has been developed to reduce the computational complexity of the SD algorithm.

It has been demonstrated that the proposed iterative algorithm and the SD algorithms outperform several existing algorithms in terms of BER performance. In addition, the proposed algorithms can exploit the frequency diversity introduced by the channel variations and, therefore, improved performance can be achieved at higher Doppler frequencies.

6.2 Future Work

In what follows, two research topics that would extend the presented work are proposed.

6.2.1 PAPR Reduction in OFDM Systems with Complex Signals

Although the PAPR-reducton algorithms described offer improved performance when compared with several existing algorithms, the computational complexity involved is still high for application in a communication terminal. In [75]-[76], several low-complexity PAPR-reduction algorithms have been proposed based on a peak-cancelling method. By combining the proposed algorithms with the peak-cancelling algorithms reported, it should be possible to achieve a balance between reduction in PAPR and reduction in computational complexity. Peak-cancelling algorithms tend to introduce distortion and the effect of distortion in combined algorithms needs to be investigated carefully.

6.2.2 ICI Reduction in OFDM Systems with Complex Signals

ICI reduction in OFDM systems with complex signals has been investigated in Chapter 5 and several detection algorithms have been proposed to achieve *near-optimal* solutions for the case where hard decisons are applied. Nevertheless, no coding scheme has been considered. In practice, forward error-correction coding is applied in OFDM systems to mitigate the effects of channel impairment [10]-[12]. In this regard, it is worthwhile to extend the current work to take into account the coding schemes used in OFDM systems.

In an attempt to improve the decoding performance, intense research has been focused on soft iterative decoding algorithms, and results have been reported on iterative decoding of concatenated codes with system performance approaching the Shannon limit in single-input single-output systems (see [77] and references cited there). In iterative decoding algorithms, a critical step is to calculate the *a posteriori* probability of each bit of the transmitted signal. For multiple-input multiple-output

systems (MIMO), it is not clear what is the best way to obtain such soft information with less computation. It has been noted in [78] that if soft information is obtained by means of an exhaustive search, the computational complexity grows exponentially with the number of variables. It has been shown in Chapter 2 that an OFDM system in a fast time-varying channel is equivalent to a MIMO system. Hence, for OFDM systems with a large number of subcarriers, the exhaustive search for soft information is intractable in practice. Therefore, the development of feasible iterative decoding algorithms should be explored for ICI reduction in OFDM systems with complex signals where forward error-control coding schemes are involved.

Bibliography

[1] J. Bingham, "Multicarrier modulation for data transmission: an idea whose time has come," *IEEE Commun. Mag.*, pp. 5-14, May 1990.

[2] R. V. Nee and R. Prasad, *OFDM for Wireless Multimedia Communications*, Artech House Publisher, 2000.

[3] R. W. Chang, "Synthesis of band-limited orthogonal signals for multichannel data transmission," *Bell Syst. Tech. J.*, vol. 45, pp. 1775-1796, Dec. 1966.

[4] B. R. Salzberg, "Performance of an efficient parallel data transmission system," *IEEE Trans. Commun. Tech.*, vol. COM-15, pp. 805-813, Dec. 1967.

[5] R. W. Chang, "Orthogonal frequency division multiplexing," *U.S. Patent*, no. 3488445, Jan. 1970.

[6] S. B. Weinstein and P. M. Ebert, "Data transmission by frequency-division multiplexing using the discrete Fourier transform," *IEEE Trans. Commun. Tech.*, vol. COM-19, pp. 628-634, Oct. 1971.

[7] J. W. Cooley and J. W. Tukey, "An algorithm for the machine calculation of complex Fourier series," *Math. Comp.*, vol. 19, pp. 297-301, 1965.

[8] W. Y. Zou and Y. Wu, "COFDM: an overview," *IEEE Trans. Broadcast.*, vol. 41, pp. 1-8, Mar. 1995.

[9] A. Peled and A. Ruiz, "Frequency domain data transmission using reduced computational complexity algorithms," *Proc. IEEE Int. Conf. Acoustics, Speech, and Signal Processing*, vol. 5, pp. 964-967, Apr. 1980.

[10] P. G. M. de Bot and P. M. J. Baggen, "Error correcting coding for OFDM broadcasting over frequency selective channels," *Proc. IEE Coll. Digital Terr. Telev.*, vol. 3, pp. 1-4, Nov. 1993.

[11] B. Le Floch, M. Alard, and C. Berrou, "Coded orthogonal frequency division multiplex," *Proc. IEEE*, vol. 83, pp. 982-996, Jun. 1995.

[12] R. D. Wesel and J. M. Cioffi, "Fundamentals of coding for broadcast OFDM," *Proc. IEEE Asilomer Conf. Signals, Systems, and Computers*, vol. 1, pp. 2-6, Nov. 1995.

[13] ETSI, "Radio broadcasting systems: digital audio broadcasting to mobile,

portable and fixed receivers," *European Telecommunication Standard*, ETS 300-401, Feb. 1995.

[14] ETSI, "Digital video broadcasting: framing structure, channel coding, and modulation for digital terrestrial television," *European Telecommunication Standard*, ETS 300-744, Aug. 1997.

[15] IEEE 802.11, "IEEE standard for wireless LAN medium access control (MAC) and physical layer (PHY) specifications," Nov. 1997.

[16] C. Rapp, "Effects of HPA-nonlinearity on a 4-DPSK/OFDM signal for a digital sound boradcasing system," *Proc. Second Euro. Satellite Commun.*, pp. 179-184, Oct. 1991.

[17] S. Merchan, A. G. Armada, and J. L. Garcia, "OFDM performance in amplifier nonlinearity," *IEEE Trans. Broadcast.*, vol. 44, pp. 106-114, Mar. 1998.

[18] T. Pollet, M. van Bladel, and M. Moeneclaey, "BER sensitivity of OFDM systems to carrier frequency offset and wiener phase noise," *IEEE Trans. Commun.*, vol. 43, pp. 191-193, Feb.-Apr. 1995.

[19] M. Russell and G. L. S. Stuber, "Interchannel interference analysis of OFDM in a mobile environment," *Proc. IEEE Conf. Vehicular Tech.*, vol. 2, pp. 820-824, Jul. 1995.

[20] P. Robertson and S. Kaiser, "The effects of Dopper spreads in OFDM(A) mobile radio systems," *Proc. IEEE Conf. Vehicular Tech.*, vol. 1, pp. 329-333, Sep. 1999.

[21] P. Robertson and S. Kaiser, "Analysis of the loss of orthogonality through Doppler spread in OFDM systems," *Proc. IEEE Conf. Global Telecomm.*, vol. 1b, pp. 701-706, Dec. 1999.

[22] Y. Li and L. J. Cimini, Jr., "Bounds on the interchannel interference of OFDM in time-varying impairments," *IEEE Trans. Commun.*, vol. 49, pp. 401-404, Mar. 2001.

[23] P. H. Moose, "A technique for orthogonal frequency division multiplexing frequency offset correction," *IEEE Trans. Commun.*, vol. 42, pp. 2908-2914, Oct. 1994.

[24] M. Luise and R. P. H. Reggiannini, "Carrier frequency acquisition and tracking for OFDM systems," *IEEE Trans. Commun.*, vol. 44, pp. 1590-1598, Nov. 1996.

[25] T. M. Schmidl and D. C. Cox, "Robust frequency and timing synchronization for OFDM," *IEEE Trans. Commun.*, vol. 45, pp. 1613-1621, Dec. 1997.

[26] J. J. van de Beek, M. Sandell, and P. O. Borjesson, "ML estimation of time

and frequency offset in OFDM systems," *IEEE Trans. Signal Process.*, vol. 45, pp. 1800-1805, Jul. 1997.

[27] M. Hlaing Minn, V. K. Bhargava, and K. B. Letaief, "A robust timing and frequency synchronization for OFDM systems," *IEEE Trans. Wireless Commun.*, vol. 2, pp. 822-839, Jul. 2003.

[28] K. Shi and E. Serpedin, "Coarse frame and carrier synchronization of OFDM systems: a new metric and comparison," *IEEE Trans. Wireless Commun.*, vol. 3, pp. 1271-1284, Jul. 2004.

[29] D. J. G. Mestdagh, P. Spruyt, and B. Biran, "Analysis of clipping effect in DMT-based ADSL systems," *Proc. IEEE Int. Conf. Commun.*, pp. 293-300, 1994.

[30] X. Li and L. J. Cimini, Jr., "Effects of clipping and filtering on the performance of OFDM," *IEEE Commun. Lett.*, vol. 2, pp. 131-133, May 1998.

[31] H. Ochiai and H. Imai, "Performance analysis of deliberately clipped OFDM signals," *IEEE Trans. Commun.*, vol. 50, pp. 89-101, Jan. 2002.

[32] A. E. Jones and T. A. Wilkinson, "Combined coding for error control and increased robustness to system nonlinearities in OFDM," *Proc. IEEE Conf. Vehicular Tech.*, pp. 904-908, May 1996.

[33] R. D. J. Van Nee, "OFDM codes for peak-to-average power reduction and error correction," *Proc. IEEE Conf. Global Telecomm.*, pp. 740-744, Nov. 1996.

[34] J. A. Davis and J. Jedwab, "Peak-to-mean power control and error correction for OFDM transmission using Golay sequences and Reed-Muller codes," *Electron. Lett.*, vol. 33, pp. 267-268, Nov. 1997.

[35] K. G. Paterson and V. K. Tarokh, "On the existence and construction of good codes with low peak-to-average power ratios," *IEEE Trans. Inform. Theory*, vol. 46, pp. 1974-1987, Sep. 2000.

[36] C. Robing and V. K. Tarokh, "A construction of OFDM 16-QAM sequences having low peak powers," *IEEE Trans. Inform. Theory*, vol. 47, pp. 2091-2094, Jul. 2001.

[37] V. .C. Chan, R. Venkataramani, and V. K. Tarokh, "A new construction of 16-QAM Golay complementary sequences," *IEEE Trans. Inform. Theory*, vol. 49, pp. 2953-2959, Nov. 2003.

[38] M. Breiling, S. Mueller-Weinfurtner, and J. Huber, "SLM peak-power reduction without explicit side information," *IEEE Commun. Lett.*, vol. 5, pp. 239-241, Jun. 2001.

[39] S. Mueller, R. Bauml, R. Fischer, and J. Huber, "OFDM with reduced peak-to-

average power ratio by multiple signal representation," *Annals of Telecommunications*, Feb. 1997.

[40] H. Ochiai and H. Imai, "Performance of the deliberate clipping with adaptive symbol selection for strictly band-limited OFDM systems," *IEEE J. Select. Areas Commun.*, vol. 18, pp. 2270-2277, Nov. 2000.

[41] J. Tellado and J. M. Cioffi, "PAR reduction in multicarrier transmission systems," *ANSI document, T1E1.4 Technical Subcommittee*, contribution number 97-367, Dec. 1997.

[42] D. Jones, "Peak power reduction in OFDM and DMT via active channel modification," *Proc. 33rd Asilomar Conf. Signals, Systems and Computers*, pp. 1076-1079, 1999.

[43] B. S. Krongold and D. L. Jones, "PAR reduction in OFDM via active constellation extension," *IEEE Trans. Broadcast.*, vol. 49, pp. 258-268, Sep. 2003.

[44] M. Sharif and B. Hassibi, "Existence of codes with constant PMEPR and related design," *IEEE Trans. Signal Process.*, vol. 52, pp. 2836-2846, Oct. 2004.

[45] Y.-S. Choi, P. J. Voltz, and F. A. Cassara, "On channel estimation and detection for multicarrier signals in fast and selective Rayleigh fading channels," *IEEE Trans. Commun.*, vol. 49, pp. 1375-1387, Aug. 2001.

[46] X. Cai and G. B. Giannakis, "Bounding performance and suppressing intercarrier interference in wireless mobile OFDM," *IEEE Trans. Commun.*, vol. 51, pp. 2047-2056, Dec. 2003.

[47] A. Stamoulis, S. N. Diggavi, and N. A. Dhahir, "Intercarrier interference in MIMO OFDM," *IEEE Trans. Commun.*, vol. 50, pp. 2451-2464, Oct. 2002.

[48] O. L. Mangasarian, *A Newton Method for Linear Programming*, Data Mining Institute Technical Report 02-02, University of Wisconsin, Mar. 2002.

[49] C. Charalambous, "Acceleration of the least pth algorithm for minimax optimization with engineering applications," *Math. Programming*, vol. 17, pp. 270-297, 1979.

[50] P. Raghavan, "Probabilistic construction of deterministic algorithms approximating packing integer program," *J. Computer and System Sciences*, vol. 37, pp. 130-143, 1988.

[51] J. Luo, K. Pattipati, and P. Willett, "A class of coordinate descent methods for multiuser detection," *Proc. IEEE Int. Conf. Acoustics, Speech, and Signal Processing*, vol. 5, pp. 2853-2856, Jun. 2000.

[52] U. Fincke and M. Pohst, "Improved methods for calculating vectors of short

length in a lattice, including a compelxity analysis" *Math. Comp.*, vol. 44, pp. 463-471, Apr. 1985.

[53] B. Hassibi and H. Vikalo, "On the sphere-decoding algorithm I. expected complexity," *IEEE Trans. Signal Process.*, vol. 53, pp. 2806-2818, Aug. 2005.

[54] L. Brunel, "Multiuser detection techniques using maximum likelihood sphere decoding in multicarrier CDMA systems," *IEEE Trans. Wireless Commun.*, vol. 3, pp. 949-957, May 2004.

[55] W. Burchill and C. Leung, "Matched filter bound for OFDM on Rayleigh fading channels," *Electron. Lett.*, vol. 31, pp. 1716-1717, Sep. 1995.

[56] N. J. Bass and D. P. Taylor, "Matched filter bounds for wireless communication over Rayleigh fading dispersive channel," *IEEE Trans. Commun.*, vol. 49, pp. 1525-1528, Sep. 2001.

[57] A. J. Paulraj and C. B. Papadias, "Space-time processing for wireless communications," *IEEE Signal Process. Mag.*, vol. 14, pp. 49-83, Nov. 1997.

[58] T. S. Rappaport, *Wireless Communications: Principles & Practice*, Prentice-Hall, NJ, 1996.

[59] F. Adachi, M. Feeney, A. Williamson, and J. Parsons, "Crosscorrelation between the envelopes of 900 Mhz signals received at a mobile radio base station," *IEE Proc.*, 133(6):506-512, Oct., 1986.

[60] W. R. Braun and U. Dersch, "A physical mobile radio channel model," *IEEE Trans. Vehicular Tech.*, VT-40(2): 472-482, May 1991.

[61] J. Sykora, "Tapped delay line model of linear randomly time-variant WSSUS channel," *Electron. Lett.*, vol. 36, pp. 1656-1657, Sep. 2000.

[62] J. G. Proakis, *Digital Communications*, 4th ed., McGraw-Hill, 2000.

[63] N. Benvenuto, S. Tomasin, and L. Tomba "Equalization methods in OFDM and FMT systems for broadband wireless communications," *IEEE Trans. Commun.*, vol. 50, pp. 1413-1418, Sep. 2002.

[64] L. W. Couch, *Digital and Analog Communication Systems*, 6th ed., Prentice-Hall, NJ, 2000.

[65] J. M. Cioffi, "A multicarrier primer," *ANSI document, T1E1.4 Technical Subcommittee*, contribution number 91-157, 1991.

[66] J. Tellado, *Peak to Average Power Ratio Reduction for Multicarrier Modulation*, Ph.D. Dissertation, Stanford University, Sep. 1998.

[67] S. Verdú, *Multiuser Detection*, Cambridge University Press, Cambridge, UK, 1998.

[68] H. Sari, Y. Levy, and G. Karam, "An analysis of orthogonal frequency-division multiple access," *Proc. IEEE Conf. Global Telecomm.*, vol. 3, pp. 1635-1639, Nov. 1997.

[69] Q. Wang and L. Y. Onotera, "Coded QAM using a binary convolutional code," *IEEE Trans. Commun.*, vol. 43, pp. 2001-2004, Jun. 1995.

[70] C. Tellambura, "Phase optimization criterion for reducing peak-to-average power ratio for OFDM," *Electron. Lett.*, pp. 169-170, Jan. 1998.

[71] J. Spencer, *Ten Lectures on the Probabilistic Method*, SIAM, Philadelphia, 1987.

[72] L. Brunel and J. Boutros, "Lattice decoding for joint detection in direct sequence CDMA systems," *IEEE Trans. Inform. Theory*, vol. 49, pp. 1030-1037, Apr. 2003.

[73] M. Varanasi, "Decision feedback multiuser detection: a systematic approach," *IEEE Trans. Inform. Theory*, vol. 45, no. 1, pp. 219-240, Jan. 1999.

[74] L. Babai, "On Lovasz' lattice reduction and the nearest lattice point problem," *Combinatorica*, vol. 6, no. 1, pp. 1-13, 1986.

[75] A. De Wild, *The Peak to Average Power Ratio Reduction of OFDM*, M. Sc. Thesis, Delft University of Technology, Sep. 1997.

[76] T. May and H. Rohling, "Reducing the peak-to-average power ratio in OFDM radio transmission systems," *Proc. IEEE Conf. Vehicular Tech.*, vol. 3, pp. 2774-2778, May 1998.

[77] J. P. Woodard and L. Hanzo, "Comparative study of turbo decoding techniques: an overview," *IEEE Trans. Vehicular Tech.*, vol. 49, pp. 2208 2233, Nov. 2000.

[78] A. Stefanov and T. M. Duman, "Turbo-coded modulation for systems with transmit and receive antenna diversity over block fading channels: System model, decoding approaches, and practical considerations," *IEEE J. Select. Areas Commun.*, vol. 19, pp. 958-968, May 2001.

Appendix A

Proof to (4.9)

Let $\{\tilde{\boldsymbol{s}}, \tilde{n}\}$ and $\{\boldsymbol{s}^\star, n^\star\}$ be the solutions of the problems in (4.3) and (4.8), respectively. From the formulation of (4.3), it can be easily verified that

$$\begin{aligned}
&\left| \sum_{k=0,k\notin I}^{N-1} X_k e^{\frac{j2\pi k\tilde{n}}{N}} + \sum_{k=1}^{K} Y_{i_k} e^{\frac{j2\pi i_k \tilde{n}}{N}} + \sum_{k=1}^{K} \tilde{s}_k Z_{i_k} e^{\frac{j2\pi i_k \tilde{n}}{N}} \right| \\
&\quad \leq \max_{0\leq n\leq N-1} \left| \sum_{k=0,k\notin I}^{N-1} X_k e^{\frac{j2\pi kn}{N}} + \sum_{k=1}^{K} Y_{i_k} e^{\frac{j2\pi i_k n}{N}} + \sum_{k=1}^{K} \tilde{s}_k Z_{i_k} e^{\frac{j2\pi i_k n}{N}} \right| \\
&\quad \leq \max_{0\leq n\leq N-1} \left| \sum_{k=0,k\notin I}^{N-1} X_k e^{\frac{j2\pi kn}{N}} + \sum_{k=1}^{K} Y_{i_k} e^{\frac{j2\pi i_k n}{N}} + \sum_{k=1}^{K} s_k^\star Z_{i_k} e^{\frac{j2\pi i_k n}{N}} \right| \qquad \text{(A.1)}
\end{aligned}$$

It follows from (4.8) that

$$\begin{aligned}
&\max_{0\leq n\leq N-1} \left| \sum_{k=0,k\notin I}^{N-1} X_k e^{\frac{j2\pi kn}{N}} + \sum_{k=1}^{K} Y_{i_k} e^{\frac{j2\pi i_k n}{N}} + \sum_{k=1}^{K} s_k^\star Z_{i_k} e^{\frac{j2\pi i_k n}{N}} \right|^2 \\
&\quad = \max_{0\leq n\leq N-1} \left\{ \left| c_n + \sum_{k=1}^{K} s_k^\star d_{nk} \right|^2 + \left| c_{n+N} + \sum_{k=1}^{K} s_k^\star d_{n+N,k} \right|^2 \right\} \\
&\quad \leq V_1 \qquad \text{(A.2a)}
\end{aligned}$$

where

$$\begin{aligned}
V_1 &= 2 \max_{0\leq n\leq 2N-1} \left| \sum_{l=1}^{N} c_n + s_k^\star d_{nk} \right|^2 \\
&= 2 \left| \sum_{k=1}^{K} c_{n^\star} + s_k^\star d_{n^\star k} \right|^2 \qquad \text{(A.2b)}
\end{aligned}$$

Hence, we have

$$\max_{0\le n\le N-1}\left|\sum_{k=0,k\notin I}^{N-1} X_k e^{\frac{j2\pi kn}{N}}+\sum_{k=1}^{K} Y_{i_k} e^{\frac{j2\pi i_k n}{N}}+\sum_{k=1}^{K} s_k^{\star} Z_{i_k} e^{\frac{j2\pi i_k n}{N}}\right| \le \sqrt{2}\left|\sum_{k=1}^{K} c_{n^\star}+s_k^{\star} d_{n^\star k}\right| \tag{A.3}$$

We note that

$$\left|\sum_{k=1}^{K} c_{n^\star}+s_k^{\star} d_{n^\star k}\right|^2 \le V_2 \tag{A.4a}$$

where

$$\begin{aligned} V_2 &= \max_{0\le n\le 2N-1}\left|\sum_{k=1}^{K} c_n+s_k^{\star} d_{nk}\right|^2 \\ &= \max_{0\le n\le 2N-1}\left|\sum_{k=1}^{K} c_n+\tilde{s}_k d_{nk}\right|^2 \\ &\le V_3 \end{aligned} \tag{A.4b}$$

and

$$\begin{aligned} V_3 &= \max_{0\le n\le N-1}\left(\left|\sum_{k=1}^{K} c_n+\tilde{s}_k d_{nk}\right|^2+\left|\sum_{k=1}^{K} c_{n+N}+\tilde{s}_k d_{n+N,k}\right|^2\right) \\ &= \left|\sum_{k=0,k\notin I}^{N-1} X_k e^{\frac{j2\pi k\tilde{n}}{N}}+\sum_{k=1}^{K} Y_{i_k} e^{\frac{j2\pi i_k \tilde{n}}{N}}+\sum_{k=1}^{K} \tilde{s}_k Z_{i_k} e^{\frac{j2\pi i_k \tilde{n}}{N}}\right|^2 \end{aligned} \tag{A.4c}$$

By using (A.1), (A.3), and (A.4), we can write

$$\left|c_{n^\star}+\sum_{k=1}^{K} s_k^{\star} d_{n^\star k}\right| \le \left|c_n+\sum_{k=1}^{K} \tilde{s}_k d_{nk}+jc_{n+N}+j\sum_{k=1}^{K} \tilde{s}_k d_{n+N,k}\right| \le \sqrt{2}\left|c_{n^\star}+\sum_{k=1}^{K} s_k^{\star} d_{n^\star k}\right|$$

which proves the relationship in (4.9).

Appendix B

Derivation of Upper Bound in (4.18)

First, it can be seen from (4.17) that $U_n(\lambda, s_1, \ldots, s_j)$ is an upper bound for the conditional probability $\Pr\left(\left|c_n + \sum_{k=1}^{K} s_k d_{nk}\right| \geq \lambda | s_1, \ldots, s_j\right)$. Second, we note that

$$\begin{aligned}
&\sum_{n=0}^{2N-1} U_n(\lambda, s_1, \ldots, s_{j-1}) \\
&= \sum_{n=0}^{2N-1} \left[2e^{-\gamma\lambda} \cosh\left(\gamma c_n + \gamma \sum_{k=1}^{j-1} s_k d_{nk} \right) \prod_{k=j}^{K} \cosh(\gamma d_{nk}) \right] \\
&= \sum_{n=0}^{2N-1} \left\{ e^{-\gamma\lambda} \left[\cosh\left(\gamma c_n + \gamma \sum_{k=1}^{j-1} s_k d_{nk} + \gamma d_{nk} \right) \right.\right. \\
&\quad \left.\left. + \cosh\left(\gamma c_n + \gamma \sum_{k=1}^{j-1} s_k d_{nk} - \gamma d_{nk} \right) \right] \prod_{k=j+1}^{K} \cosh(\gamma d_{nk}) \right\} \\
&= \frac{1}{2} \left[\sum_{n=0}^{2N-1} U_n(\lambda, s_1, \ldots, s_{j-1}, 1) + \sum_{n=0}^{2N-1} U_n(\lambda, s_1, \ldots, s_{j-1}, -1) \right] \\
&\geq \min_{s_j \in \{1,-1\}} \sum_{n=0}^{2N-1} U_n(\lambda, s_1, \ldots, s_j) \qquad \text{(B.1)}
\end{aligned}$$

Furthermore, we note that

$$\begin{aligned}
\sum_{n=0}^{2N-1} U_n(\lambda) &= \sum_{n=0}^{2N-1} 2e^{-\gamma\lambda} \cosh(\gamma c_n) \prod_{k=1}^{K} \cosh(\gamma d_{nk}) \\
&\leq V_1 \qquad \text{(B.2a)}
\end{aligned}$$

and

$$\begin{aligned} V_1 &= \sum_{n=0}^{2N-1} 2e^{-\gamma\lambda} e^{\gamma^2 c_n^2/2} \prod_{k=1}^{K} e^{\gamma^2 {d_{nk}}^2/2} \\ &= \sum_{n=0}^{2N-1} 2e^{-\gamma\lambda} e^{\left(c_n^2 + \sum_{k=1}^{K} {d_{nk}}^2\right)\gamma^2/2} \\ &\leq V_2 \end{aligned} \tag{B.2b}$$

with

$$\begin{aligned} V_2 &= \sum_{n=0}^{2N-1} 2e^{-\gamma\lambda} e^{\varepsilon\gamma^2/2} \\ &= 4Ne^{-\gamma\lambda+\varepsilon\gamma^2/2} \end{aligned} \tag{B.2c}$$

where the inequality $\cosh(x) \leq e^{x^2/2}$ has been used and $\varepsilon = \max\limits_{0\leq n\leq 2N-1} \left(c_n^2 + \sum_{k=1}^{K} d_{nk}^2\right)$. It can be readily verified that function $e^{-\lambda\gamma+\varepsilon\gamma^2/2}$ has a global minimum when γ assumes the value $\gamma = \lambda/\varepsilon$. In such a case, (B.2) becomes

$$\sum_{n=0}^{2N-1} U_n(\lambda) \leq 4Ne^{-\lambda^2/(2\varepsilon)} \tag{B.3}$$

From (B.3), it is obvious that condition (4.13c) is satisfied if $\lambda > \sqrt{2\varepsilon \log(4N)}$.

Appendix C

Derivation of Upper Bound in (4.33)

First, it can be seen from (4.25) that $G_n(\lambda, s_1, \ldots, s_j)$ is an upper bound for the conditional probability $\Pr\left(\left|c_n + \sum_{k=1}^{K} s_k d_{nk}\right| \geq \lambda | s_1, \ldots, s_j\right)$. Second, we note that

$$\begin{aligned} \sum_{n=0}^{2N-1} G_n(\lambda, s_1, \ldots, s_{j-1}) &= \sum_{n=0}^{2N-1} \left[2e^{-\gamma\lambda} g\left(\gamma c_n + \gamma \sum_{k=1}^{j-1} s_k d_{nk}\right) \prod_{k=j}^{K} g(\gamma d_{nk}) \right] \\ &\geq V_1 \end{aligned} \tag{C.1}$$

and

$$\begin{aligned} V_1 &= \sum_{n=0}^{2N-1} \left\{ e^{-\gamma\lambda} \left[g\left(\gamma c_n + \gamma \sum_{k=1}^{j-1} s_k d_{nk} + \gamma d_{nk}\right) + g\left(\gamma c_n + \gamma \sum_{k=1}^{j-1} s_k d_{nk} - \gamma d_{nk}\right) \right] \right. \\ &\quad \left. \prod_{k=j+1}^{K} g(\gamma d_{nk}) \right\} \\ &= \frac{1}{2} \left[\sum_{n=0}^{2N-1} G_n(\lambda, s_1, \ldots, s_{j-1}, 1) + \sum_{n=0}^{2N-1} G_n(\lambda, s_1, \ldots, s_{j-1}, -1) \right] \\ &\geq \min_{s_j \in \{1,-1\}} \sum_{n=0}^{2N-1} G_n(\lambda, s_1, \ldots, s_j) \end{aligned} \tag{C.1a}$$

where inequality (4.26) has been used. Furthermore, we note that

$$\begin{aligned} \sum_{n=0}^{2N-1} G_n(\lambda) &= \sum_{n=0}^{2N-1} 2e^{-\gamma\lambda} g(\gamma c_n) \prod_{k=1}^{K} g(\gamma d_{nk}) \\ &\leq V_2 \end{aligned} \tag{C.2a}$$

and

$$\begin{aligned} V_2 &= \sum_{n=0}^{2N-1} 2e^{-\gamma\lambda} e^{k_1\gamma^2 c_n^2} \prod_{k=1}^{K} e^{k_1\gamma^2 {d_{nk}}^2} \\ &= \sum_{n=0}^{2N-1} 2e^{-\gamma\lambda} e^{\left(c_n^2 + \sum_{k=1}^{K} {d_{nk}}^2\right) k_1\gamma^2} \\ &\leq V_3 \end{aligned} \tag{C.2b}$$

with

$$\begin{aligned} V_3 &= \sum_{n=0}^{2N-1} 2e^{-\gamma\lambda} e^{\varepsilon k_1\gamma^2} \\ &= 4Ne^{-\gamma\lambda + \varepsilon k_1\gamma^2} \end{aligned} \tag{C.2c}$$

where the inequality $\mathrm{g}(x) \leq e^{k_1 x^2}$ has been used and $\varepsilon = \max\limits_{0\leq n\leq 2N-1} \left(c_n^2 + \sum_{k=1}^{K} d_{nk}^2\right)$. It can be readily verified that function $e^{-\lambda\gamma + \varepsilon k_1\gamma^2}$ has a global minimum when γ assumes the value $\gamma = \lambda/(2k_1\varepsilon)$. In such a case, (C.2) becomes

$$\sum_{n=0}^{2N-1} G_n(\lambda) \leq 4Ne^{-\lambda^2/(4k_1\varepsilon)} \tag{C.3}$$

From (C.3), it is obvious that condition (4.13c) is satisfied if $\lambda > \sqrt{4k_1\varepsilon \log(4N)}$.